Towards Realization of Magnetocaloric and Magnetoelectric Applications based on Bulk and Thin film forms of Sodium substituted Lanthanum Manganites

Thesis submitted to
COCHIN UNIVERSITY OF SCIENCE AND TECHNOLOGY
in partial fulfilment of the requirements for the
award of the degree of

Doctor of Philosophy

Sethulakshmi N

Department of Physics
Cochin University of Science and Technology
Cochin- 682022
India

September 2014

Author:
Sethulakshmi N
Magnetics Laboratory
Department of Physics
Cochin University of Science and Technology
Cochin -682022
Kerala. India.

E-Mail: nlsethu@gmail.com

Residence:
House No. 76, First floor
17th cross, 8th main
Bandappa garden
Muthyala Nagar
Bangalore – 560054

Supervising Guide:
Prof. (Dr.) M. R. Anantharaman
Professor, Department of Physics
Cochin University of Science and Technology
Cochin - 682 022
Kerala. India.

Cover Page Illustration:

Front: Magnetocaloric and magnetoelectric effects

Back: Field effect device model and hysteresis curves

September 2014

DECLARATION

I hereby declare that the Ph.D. thesis work entitled, **"Towards Realization of Magnetocaloric and Magnetoelectric Applications based on Bulk and Thin film forms of Sodium substituted Lanthanum Manganites"** is based on the original work carried out by me under the guidance of **Prof. M R Anantharaman,** in the Department of Physics, Cochin University of Science and Technology, Cochin-22 and has not been included in any other thesis submitted previously for the award of any degree.

Sethulakshmi N

Cochin – 22

September 2014

Department of Physics
Cochin University of Science and Technology
Cochin – 682022

Certificate

Certified that the present Ph.D. thesis work entitled **"Towards Realization of Magnetocaloric and Magnetoelectric Applications based on Bulk and Thin film forms of Sodium substituted Lanthanum Manganites"**, submitted by **Mrs. Sethulakshmi N** is an authentic record of research work carried out by her under my supervision in the Department of Physics in partial fulfillment of the requirements for the Degree of Doctor of Philosophy of Cochin University of Science and Technology, and has not been included in any other thesis submitted previously for the award of any degree.

.

September 2014
Cochin -22

Prof. M. R. Anantharaman

Supervising Guide
Department of Physics
CUSAT

Department of Physics
Cochin University of Science and Technology
Cochin – 682022

Certificate

Certified that all the relevant corrections and modifications suggested by the audience during the Pre-synopsis seminar and recommended by the Doctoral Committee of the candidate has been incorporated in the thesis.

September 2014
Cochin -22

Prof. M. R. Anantharaman

Supervising Guide
Department of Physics
CUSAT

Acknowledgements

It is a matter of great joy to present my doctoral thesis. I am grateful to several people who have played significant roles in my life and academic career over these years. I would like to acknowledge each and every one in helping and guiding me to achieve this goal.

First of all, I would like to express my sincere gratitude towards my Supervising guide, Prof. M.R. Anantharaman, Professor, Department of Physics, Cochin University of Science and Technology, for his support, encouragement and personal attention throughout my research period. I will always be grateful to him for his valuable advice and guidance without which the successful completion of this work would not have been possible. I acknowledge my former Supervisor, Prof. M. Sabir for all his support during the initial months of my research.

I am also grateful to Prof. B. Pradeep, Head of the Department, Department of Physics, Cochin University of Science and Technology for his help and support. My sincere thanks to all faculty members of the Department of Physics, Cochin University of Science and Technology for their unstinted support to me during the course of my research.

I would like to express my sincere gratitude to the Department of Science and Technology (DST), for selecting me for the DST INSPIRE fellowship (JRF and SRF) and supporting me in my doctoral research. I would like to thank all the staff members especially in the academic block of Cochin University of Science and Technology who have always been of great help in ironing out any administrative issues, doubts.

I sincerely thank DST DAAD Indo-German Personnel Exchange Programme for giving me an opportunity to work in the Institute of Physics, Technical University of Chemnitz, Germany and for extending financial support to make this possible. I am also thankful to Dr. Manfred Albrecht, Professor, Institute of Physics, Technical University of Chemnitz, Germany for his guidance and help during my period of work in Germany. I am grateful to Dr. Andreas Leibig, Mr. Fabian Gass, Mr. Mark Lindoff, Mr. Marcus Daniel and Ms. Birgit of the Technical University of Chemnitz, Germany for their guidance and for making my stay memorable. I made a good friend in Ms. Xialoei during my stay in Germany. Her friendship and warmth made my stay comfortable and pleasant in a foreign country. I am also thankful to Mr. Ananthasivan and family for their help, support and care throughout my stay in Germany.

I also bestow my sincere gratitude to the INUP programme of Centre for Nanoelectronics, IIT- Bombay especially to the co-ordinators, Dr. K Nageshwari, Prof. Anil Kottantharayil, and Prof. Ramgopal Rao. Their support was crucial for my work regarding thin film deposition and characterization techniques. I also thank INUP programme, IPC and

Materials Engineering Departments of IISc Bangalore for allowing me to make use of their facilities to take various measurements for my research.

Mere words are insufficient to express my gratitude to Dr. G. Srinivasan, Distinguished Professor, Oakland University, Rochester, USA for his valuable suggestions and guidance which has contributed immensely to the successful completion of this research work. With deepest gratitude, I thank Dr. K. G Suresh, Professor, Department of Physics, IIT Bombay for PPMS measurements. I also thank Dr. S Vasudevan, Prof. S. Ramakrishnan, Prof. Rajeev Ranjan, Prof. S. Ranganathan from IISc Bangalore for their guidance and support. I am thankful to Dr. Imad Al Omari, Dr. Salim Al Harthi, SQU Oman for all their help regarding the material characterization.

At this juncture, I want to thank Mr. Sandeep Kumbar, Ms. Shailaja of IIT Bombay and Mrs. Radhika, Ms. Lalitha, Mr. Prasad, Mr. Manikant and Mr. Sterin of IISc Bangalore for their unconditional help during my research at the IIT-B and IISc.

I would like to sincerely acknowledge the help and guidance provided by the teachers right from my school days for moulding me well. I am also grateful to the teachers and staff of St. Teresas College, Ernakulam and Sacred Hearts College, Thevara for inculcating research interest in me and guiding me forward.

I am thankful to my close friend from my college days, Mrs. Minnu Praveen for all her help, support and love. I would like to quote the

proverb “A friend in need is a friend indeed” to express my love and gratitude towards her.

Magnetic Laboratory shortly called Maglab in the Department of Physics, CUSAT where I worked all these years has been a second home. The lab was always filled with lots of fruitful discussions, friendly chats which I will cherish throughout my life. During these years, I was fortunate to develop good friendships with my colleagues in the maglab. I was fortunate to get an excellent friend in Vinayasree whom I fondly call Vinayachechi. I will always cherish the wonderful times we had in Maglab and during our travel and stay in IIT Bombay. I am also thankful to other members of Maglab, Geetha chechi, Babu Sir, Sudeep, Lija K Joy, Lisha Raghavan, Sivaraj, K S, Aravind P B, Jinisha B, Anupama E, Pooja and Bintu.

I am sincerely thankful to Dr. Senoy Thomas for all the valuable suggestions he provided throughout the research period. I also thank Dr. Sagar S, Dr. T N Narayanan, Dr. Swapna S Nair, Dr. Sajeev US, Dr. Hysen Thomas, Dr. Reena Mary A P, Dr. Vijutha Sunny, Dr. Veena Gopalan E, Dr. Jamal for their valuable advice.

I was also fortunate to get good friends like Hasna, Poornima chechi, Beena, Subha and Shajira.

I was fortunate to get a good friend in Mrs. Shiji Rahul who has been my hostel roommate over these years for providing a friendly atmosphere in the hostel enriched with good discussions and many cherishable moments.

I also remember with pleasure all my friends in Athulya hostel like Leena, Dhanya, Rakhi, Ramsi, Vineetha and Honey.

Last, but not the least, I will always be grateful to my family members for undergoing all sorts of hardships in helping me pursue my doctoral research. I would like to express my gratitude and love to my husband Dr. Arun Vishwanathan for his unconditional support and love without which I would not have completed this research work. Words are insufficient to express my gratitude and love to my (Appa) father, (Amma) mother and brother Suresh from the initial days of research work. I am fortunate enough to get married into a family where I got a loving Appa and Amma. They have helped, supported and guided me immensely unmindful of the hardships and pain they suffered during these years.

My family has been there with me at each stage of my research work lending their support and encouragement.

I use this occasion to express my gratitude by dedicating this thesis to them.

I am also grateful to God Almighty for guiding me through each and every stage of this work. Without His blessings I would not have been able to complete this Thesis.

Sethulakshmi N

PREFACE

Manganites are potential candidates for multifunctional applications since there is close entanglement between charge, spin and orbital degrees of freedom. These are a special class of materials called half metallics where electrons with one particular spin dominates over the other or have higher density of states unlike metals and their structural, magnetic and electrical properties are interrelated. Some major phenomena exhibited by them are crystal field effect, Jahn Teller distortion, spin dependent electron transport and magnetoresistance. Magnetoresistance which was first observed in manganites have been now exploited for the development of artificial structures of Fe/Co/Fe for GMR (Giant Magnetoresistance) based read heads in storage devices, bolometric sensors and spin valves.

Jonker and Van Santen in 1950's established the correlation between Curie temperature, resistivity and saturation magnetization and thus manganites came to the limelight of research. Later magnetic as well as conduction mechanism was explained on the basis of a single theory of double exchange proposed by Zener. Interest in rare earth manganites grew stronger after the discovery of colossal

magnetoresistance in 1991. Manganites exhibit perovskite structure ($AMnO_3$) where A site ions basically of rare earth elements (Eg: La, Y, Dy and Pr) are surrounded by MnO_6 octahedra formed by Mn ions and oxygen ions. Magnetic, structural and electrical properties can be tuned by substituting different elements for A sites thereby introducing mixed valency for Mn ions.

Manganites with La sites substituted by lower valence ions than La^{3+} are categorized as hole doped manganites and substitutions with higher valence ions than La^{3+} are termed as electron doped manganites. Substituting elements also change the lattice structure and tolerance factor apart from introducing holes or electrons in the manganite structure. Magnetic property of doped manganites is associated basically with the change in the ratio of Mn^{3+}/Mn^{4+} ions due to divalent ion substitutions by Ca, Sr, Ba and tetravalent ions of Ce for La ions. Magnetism is governed by spin ordering of t_{2g} levels of Mn^{3+} and Mn^{4+} ions mediated by oxygen. When the spin ordering of t_{2g} levels of adjacent Mn^{3+} and Mn^{4+} ions are parallel to each other, there is ferromagnetic alignment essentially with an exchange of electron from e_g level of Mn^{3+} to Mn^{4+} while superexchange mechanism between same valence ions (Mn^{3+}-O- Mn^{3+} or Mn^{4+}-O- Mn^{4+}) result in antiferromagnetic alignment without any electron transfer. Vacancies at La or O sites, difference in ionic radii, valency of La or substituting ions and lattice mismatch are some other factors that affect the magnetic property of doped manganites.

Hole doped manganites with monovalent substitutions for La sites are another effective way of achieving different Mn valencies since substitution of monovalent ion by ‘x’ amount convert ‘2x’ Mn^{3+} ions to Mn^{4+} ions which is double the amount of Mn^{4+} obtained for ‘x’

amount of divalent substitution. Monovalent ions like K^+, Na^+ and Li^+ are best suited for La sites since their ionic radii are close to La^{3+} thus keeping tolerance factor almost constant even after substitution despite the difference in valencies of La^{3+} and Na^+. Thus monovalent susbstituted manganites are of interest from structural, electrical and magnetic properties point of view. It is thus possible to develop hole doped rare earth lanthanum manganites by controlling the substitution of monovalent ion like sodium and getting it reflected on the magnetic phase of the material. Thus a magnetic material using sodium substituted lanthanum manganites with appreciable saturation magnetization near 300 K and magnetic ordering temperature in the high temperature regime is of interest to the scientific community.

Hence monovalent substituted manganites assume importance both from theoretical and applied perspectives. Literature reports especially on higher substitution levels of monovalent ions are scarce or seldom reported. Thus there exist possibility of developing excellent compositions out of monovalent substitutions with large magnetic moments and possessing different magnetic phases. Magnetic phase of these kind of materials can be ferromagnetic, antiferromagnetic, canted antiferromagnetic, charge ordered and spin glass states. Such doped manganites are candidate materials for investigating correlated systems with co-existant FM-AFM phases.

Magnetic materials with large magnetic moments can find applications in the field of magnetic refrigeration. Refrigeration mechanism based on magnetic materials relies on the principle of magnetocaloric effect (MCE) which is termed as reversible change in temperature in the presence and absence of magnetic field. For

considering MCE, a magnetic material is viewed as two subsystems consisting of a magnetic part and a lattice part. Upon application and removal of magnetic field, a transfer of entropy between these subsystems takes place which is manifested as change in temperature. Magnetic refrigeration is an ecofriendly cooling technology utilizing only magnetic materials and do not pose any threat to ozone depletion when compared to CFC gases used in conventional refrigeration. Currently, Gd and Gd based silicides are reported to be the frontrunners with maximum magnetic entropy change (ΔS_M) of 40 $J.Kg^{-1}K^{-1}$. Other potential MCE materials are Laves phases, Mn As Alloys all with low operating temperatutes below 300 K. Thus quest for MCE materials with appreciable ΔS_M value operating at temperatures close to room temperature is on and among them; manganites occupy a prominent place since the magnetic properties of the material can be tailored by appropriate substitution.

Magnetoelectrics as well as multiferroics are currently fascinating areas of research. Multiferroic materials possess two or more ferroic orders in the same phase and such materials do not practically exist and an immediate cousin is a magnetoelectric material. A magnetoelectric material is basically a composite comprising of ferromagnetic and ferroelectric material essentially with a coupling between these ferroic orders called magnetoelectric coupling. Manganites can serve as effective candidates for ferromagnetic component and deposition of such a manganite film on a good ferroelectric material can be devised to provide a magnetoelectric composite provided there is a coupling between electric and magnetic ordering. Magnetoelectrics are the next generation switching devices where the electric/ magnetic field

can control magnetization/electric polarization respectively further leading to four state storage devices. One of the practical ways of inducing a coupling between ferroelectric (which is also piezoelectric) and ferromagnetic constituents in a material is via strain. In such a material, strain effects produce substantial changes in electrical / magnetic parameters with the applied magnetic/electric fields and the material as a whole function as a field effect device.

The present thesis work focuses on hole doped lanthanum manganites and their thin film forms. Hole doped lanthanum manganites with higher substitutions of sodium are seldom reported in literature. Such high sodium substituted lanthanum manganites are synthesized and a detailed investigation on their structural and magnetic properties is carried out. Magnetic nature of these materials near room temperature is investigated explicitly. Magneto caloric application potential of these materials are also investigated. After a thorough investigation of the bulk samples, thin films of the bulk counterparts are also investigated. A magnetoelectric composite with ferroelectric and ferromagnetic components is developed using pulsed laser deposition and the variation in the magnetic and electric properties are investigated. It is established that such a composite could be realized as a potential field effect device.

Thus the main objectives of present investigation are as follows:

- ✓ Synthesis of bulk samples belonging to sodium substituted lanthanum manganite series, $La_{1-x}Na_xMnO_3$ (x= 0.5 to 0.9)

- ✓ Study the effect of sodium substitution on crystal structure, lattice parameters, magnetization and transition temperatures
- ✓ Evaluation of magnetic entropy change with temperature and Na concentration
- ✓ Determining the amount of Mn^{4+} and Mn^{3} ions and ascertaining the role of Mn^{4+}/Mn^{3+} ratio in the magnetism exhibited by these compounds
- ✓ Deposition of Thin films of sodium substituted lanthanum manganite thin films using Pulsed Laser Deposition on silicon substrate
- ✓ Investigate the magnetic properties and magnetocaloric effect for different compositions
- ✓ Devising a magnetoelectric field effect device using thin films deposited on a Piezoelectric substrate of PMN PT
- ✓ Study the variation of electrical and magnetic properties with sodium concentration
- ✓ Correlation of results

The Thesis is entitled "Towards Realization of Magnetocaloric and Magnetoelectric Applications based on Bulk and Thin film forms of Sodium substituted Lanthanum Manganites" and consists of eight chapters.

Chapter 1 gives an introduction to the family of perovskites, their structure with a summary of work already carried out in the area of manganites. Basic concepts of magnetocaloric effect and magnetoelectric materials are also discussed.

Chapter 2 contains the theoretical concepts associated with structure, spin dependent transport and magnetism in manganites. It also throws light into the theoretical background of magnetic entropy change and adiabatic temperature change associated with magnetocaloric effect.

Chapter 3 deals with various experimental techniques employed for the characterization of these materials. An overview of the working principle of each characterization tool will be discussed.

In **Chapter 4**, synthesis of bulk samples of higher sodium substituted lanthanum manganites will be discussed. Effect of sodium substitution on the structural and magnetic properties is investigated. Magnetic properties near room temperature are thoroughly investigated and the role of Mn valence ions in deciding magnetic behaviour is determined.

In **Chapter 5**, magnetic isotherms of the synthesized samples are drawn and the nature of magnetic transition is established. Isotherms are further utilized to determine magnetic entropy change. Maximum magnetic entropy change and corresponding adiabatic temperature change are also determined. Variation of transition temperature with sodium concentration is also reported in this chapter.

Chapter 6 describes thin film deposition of the bulk counterparts on a normal silicon substrate using Pulsed Laser Deposition. Stoichiometry of deposited films is confirmed from compositional analysis. Structural and magnetic properties of thin films along with magnetic entropy variation with sodium substitutions are also investigated.

In **Chapter 7,** a magnetoelectric composite using manganite thin film deposition on a ferroelectric substrate like PMN PT is discussed and

the variation of magnetization and electric polarization in such a composite is studied. Phenomenon of strain induced magnetism and the potential of such a magnetoelectric composite for a field effect device is realized.

Chapter 8 is the final chapter where salient features of the present work are highlighted. The overall conclusions as well as the scope for further investigations are also brought out.

CONTENTS

Research Publications

In International Journals

Near fifty percent sodium substituted lanthanum manganites—A potential magnetic refrigerant for room temperature applications
N. Sethulakshmi, I. A. Al-Omari,K. G. Suresh and M. R. Anantharaman
APPLIED PHYSICS LETTERS 104, 092407 (2014).

Large enhanced dielectric permittivity in polyaniline passivated core-shell nano magnetic iron oxide by plasma polymerization
Lija K. Joy, V. Sooraj, U. S. Sajeev, Swapna S. Nair, T. N. Narayanan, **N. Sethulakshmi**, P. M. Ajayan, and M. R. Anantharaman
APPLIED PHYSICS LETTERS 104,121603 (2014).

Contact potential induced enhancement of magnetization in polyaniline coated nanomagnetic iron oxides by plasma polymerization
N. Sethulakshmi, V. Sooraj, U. S. Sajeev, Swapna S. Nair, T. N. Narayanan, Lija K. Joy, P. A. Joy, P. M. Ajayan, and M. R. Anantharaman, APPLIED PHYSICS LETTERS 103, 162414 (2013).

On Magnetic Ordering in Heavily Sodium substituted Hole doped Lanthanum Manganites

N Sethulakshmi, A N Unnimaya, I A Al - Omari, Salim Al – Harthi, S Sagar, Senoy Thomas and M R Anantharaman (under review in JOURNAL OF MAGNETISM AND MAGNETIC MATERIALS)

Influence of Higher Sodium substitutions on the magnetic Entropy change in Lanthanum Manganites

N. Sethulakshmi, I. A. Al – Omari and M. R. Anantharaman (under review in MATERIALS RESEARCH BULLETIN)

Conference Publications

Towards a field effect device using multiferroic rare earth manganites [best poster presentation]

National Conference on Emerging Technologies for Processing and Utilization of Beach Sand Minerals organized by Rare Earth Association of India (REAI) and IRE Retired Employees Organization(IREREO)March 1-2, 2013

On* ferromagnetic *ordering and MCE behavior in monovalent Lanthanum manganites

International Conference on Advanced Functional Materials (ICAFM-2014) at Thiruvananthapuram, being jointly organised by CSIR-

NIIST, IIM Trivandrum Chapter, ICS Kerala Chapter, MRSI Trivandrum Chapter and SPS Trivandrum Chapter

Magnetocaloric effect – A new solution to energy crisis

National Seminar on Frontiers of Nanotechnology , organised by Sree Sankara Vidya peetom college, valayanchirangara on 6-7 March 2014

CHAPTER 1

Introduction

Man's thirst for new materials is never quenched and has been an ongoing process carried forwarded through various periods of human history from the Stone Age to Iron Age through Bronze Age. The occurrence of Industrial revolution and spin offs of World wars and space technology have given birth to new and novel materials. Thus the study of materials science and their characterization have given birth to a new branch called Material science and Engineering which represents a blend of scientific discoveries and practical applications of materials. Material science and Engineering is rapidly advancing and scaling new heights with the invention of new devices and modification of existing technologies with newer materials. It is an ever green and a highly fascinating field since advances in materials directly influence technological developments. [1-3].

From materials science point of view, materials are classified as metals, polymers, ceramics, semiconductors and composites. Metals are excellent electrical and thermal conductors while in semiconductors, electrical property is dependent on the temperature and the concentration of doping elements. Metals are extensively utilized in electrical and thermal works, in the manufacturing of various items ranging from small utensils to aircraft frames, in chemical plants as well as in the medical field [4].

Semiconductors have also played a pivotal role in the integrated circuitory which revolutionized the electronics and computer industries. Larger molecular structure, low density and flexibility of polymers also are in demand for adhesives and lubricants to implantable devices like orthopedic plates, artificial joints and heart valves. Ceramics which combine metallic and nonmetallic properties are capable of withstanding high temperatures even though they are mechanically brittle. Composites are perfectly engineered materials comprising of one or more material types and hence combine the best qualities of its constituents. One major example for composites is fibre glass which has the strength of glass and flexibility of polymer. Each class of material has specific applications but the search for advanced materials is increasing with man's quest to do wonders with technology [2].

Presently, huge innovations and research are on in the areas of information storage, communication, energy resources and medical therapy. Magnetic materials are of great value in all these fields. Phenomenon of magnetism is exploited in storage devices like hard disks, CD-ROM, electric motors, generators, transformer cores, loudspeakers, automobiles, magnetic resonance imaging equipment and many other electronic gadgets. With time many new applications are continuously emerging [3,4].

1.1. Magnetic Materials

"Modern technology would be unthinkable without magnetic materials and magnetic phenomena"

Rolf E. Hummel, Understanding Materials Science, 1998

Magnetic materials play an important role in new fields of technological advances as rightly quoted by Rolf E Hummel. Magnetic materials have been known to mankind since the discovery of 'load stone' (Fe_3O_4) or magnetite, which is a naturally occurring magnet. A simple description of magnetism could be "property of materials by which they respond to the external magnetic field". The response of the material to magnetic field (H) can be given by magnetic induction, B. Magnetic induction B can be given by $B = \mu_0 (H + M)$ where H is the external applied magnetic field in A/m, M is the magnetization of the material (magnetic moment per unit volume) in A/m and μ_0 is the magnetic permeability of free space in weber/Am making B in weber/m^2 which is otherwise termed as Tesla. Other key terms describing the magnetic nature are permeability and susceptibility. Permeability (μ) can be defined as the measure of how permeable is the material to the external magnetic field. It is given by the ratio of B and H (μ=B/H). Susceptibilty (χ) defines the measure of response in the magnetic characteristics with respect to the applied magnetic field and is given by the ratio of M and H (χ=M/H). In SI units, Susceptibility is dimensionless while permeability has the unit of Henry/m. Relationship between the two can be given by $\mu/\mu_0 = 1+\chi$ [5].

1.2. Classification of Magnetic Materials

Magnetic materials are broadly classified depending on the origin of magnetic moment and by their response characteristic to the external magnetic field, temperature atc. Before dwelling into the classification, origin of magnetic moment or magnetization in the materials need to be analyzed. The magnetism is an atomic phenomenon.

A normal atom with electrons orbiting around the nucleus is associated with an orbital angular momentum in addition to the momentum contributions from the spin of each electron. The orbital and spin angular momentum are the fundamental contributors to the magnetic moment of the atom. The presence of an external magnetic field further alters the orbital angular momentum leading to an effective change in the magnetization of the material. Magnetic materials are classified into different categories namely diamagnetic, paramagnetic, ferromagnetic, anti ferromagnetic and ferromagnetic materials depending on their magnetic susceptibility [4,5].

1.2.1. Diamagnetism

This type of magnetism is present in all materials as the magnetization arises from the change in the orbital motion of electrons in the presence of magnetic field. The diamagnetic behaviour is a weak phenomenon and is dormant in materials where there are no unpaired electrons (i.e, completely filled orbitals) whereas in materials with unpaired electrons the diamagnetic behavior is overshadowed by other types of magnetism like ferro/paramagnetism. When a diamagnetic material is placed in a magnetic field (consider the case, field is perpendicular to the orbiting electrons) there will be a rate of change of magnetic flux associated with it. This will induce an electromotive force (emf) proportional to rate of change of flux opposing the field (Lenz's law) and thus the induced magnetic moments are directed opposite to the applied field. Thus, stronger the external field more negative is the magnetization induced and hence the magnetic susceptibility is negative.

In the actual picture, the rate of change of flux is achieved by decreasing the velocity of the electrons which adversely decreases the magnetic moment also and it is this decreased moment we observe as diamagnetic effect. All the noble gases and superconducting materials are diamagnetic. Diamagnetic materials find applications in alloys of dia and paramagnetic materials (paramagnetic materials have positive susceptibility) to reduce the susceptibility close to zero for delicate magnetic measurements. Recently the anisotropic diamagnetic property is explored for the alignment of liquid crystals [5-7].

1.2.2. Paramagnetism

The materials which have permanent magnetic moments even in the absence of external magnetic field are called paramagnetic materials. The magnetic moments arise from the spin contributions of the unpaired electrons in the atomic/molecular orbitals. These magnetic moments are only weakly coupled to each other and are randomly oriented due to thermal agitation making the net magnetic moment zero in the absence of a magnetic field. When magnetic field is applied, the moments will be aligned in the direction of the field and hence the susceptibility in this case is positive. Salts of transition metal elements, metals like aluminium, and gases like oxygen are examples of paramagnetic materials. The ferromagnetic materials make transition to paramagnetic state at high temperatures provided the thermal energy overcomes the cooperative aligment of magnetic moments. In general, paramagnetic effects are quite small and the magnetic susceptibility is of the order of 10^{-3} to 10^{-5} for most paramagnets and inversely proportional

to temperature, but may be as high as 10^{-1} for synthetic paramagnets such as ferrofluids and the permeability is slightly greater than one [5,8].

1.2.3. Ferromagnetism

It is the basic type of magnetism found in permanent magnetic materials like nickel, iron. In ferromagnets, the magnetic moments are strongly coupled to each other unlike paramagnetic materials and the moments align parallel to each other competing the thermal agitation yielding a net magnetic moment in the absence of a magnetic field. This magnetization in the absence of magnetic field is called spontaneous magnetization (M_s) and has its origin mainly from the spin contributions of the electrons. A remarkable feature of ferromagnetic materials is the hysteresis behaviour which is defined as the property of these materials to retain their magnetization even after the removal of magnetic field. After achieving saturation magnetization on the application of external magnetic field, the remaining magnetization present in the material on decreasing the field to zero is called remanent magnetization (M_r). The reverse field required to reduce the magnetization to zero is called coercivity (H_c). The application potentials of ferromagnetic materials are determined based on these hysteresis loop parameters. Ferromagnetic materials are further classified into soft and hard materials. The materials which require large coercive fields for achieving zero magnetization (large field for saturation also) are called hard ferromagnets while soft magnets are easily saturated and demagnetized [5].

Magnetism in ferromagnetic materials is explained by means of magnetic domains. Domains are small regions within the ferromagnetic material where the magnetic domains are aligned parallel to one another. In the demagnetized state, the magnetization vectors of different domains have different orientations and the net moment is zero. On magnetizing the material the domains align parallel to another. These domains are separated by boundaries called domain walls or bloch walls. They are about four-millionths of an inch (~10 μm) in thickness and within this region the direction of magnetization changes by either 90^0 or 180^0[5-9].

1.2.4. Ferrimagnetism

The ferrimagnetic materials are often referred to as weak ferromagnetic materials. The magnetism in ferromagnetic materials are explained based on the two sublattice model wherein the adjacent magnetic moments are aligned antiparallel but have a spontaneous magnetization as the magnetic moments are not equal. Thus the two interpenetrating sublattices are not equal; one has higher magnetization compared to the other. The ferrimagnetic materials are insulators unlike the ferromagnetic metals. Ferrites are ferrimagnetic transition metal oxides which find large number of technological applications mainly in high frequency regime as the eddy currents due to ac fields will not influence the insulators. Yttrium iron garnet (YIG) and magnetite also fall under the category of ferrites. Figure 1.1 shows different types of magnetic ordering or dipole alignment with respect to an applied magnetic field [5,7].

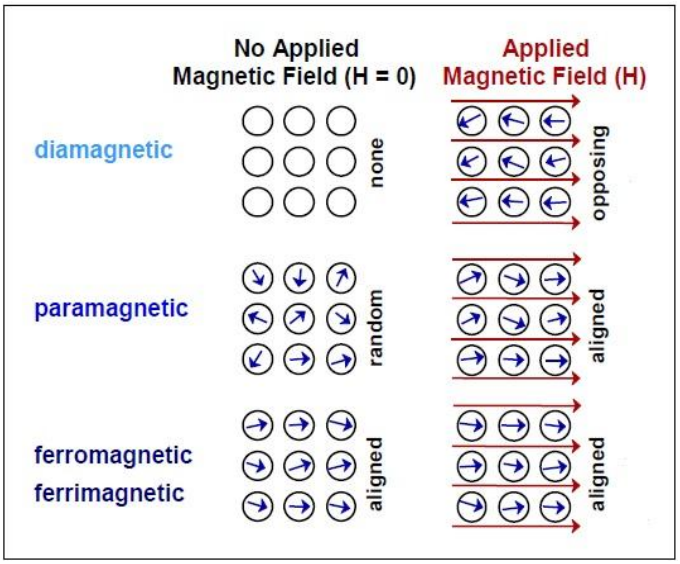

Figure 1.1: Different types of magnetic ordering

1.2.5. Antiferromagnetism

Materials where the cooperative alignment of adjacent magnetic moments is antiparallel correspond to antiferromagnetic materials. Antiferromagnetism can also be described consisting of two interpenetrating sublattices with equal moments cancelling each other. Antiferromagnetic materials have no spontaneous magnetization and their response to magnetic field at particular temperature is similar to paramagnetic materials but with larger positive susceptibility. The susceptibility is temperature dependent and decreases with decrease in temperature below the transition temperature, T_N (Neel temperature). Figure 1.2 shows the magnetic dipole alignment in antiferromagnetic materials and M-H curves for different types of magnetism.

Chromium, Nickel oxide and hematite show antiferromagnetic ordering. Antiferromagnetic materials find applications in spin valves because of their property of exchange bias coupling. Another area of possible application is in CMR materials (Colossal magnetoresistance) where the antiferromagnetic to ferromagnetic transition is accompanied by a metal insulator transition [7,9].

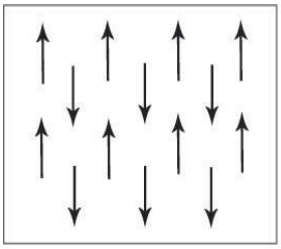

(a)

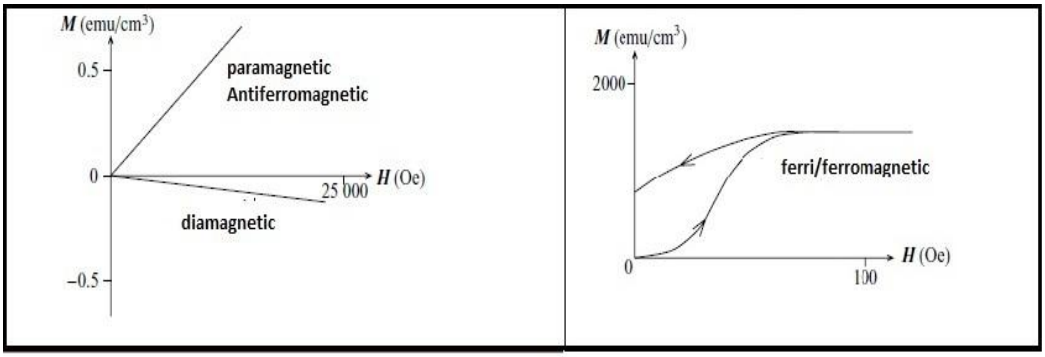

(b)

Figure 1.2: (a) Alignment of magnetic dipoles in Antiferromagnetic materials (b) M Vs H curves for different types of magnetic materials [5]

Correlated materials also display interesting magnetic phenomena in addition to their excellent structural, electrical and thermal properties. They find applications in diverse fields such as storage devices, bolometric sensors, magneto-resistance devices and spin valves and are on par or above conventional magnetic materials.

1.3. Correlated materials

Correlated materials are basically oxides comprised of transition metal elements. In transition metals with open (or partially filled) d or f orbitals, spatial confinement of electrons in orbitals is larger providing a strong coulomb repulsion between them. Such strongly interacting or 'correlated' electrons appear localized with a pronounced influence of each single electron on others. Net results of such a correlated behaviour are large interplay between spin, charge and orbital moment and the extreme sensitivity of the material properties to slight changes in temperature, pressure and ionic concentration [10,11]. Even though these systems comprise of simple transition metals, they exhibit some of the most intriguing properties in the field of condensed matter physics. Remarkable properties like ferromagnetic/ antiferrromagnetic ordering, metal - insulator transition in oxides of transition metals, superconductivity in cuprates like $La_{2-x}Sr_xCuO_4$ and volume change associated with phase transitions in actinides are the effects of correlated electron behaviour [11,12]. Correlated systems can be categorized as high T_C materials, mott insulators, spintronic materials, heavy fermions, MR materials and perovskite manganites depending on the properties exhibited by them. Density function theory (DFT) and Dynamic mean

field theory (DMFT) have been developed to explain the correlation physics of electrons. In the application level, these materials are highly sought for developing superconducting magnets, magnetic storage devices, smart windows to control temperature in a room and in spintronics [13,14].

Perovskite manganites are excellent electron correlated systems possessing different phase states and transitions with a close correlation between structure, electron transport and magnetic properties. Manganites belong to perovskite family and are highly investigated materials owing to their technological applications in electro optic modulators, dielectric resonators, electrostrictive actuators and in refractories. It has also been established that perovskites like $GdFeO_3$ play a substantial role in magnetic bubble memories [15].

1.4. Perovskites

Perovskites are generallly ceramic materials with a combination of metals with a non metal like oxygen having a general formula ABO_3. The first perovsite characterized was Calcium Titanate ($CaTiO_3$) by the scientist G. Rose in 1839 and was named after the mineralogist, and then Russian vice-president, Count Lev Aleksevich Perovski. Later it was discovered that the most abundant mineral on earth, the magnesium silicate ($MgSiO_3$) is a perovskite [5,15].

Perovskites have the general structural formula ABO_3 where A sites are occupied by trivalent or divalent alkali/alkaline earth metal ions and the B sites by transition metal ions. They have a cubic structure which can be viewed as the A site ions forming the corners of

the cube, transition metal ion at the body centre and the oxygen anions at the face centres. An alternate crystal picture includes corner shared BO_6 octahedra with A ions at centre. Structure of perovskite is shown in figure 1.3. Perovskite cubic structure is an ideal case and the structure can distort to rhombohedral, orthorhombic, hexagonal or monoclinic depending on the term called tolerance factor given by

$$t = \frac{< r_A > + r_O}{\sqrt{2}(r_{Mn} + r_O)} \qquad (1.1)$$

where r_A is the radius of A site ion, r_O is the radius of oxygen ion, r_{Mn} is the radius of Mn ion. For the ideal cubic case, value of t corresponds to one [15, 16]. Perovskite materials are in the limelight since 1950's.

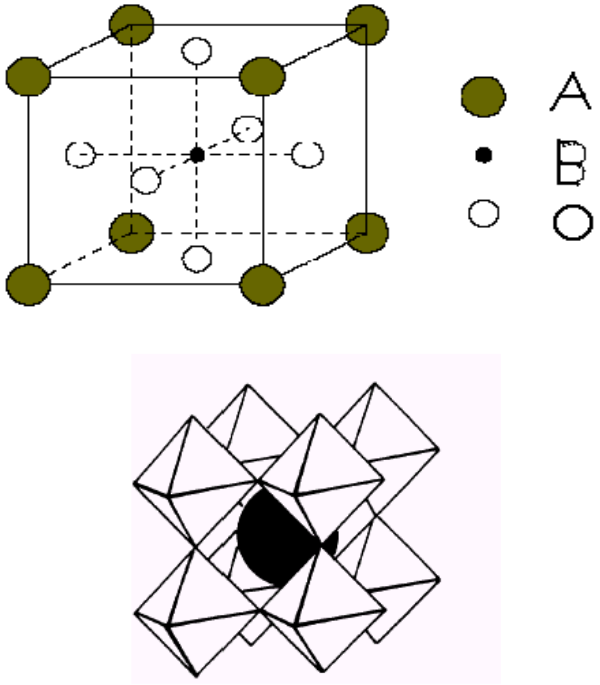

Figure 1.3: Perovskite structure

Materials belonging to this family were investigated extensively and a variety of research outputs were reported in the fields of conductivity, magnetization, specific heat, Hall effect, Seebeck effect, I-V characteristics, magnetostriction, magneto résistance etc. Perovskites retain good thermal and thermodynamic stabilities which are the basic requirements for catalytic applications and for electrode applications in magnetohydrodynamic generators [15].

1.5. Manganites

Manganites, named after the key ingredient manganese with the general chemical composition $AMnO_3$ or $A_{1-x}R_xMnO_3$; (A = La, Pr, Nd), (R = Ca, Sr, Ba) is a prominent member of the perovskite family. They came to the focus of research because of two remarkable features : Metal - Insulator transition and exchange interaction mediated magnetism [17]. The ferromagnetic transition in these materials take place at a particular level of ion doping (finite 'x'value, $x \neq 0$) with an appreciable change in conductivity. Colossal Magneto-Resistance (CMR) was first observed in the doped derivatives of manganites [La-Ca-Mn-O films at T=77K in an applied field of 5Tesla] which was followed by a stream of work in the transport, magnetic, electrical and thermal properties of manganites [18,19]. New theories like double exchange mechanism and semi covalent exchange have been put forwarded to explain the magnetic behavior of Mn ions. Thus the importance of manganites is growing day by day [17]. At present active research is on in manganites, their doped components, multilayer structures, composites etc. to realize their

potentials in the field of magnetoelectrics, magnetic storage, switching devices, magnetocaloric effects and spintronics [20-26].

1.6. Historical Background

Successful entry of Manganites to the field of research was through the works of Jonker and Van Santen in 1950 and they discovered a striking correlation between the Curie Temperature (T_C), Saturation magnetization (Ms) and Electric resistivity (ρ) as function of x in samples of $La_{1-x}A'_xMnO_3$; A'= Ca^{2+}, Sr^{2+}, Ba^{2+} [17,19]. For polycrystalline samples of $La_{0.7}Sr_{0.3}MnO_3$, Tc_{max} of 370K, σ_{max} of $300\Omega^{-1}cm^{-1}$ and Ms_{max} of 90G/g [16] were observed. In the following year, Zener came up with a novel concept of exchange mechanism later named as Zener's double exchange mechanism which until today stands as one of the fundamental theories explaining magnetism in manganites. This was followed by contributions from Anderson and Hasegawa in 1955 and de Gennes in 1960 [27-29].

Zener stated that in the case of doped manganites, the magnetic behaviour is due to the combined effect of mixed valence ions Mn^{3+} and Mn^{4+}. The transfer of electron from Mn^{3+} to O^{2-} and to Mn^{4+} causes high conductivity and as the hopping electron retains its spin, spins of two adjacent Mn ions need to be parallel. This theory could successfully explain the experimental results observed at that time as the observation of crystal structure of different samples with same lattice constants confirmed that simple exchange interaction could not be the reason for magnetism [27,28]. Jonker has also stated that as crystal structure approaches cubic phase, magnetization have only spin

contributions from ions [27,30]. This was close to the double exchange theory, i.e, for cubic phase, Mn-O-Mn planes are linear and hence maximum double exchange and hence higher magnetization. Many significant investigations followed after Zener's theory in this field. Studies on cobaltites [31], low temperature studies on manganites, dc & ac resistivity, magnetization, hall effect and Seebeck effect need special mention here [32]. Volger proposed that maximum T_C and minimum resistivity at x=0.3 doped samples could be an indication for a correlation between magnetism and electrical conductivity [32].

In 1955, Wollan and Koehler performed neutron diffraction studies on $La_{1-x}Ca_xMnO_3$ samples and prepared a magnetic structure based phase diagram [33]. Later, high quality millimeter sized long single crystals of manganites (LaPb) MnO3 [34] were developed and reports in this area confirmed the earlier observed results [35]. The concept of spin polarized conduction band came up for explaining magnetic behavior due to the non Heisenberg nature of ferromagnetic transition [35].

The next major development in the field of manganites took place when the oxygen stoichiometry and transport properties were investigated [36]. They were unsuccessful in Hall effect measurements but interpreted that charge localization into magnetic or lattice polaron conduction by hopping in paramagnetic region above T_C but the reason for such a charge localization was undefined. The lattice interaction and magnetic behavior was brought to picture by Louca [37,38] from the study on local structure of manganites.

These earlier investigations provided some remarkable insights on the correlation between magnetism and resistivity. Magnetic

behaviour can be due to double exchange interaction between $Mn^{3+}$and Mn^{4+} ions and is maximum when Mn ions are collinear with anions. It is also found that oxygen stoichiometry and divalent ion substitution have profound influence on double exchange mechanism. It is worth mentioning the pioneering theoretical contributions during this period namely Double exchange theory and its modifications by Zener, Anderson, Hasegawa, Goodenough and de Gennes, concept of magnetic and lattice polaron, concept of small lattice polarons, narrow band model and Jahn Teller distortion [27-29, 39-41].

The concept of mixed valence states and their control over the properties of manganites especially on the metallic conduction and the magnetic ordering was put forth by Verwey and de Boer. They observed that mixed valence states of Fe such as Fe^{3+} ($3d^5$) and Fe^{2+} ($3d^6$) in the B sites of spinel structured magnetite led to conduction and ferromagnetic B± B exchange interactions [42]. Followed by their analysis, lot of research works were dedicated to mixed valence states and were extended to perovskite oxides too [42-46]. In perovskites or specifically in manganites, mixed valency can be achieved by substituting different elements at A sites. Divalent cations which can occupy A sites include calcium, barium, strontium and lead and trivalent cations basically rare earths like yttrium, lanthanum, praseodymium and neodymium. Such elemental substitution led to different classes of manganites like hole and electron doped categorized respectively depending on the valency of substituting ions is smaller or larger than the A site ions.

1.7. Doped Manganites

Doped manganites refer to element substituted manganite systems and the word 'doped' signifies whether it is electron doped or hole doped. Hole doping refers to replacing rare earth trivalent ions by divalent ions like Ca, Sr and Ba resulting in the mixed state of Mn^{3+} and Mn^{4+} for manganese ions. There has been extensive studies on hole doped systems like $La_{1-x}Ca_xMnO_3$ and $La_{1-x}Sr_xMnO_3$ which proved them to be paramagnetic at high temperatures and ferromagnetic at low temperatures. In electron doping, the rare earth sites are substituted by trivalent ions like Ce, Y and Ga resulting in mixed valence state of Mn^{2+}/Mn^{3+} ions. Magnetic ordering in these types of materials relies upon exchange interaction between Mn^{3+} and Mn^{2+} ions [47-50].

Substitutions for A sites by divalent or trivalent ions have been investigated and a lot of interesting properties have come up, for instance, Colossal Magneto-resistance (CMR) effect [51-53]. Variation of the ionic radii at A sites can result in buckling or distortion of MnO_6 octahedra from cubic phase to several lower symmetry structures having reduced co-ordination numbers for A and Mn ions [54]. Orthorhombic, rhombohedral, tetragonal and monoclinic are the most common non cubic structures of manganites Magnetic ordering in these materials arise from the spin ordering of adjacent Mn ions mediated by hopping of electrons from Mn^{3+} to Mn^{4+}ions. On the basis of the electron hopping amplitude, which is also called as bandwidth, doped manganites are again classified as large bandwidth, intermediate bandwidth and lower bandwidth manganites.

1.8. Lanthanum Manganites

Lanthanum manganite is the first member of the manganite series and are being extensively investigated ever since the discovery of CMR effect in them. Lanthanum manganites and its derivatives, $La_{1-x}A_xMnO_3$ with A ions of Sr^{2+}, Ca^{2+} are found to be exhibiting interesting properties such as magnetoresistance, ferro/antiferro magnetic ordering, magnetic entropy change, near room temperature metal - insulator transition, high magnetic transition temperature and these properties are tunable by the type of substituting element, their valency, ionic radii and concentration. Thus these are exciting materials from fundamental and application point of view [19,27,42].

Catalytic activity of manganites, particularly, lanthanum manganites (LMO) is utilized in the oxidation of CO and hydrocarbons [55,56]. Different valence ion substitution at La or Mn sites (called doped LMO) lead to cation or anion vacancies providing enhanced mobility and reactivity of oxygen ions essential for the catalytic activity [57]. Another major area dominated by doped LMO are in solid oxide fuel cells (SOFCs) where they serve as cathode materials similar to yttria stabilized zirconia (YSZ) electrolytes due to their excellent electronic and ionic conductivity, thermal, mechanical and chemical stability [58,59]. These materials also find applications in a wide area ranging from magneto-resistive random access memory (MRAM), magnetic tunnel junctions (MTJs), data storage, read - write heads to bolometric sensors [19,60].

1.9. Magnetoelectrics and Multiferroics

Magnetoelectrics as well as multiferroics are one of the most interesting and challenging field of contemporary research as these materials possess immediate applications in the area of switching devices, sensors and spintronics. Multiferroics refer to materials possessing two or more ferroic orders of polarization such as ferroelectricity, ferromagnetism or ferroelasticity. Generally a material exhibiting ferroelectric and ferromagnetic property in a specific temperature range is a multiferroic material while those materials in which these two properties can be coupled forms a magnetoelectric multiferroic material [61,62]. A magnetoelectric material has huge potential in storage devices as switchable memory devices where a magnetic field can influence the electric polarization and electric field could change magnetization behaviour. Single-phase materials in which ferromagnetism and ferroelectricity arise independently also exist, but are rare. As the new century unfolds, the study of materials possessing coupled magnetic and electrical order parameters has been revisited [63,64]. A schematic diagram showing correlation between electrically and magnetically ordered systems is shown n figure 1.4.

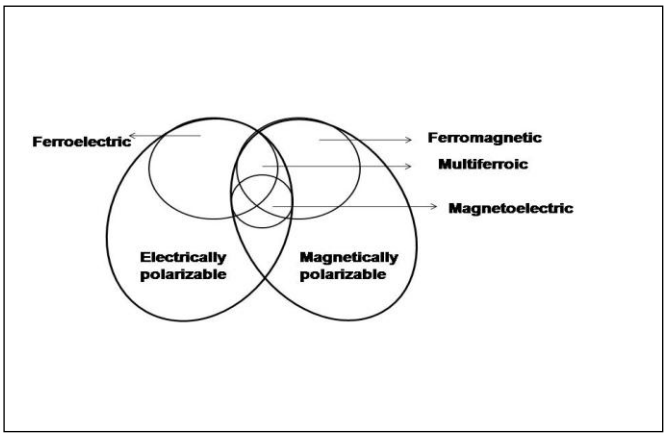

Figure 1.4: Schematic diagram showing correlation between electrical and magnetic properties [64]

An article titled" "Why are there so few multiferroics" authored by N. A Hill et al. in 2000 [62] clearly states the reason for the mutually exclusive nature for polarization phenomenon in electricity and magnetism. Ferromagnets are basically metals while ferroelectrics are insulators. Thus in ferromagnets there will be d electrons while no free electrons in d orbitals are found in ferroelectrics which imply that for a single phase multiferroic material there is discrepancy between d^0ness and d ness. Also only 13 point groups exist which allow materials with both these properties. Search for a single phase multiferroic material did not succeed and thus composite materials or materials with ionic substitutions were considered. One such ferroelectric ferromagnetic material discovered was nickel iodine boracite, $Ni_3B_7O_{13}I$ followed by a lot of investigations in mixed perovskites. The first synthetic ferromagnetic ferroelectric from a perovskite was (1 - *x*)Pb $(Fe_{2/3}W_{1/3})$ O_3 - *x*Pb$(Mg_{1/2}W_{1/2})O_3$, where Mg and W ions are diamagnetic causing

ferroelectricity, and d^5 Fe^{3+} ion is responsible for the magnetic ordering. A lot of perovskites were utilized for developing such magnetoelectric systems giving rise to a new branch of materials called multiferroic perovskites [65-69]. Schematic of a multiferroic is indicated in figure 1.5.

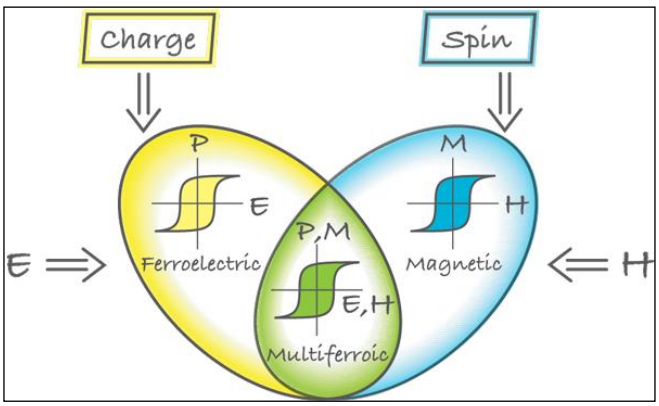

Figure 1.5: Schematic diagram of a typical multiferroic [61]

A strong coupling between spin magnetic moments and lattice structure observed in $La_{0.83}Sr_{0.17}MnO_3$ [70] is evident from magnetically induced structural phase transitions. In $Nd_{0.5}Sr_{0.5}MnO_3$, an external magnetic field can induce electronic metal insulator transition pointing towards strong correlation between electronic charge carriers and magnetic spin moments [65]. Most of the rare earth manganites crystallize in perovskite phase with antiferromagnetic ordering between adjacent Mn^{3+} ions caused by superexchange mechanism. From these observations it was made clear that although combination of ferroelectricity and ferromagnetism is rare, coupling between electric and magnetic order parameters is not rare or not an unattainable task [71-73].

1.10. Magnetocaloric Effect

Magnetic refrigeration based on magnetocaloric effect (MCE) is a promising cooling technology preferred over conventional thermomechanical cooling owing to its eco friendliness. Refrigeration mechanism based on adiabatic demagnetization was first proposed by Debye and Giaque in early 1920's . First experimental demonstration was carried out in 1933 by Nobel Laureate William F. Giaque and D.P. Macdoughgall. A near room temperature magnetic refrigerator was demonstrated by Karl A. Gscheidner in 1997[74-76] .

Currently pursued as most effective, easily accessible and highly economical cooling technology, magnetic refrigeration is solely attributed to magnetic materials and derives its strength from the coupling of magnetic domains with material lattice. An ideal magnetocaloric material operating at room temperature exhibits an appreciable change in magnetic entropy near room temperature and can effectively contribute to lowering the energy consumption upto a level of 20-30 percent. Change in magnetic entropy of a material with respect to magnetic field variations forms the basis of Magnetocaloric effect (MCE). It is perceived that change in entropy under adiabatic conditions can induce an equal but opposite change in the entropy of lattice which in turn is manifested as change in temperature of the material [74,75]. Figure 1.6 explains the mechanism of MCE where on applying magnetic field, magnetic diploes are oriented increasing the lattice entropy which gets dissipated as heat. By adiabatic demagnetization, the reverse is true in that lattice entropy is higher at the expense of magnetic entropy. This cycle gets repeated and

such a type of magnetic cooling can be effectively utilized for refrigeration. Materials exhibiting a large entropy change at low magnetic field with transition temperatures close to room temperature are considered as promising materials for magnetic refrigeration. Detailed theory of MCE will be discussed in chapter 2.

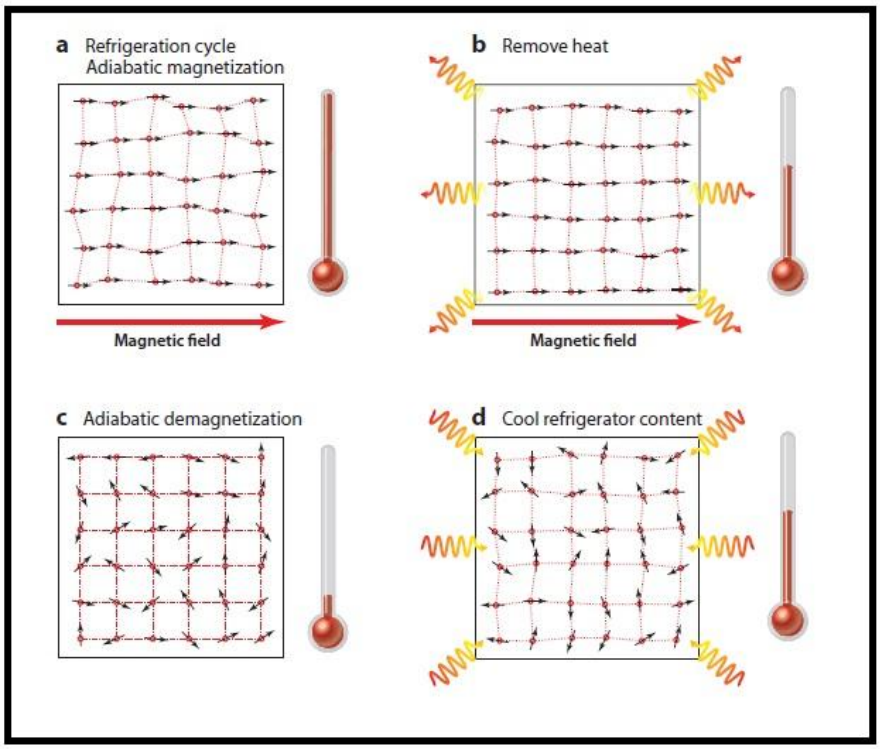

Figure 1.6: Mechanism of MCE [74]

Late 90's saw a spurt in the research activities on MCE materials, notable were on n Gd and Yb based alloys, gadolinium germanium silicides an La(Fe,Si) alloys. Giant magnetocaloric effect (GMCE) with an adiabatic temperature change (ΔT_{ad}, or $|\Delta T_{ad}|$) of 15 K and magnetic entropy change ($\Delta S_{M,}$ or $|\Delta S_M|$) of 18.5 $J.Kg^{-1}K^{-1}$ have been

observed in $Gd_5Ge_2Si_2$ at 276 K for a magnetic field of 5 T [76,77]. These silicides are prototype materials for magnetic refrigeration and various elemental substitutions like Cu, Ga, Mn and Nb for Ge and Si has led to varied entropy and adiabatic temperature changes [78]. Later GMCE have been reported in $LaFe_{11.4}Si_{1.6}$ at 210 K with a $|\Delta S_M|$ of 20 $J.kg^{-1} K^{-1}$ at a magnetic field of 5 T comparable to Gd compounds [79]. In parallel, materials like hydrogen-added YFe_2 [$YFe_2(H_{1-y}D_y)_{4.2}$] with AB_2 stoichiometry have also been studied which exhibited a $|\Delta S_M|$ of 10 $J.kg^{-1} K^{-1}$ and similar compounds like Ho_2Co and HoCoSi also reported entropy values of 11 and 30 $J.kg^{-1} K^{-1}$ respectively at 5 T in the low temperature range below 130 K [80-82]. Superparamagnetic ferrites are also being investigated since the blocking temperature (T_B) can modulate the entropy change [83]. Other materials of interest in the area of MCE are MnAs, MnFe compounds, heusler alloys, intermetallics with rare earth metals and ferromagnetic lanthanum manganites [84,74]. Some of the prominent MCE materials are indexed in figure 1.7.

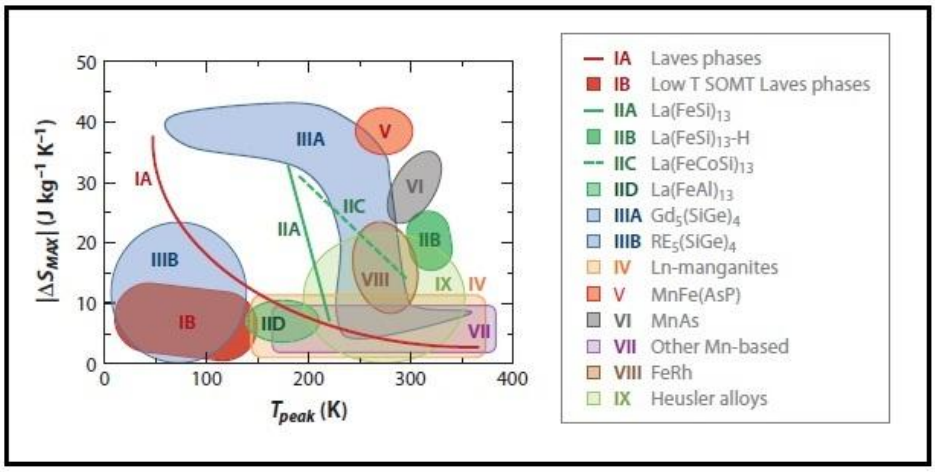

Figure 1.7: Magnetocaloric materials [74]

Lanthanum manganites with ABO_3 structure and its derivatives have secured a prominent position in the MCE phenomenon as they possess high magnetic moments. Ferromagnetic (FM) to paramagnetic (PM) transition at high temperatures often coupled with metal-insulator transition in doped manganites directed the focus towards magnetic entropy studies [84, 85]. ΔS_M of 1 $J.Kg^{-1}K^{-1}$ $La_{0.67}Ca_{0.33}MnO_3$ and 2 $J.Kg^{-1}K^{-1}$ was observed in $La_{0.67}Ca_{0.33}MnO_3$ and $La_{0.87}Sr_{0.13}MnO_3$ respectively under a magnetic field of 10 KOe [86,87]. Highest ΔS_M of 8 $J.Kg^{-1}K^{-1}$ around 250 K was found in $La_{0.7}Ca_{0.3}MnO_3$ under 2 T magnetic field [88]. Recently a ΔS_M of 5.15 $J.kg^{-1}K^{-1}$ corresponding to a magnetic field of 5 T was reported for $La_{0.67}Sr_{0.33}MnO_3$ at 370 K [89]. Efforts are on to effectively utilize the tunability of magnetic properties of doped manganites in MCE for developing manganites with high entropy values near room temperature. A possible concern in manganites is that their specific heat is higher and hence adiabatic temperature variation is smaller, but higher Curie temperature well above room temperatures can be of help as the adiabatic temperature change is proportional to temperature [89]. The advancements made in materials has led to the development of a prototype room temperature refrigeration system based on Gd and is currently on display at the Ames laboratory, USA [77].

1.11. Manganites : Bulk to Nano

Nanotechnology is the science of the new era which is advancing forward at a tremendous speed replacing the existing devices

and technology. Nanotechnology stands for engineering at atomic precision. Various materials with dimensions in the order of one billionth of a meter come under the nano category. Properties of materials are highly dependent on size, shape, dimensions and altering such parameters keeping the chemical composition intact have awakened entire scenario of interdisciplinary sciences [90,91]. It is well said by Sir Eigi Kobayashi that "Those who control materials control technology." Early roots for nanotechnology and nanoscience were from supreme visions of the scientist, Dr. Richard Feynman who gave a lecture entitled "There's Plenty of Room at the Bottom" about 55 years ago at a meeting of the American Physical Society. Concept of nanotechnology was not known at that time and the credit for first using the word 'Nanotechnology' goes to N. Taniguchi in 1974 to refer the precise tolerance requirements for designing and machining materials. A string of discoveries like Scanning Tunneling Microscopy (STM), Atomic Force Microscopy (AFM), Magnetic Force Microscopy (MFM), single walled and multi walled carbon nanotubes, graphene, lithography and phenomena of magnetic hyperthermia using nanoparticles helped in the incredible growth of nanotechnology as a broad interdisciplinary field [92,93].

In the macro scale, material properties like stiffness, magnetism, electrical conductivity all depend on interior atoms since surface atoms are minuscule. But surface atoms are relevant in adhesion or in ejection of electrons like plasma displays. It can be presumed that atoms on the surface and in the interior behave differently. In nano scale, surface atoms are higher than bulk with a larger surface to volume ratio and a combined influence of both surface and interior atoms can result in new exciting properties. It has been revealed that nanoparticles have

different chemical, electrical, optical, mechanical, thermal and magnetic properties than the bulk [91-93].

Advances in nanoscience and nanotechnology have their implications in manganites also. The co-existing metallic and insulating nature of manganites has been thought of being extended to micrometre and nanometre scales. In such nano or micro manganite thin film structures, metallic or insulating phases co-exist for particular length scales for a particular composition. Such electronic inhomogeneities within the same sample is an attractive feature since it leads to fabricate nanostructures which are spatially self organized and having diverse functionalities. Giant magnetoresistance, re-entrant M-I transitions, charge ordering, ferro/antiferro magnetic ordering, size dependent exchange bias effects, spin glass states are some recent features observed in manganite nanostructures and thin films. Nanostructures of manganites like nanorods, nanotubes and nanowires have also been developed since they possess excellent magnetotransport and electrical properties. In parallel, several methods like hydrothermal, solgel, electrospinning, lithography, template process have come to existence for the preparation of nanomaterilas. There has been reports of synthesis technique being a crucial in deciding the material properties, for instance $La_{0.7}Sr_{0.3}MnO_3$ synthesized by various routes exhibited different properties. Manganites are already known to be having diverse properties and reduced dimensionality further opens up much newer and interesting features useful for the future technology [18].

1.12. Motivation of the Present Study

Rare earth manganites are extensively investigated as they exhibit interesting phenomena such as magnetoresistance, near room temperature metal-insulator and magnetic transitions. Lanthanum manganites belong to these class of materials and have gained immense importance ever since the discovery of Colossal Magneto-resistance. These materials belong to the family of strong electron correlated systems with close coupling between lattice, electron spin and charge transport. Extensive studies are on to understand the diverse properties exhibited by them. Lanthanum manganite (LMO) is an antiferromagnetic insulator or also called a mott insulator. In the doped compositions of LMO, magnetic ordering has been found to be of different kinds such as spin canted antiferromagnetic, ferromagnetic or a combination of two orders. The reason for the exhibition of a variety of magnetic behaviour can be attributed to the fact that magnetism in LMO is highly dependent on small variations in the La, Mn sites, Mn^{4+}/ Mn^{3+} ion ratio and oxygen content [27, 94].

In the area of doped manganites, divalent substitutions at La sites (Ca, Sr, Ba, Pb) have been investigated earlier and reported in various research papers [27]. Fewer studies have focussed on the monovalent substitution for La ions. Monovalent substitutions can result in the conversion of Mn^{3+} ions to Mn^{4+} conducive for magnetic ordering and the conversion rate is twice that of divalent substitutions. Since monovalent ions (K^+, Na^+) have higher ionic radii than La^{3+} ions, their substitution can increase the effective ionic radii at La sites leading to crystallographic distortion manifested as an increase in Mn-O-Mn bond

angle. Double exchange interaction between Mn^{3+} and Mn^{4+} ions with increased bond angles (or shorter Mn-O) favours ferromagnetism with a higher Curie temperature (Tc) [94,95]. Thus monovalent substituted lanthanum mangnaites warrants a thorough investigation.

An extensive survey of literature also reveals that reports on heavily (monovalent) substituted lanthanum manganites are scarce. Monovalent ions like sodium can be substituted for La sites and such substitution multiplies the amount of charge carriers than that from divalent substitutions. Such an increase in charge carriers influences the structural, magnetic, electrical and thermal properties. Doped lanthanum manganites with sodium concentrations from 50 to 90 percent in steps of 10 will be the subject of our interest. Sodium being volatile, an effective synthesis procedure is required for maintaining the sroichiometry in the resulting compound. A modified citrate gel method will be chosen for the synthesis of these materials. A unique feature of manganites is that oxygen stoichiometry, and vacancies also affect the magnetic properties of manganites. Thus a complete investigation on the structural and magnetic properties of heavily doped manganites with sodium is worthwhile. However, substitutuion of Na for La can result in non stoichiometry and also create vacancies and hence the exact determination of the amount of Na,La, O and their valence states is all the more important. This will be yet another motive of the present investigation. The compositional analysis will be carried out by using X-ray Photoelectron Spectroscopy (XPS). XPS results will be correlated with the magnetic properties.

Hence, in the first phase of this investigation, the focus will be on the synthesis and properties of compositions with heavily

substituted Na ions. The evaluation of their magnetic properties and correlation with composition visa vis Mn^{3+}/Mn^{4+} ratio also forms a major part of the first phase of investigation. These samples will be subjected to magnetization measurements in order to determine the nature of magnetization. These compositions are expected to have large magnetizations (saturation magnetization) with near room temperature ordering. Thus Na substituted $LaMnO_3$ are potential materials for magnetic refrigeration. So evaluation of entopy change and adiabatic temperature change by plotting M-H isotherms of these compositions is another objective of the present investigation.

The magnetic entropy change stems from Maxwell's thermodynamic relations and entropy change can be evaluated from magnetic isotherms. Thus in the next phase of the study on bulk materials, magnetic entropy change of the sodium substituted LMO system and the variation of entropy with temperature and concentration of sodium will be carried out. Magnetic entropy change can then be utilized to determine the adiabatic temperature change which is a thermodynamical parameter in deciding the efficiency of a magnetocaloric material. Heat capacity measurements will also be performed on doped manganite system rather than relying on the literature values which could provide credence to the evaluated magnetocaloric parameters.

Thin film forms of these compositions are essential for further studies inorder to explore the possibility of fabricating devices based on these materials. Thin films are to be deposited on suitable substrates by choosing an appropriate deposition technique. It is known that pulsed laser deposition technique can produce quality thin films without compromising on the stoichiometry. These films are to be

characterized inorder to evaluate their structural, magnetic and magnetocaloric parameters. So preparation and characterization of thin film samples of LNMO series on Si substrates forms part of this investigation. Magnetocaloric parameters namely magnetic entropy change (ΔS_M), adiabatic temperature change (ΔT_{ad}) and relative cooling power (RCP) will also be evaluated and compared with that of their bulk values.

Magnetoelectric (ME) response is an in thing in the area of multiferroics. and materials exhibiting this phenomena can be employed to fabricate multifunctional devices. Such ME coupled devices could be ideal for storage with four states. The advantages of such memory devices are that electric polarization can be varied by magnetic field and vice versa. [72,97,98]. Thus manganites could serve as the ferromagnetic part in developing a ferroelectric-ferromagnetic (FE-FM) heterostructures. A proper choice of the substrate and the ferroelectric component could lead to development of field effect devices. We have converged on a substrate which is both ferreoelectric, piezoelectric and an ideal choice for such substrate is PMN PT. Thin films of sodium substituted lanthanum manganites deposited on ferroelectric substrates were also fabricated which mimics a field effect device. Initially, physical properties of such heterostructures need to be investigated to gauge magnetoelectric coupling. Thus the present thesis focuses on the physical properties of FE-FM heterostructures arising from the coupling between magnetic and electrical behaviour. A heterostructure consisting of FM and FE will serve as an ideal device for such applications. Substrtaes of PMN PT are available which are ferroelectric as well as piezoelectric. It will be our endeavour to deposit films of different thicknesses on PMN PT substrates

and evaluate their various properties. For this, PLD technique will be employed. Their magnetic and ferroelectric hysteresis loops will be traced to evaluate various parameters like coercivity, remenance and saturation magnetization or saturation polarization. Finally, a field effect device will be demonstrated with a FE/FM heterostructure. Recently it has been observed that strain effects of the substrate can also influence the magnetic ordering in thin films of manganites [96]. Recent reports based on theoretical calculations conducted on MoS2thin films and graphene also points to the possibility of achieving magnetization by strain [99, 100]. Hence it was through fit to investigate such phenomena on FE/FM heterostructures with PMN PT as the substrate for different thicknesses. This also will be probed during the course of this investigation. Thin films deposited on different substrates for different thickness could lead to study of substrate influence on the magnetic properties of such heterostructures.

Thus the main objectives of present investigation are as follows:

- ✓ Synthesis of bulk samples belonging to sodium substituted lanthanum manganite series, $La_{1-x}Na_xMnO_3$ (x= 0.5 to 0.9)
- ✓ Study the effect of sodium substitution on crystal structure, lattice parameters, magnetization and transition temperatures

- ✓ Evaluation of magnetic entropy change with temperature and Na concentration for the series $La_{1-x}Na_xMnO_3$ (x= 0.5 to 0.9)
- ✓ Determination of the amount of Mn^{4+} and Mn^{3} ions and ascertaining the role of Mn^{4+}/Mn^{3+} ratio in the magnetism exhibited by these compounds
- ✓ Deposition of Thin films of sodium substituted lanthanum manganite using pulsed laser deposition on silicon substrate
- ✓ Investigate the magnetic properties and magnetocaloric effect for different compositions
- ✓ Demonstrating a magnetoelectric field effect device using thin films deposited on a piezoelectric substrate of PMN PT
- ✓ Investigate the variation of strain on the magnetic properties of LNMO coated on PMN PT substrate
- ✓ Correlation of results

References

[1] William D. Callister Jr., Materials Science and Engineering – An Introduction,Sixth edition, John Wiley and Sons Inc., U.K (2009).

[2] James F. Shackelford, Madanapalli K. Muralidhara, Introduction to Materials Science for Engineers, Dorling Kindersley (India) Pvt. Ltd (2009).

[3] Yip-Wah Chung, Introduction to Materials Science and Engineering, CRC press, Taylor & Francis group, Florida (2007).

[4] S. L. Kakani, Amit Kakani, Material Science, New age international (P) Ltd, New Delhi, India (2004).

[5] N. A. Spaldin, Magnetic Materials: Fundamentals and Applications, 2nd ed., Cambridge University Press, New York (2011).

[6] R. E. Hummel, Electronic Properties of Materials, 3rd ed.,Springer, USA (2009).

[7] B. D.Cullity and C. D. Graham, Introduction to Magnetic Materials, 2nd ed., John Wiley and Sons, New Jersey (2009).

[8] J. S. Blakemore, Solid State Physics, 2nd ed., Cambridge University press, U. K (1985).

[9] Charles Kittel, Introduction to Solid State Physics, 7th ed.(reprint), Wiley India (P) Ltd., New Delhi, India (2008).

[10] Gabriel Kotliar and Dieter Vollhardt, Physics Today, 53-59, (2004).

[11] E. Dagotto, Science, **309**, 257 (2005).

[12] Y. Tokura, Rep. Prog. Phys. **69**, 797 (2006).

[13] J. Zaanen, G. A. Sawatzky, J. W. Allen Physical Review Letters **55**, 418–421(1985).

[14] J. M. Tomczak, S. Biermann, Physica Status Solidi (b), **246**, 1996–

2005 (2009).

[15] L. G. Tejuca, J. L. G. Fierro, Properties and applications of perovskite-type oxides, Marcel, Dekker Inc., New York (1993).

[16] A.S.Bhalla, R. Guo and R.Ro, Mat. Res. Innovat., **4**, 3-26 (2000).

[17] Y Tokura, Rep. Prog. Phys. **69,** 797 (2006).

[18] Anant V. Narlikar, Frontiers in Magnetic materials, Springer, Germany (2005).

[19] Lev P. Gor'kov, Vladimir Z. Kresin, Physics Reports, **400**,149–208 (2004).

[20] A. M. Shuvaev, A. A. Mukhin and A. Pimenov, J. Phys.: Condens. Matter, **23,** 113201 (2011).

[21] Phan M-H., Yu S.C., J. Magn. Magn. Mater., **308**, 325 (2007).

[22] P. Raychaudhuri, T. K. Nath, P. Sinha, C. Mitra, A. K. Nigam, S. K. Dhar and R. Pinto, J. Phys.: Condens. Matter, **9,** 10919–10927 (1997).

[23] L. M. Wang, Jian-Hong Lai, Jyh-Iuan Wu, Y.-K. Kuo, C. L. Chang, J. Appl. Phys., **102**, 023915 (2007).

[24] C. N. R. Rao, A. K. Kundu, M. M. Seikh, and L. Sudheendra, Dalton Transactions pp., 3003-3011 (2004).

[25] M. Imada, A. Fujimori, and Y. Tokura, Rev. Mod. Phys.,**70**, 1039 (1998).

[26] J. C. Loudan, N. D. Mathur, and P. A. Midgley, Nature **420**, 797 (2002).

[27] Myron B. Salamon, Marcelo Jaime, Revs. of Mod.Phys **73**,(2001).

[28] Goodenough, J. B., Phys. Rev. **100**, 564(1955).

[29] Anderson, P., and H. Hasegawa, Phys. Rev. **100**, 675 (1955).

[30] Jonker, G., and J. van Santen, Physica, **16**, 337-349 (1950).

[31] Jonker, G., Santen, J., Physica **19** 120-130 (1953).

[32] Volger, J., Physica (Amsterdam) **20**, 49 (1954).

[33] Wollan, E., and K. Koehler, Phys. Rev. **100**, 545 (1955).

[34] Morrish, A., B. Evans, J. Eaton, and L. Leung, Can. J. Phys. **47**, 2691(1969).

[35] Searle, C., and S. Wang, Can. J. Phys. **47**, 2703 (1969).

[36] Tanaka, J., M. Umehara, S. Tamura, M. Tsukioka, and S. Ehara, J. Phys. Soc. Jpn., **51**, 1236 (1982).

[37] Louca, D., and T. Egami, Phys. Rev. B, **59**, 6193 (1999).

[38] Louca, D., T. Egami, E. Brosha, H. Ro¨ der, and A. Bishop, Phys. Rev. B **56**, R8475 (1997).

[39] Kasuya, T., A. Yanase, and T. Takeda, Solid State Commun.**8**, 1543 (1970).

[40] Holstein, T., Ann. Phys., **8**, 343 (1959).

[41] Reinen, D., Solid State Chem. **27**, 71 (1979).

[42] J. M. D. Coey, M. Viret, Adv.Phys., **48**, 2, 167-293(1999).

[43] E.Pollert, S. Krupicka, and E. Kuzmicova, J. Phys. Chem. Solids **43**,12, 1137-1145(1982).

[44] R.Von Helmholt, J.Wecker, B.Holzapfel, L.Schultz, , and K.Samwer, Phys. Rev. Lett.,**71**,14 (1993).

[45] S. Pignard, H. Vincent, J.P. Senateur, J. Pierre, J. Magn. Magn. Mater. 177–181, 1227(1998).

[46] A. Gupta, T.R. Mcguire, P.R. Duncombe, M. Rupp, J.Z. Sun, W.J. Gallagher, G. Xiao, Appl. Phys. Lett. **67**, 3494(1995).

[47] Y. Morimoto, A. Asamitsu, H. Kuwahara, and Y. Tokura, Nature, **380**, 141 (1996).

[48] R. Seshadri, C. Martin, M. Hervieu, B. Raveau, and C. N. R. Rao,

Chem. Mater. **9,** 270 (1997).

[49] Pengcheng Dai, J. A. Fernandez-Baca, E. W. Plummer, Y. Tomioka, and Y. Tokura, Phys. Rev. B **64**, 224429 (2001).

[50] H. Asano, J. Hayakawa, and M. Matsui, Appl. Phys. Lett. **68,** 3638 (1996).

[51] Mira J., Rivas J., Hueso L.E., Rivadulla F. and Lopez-Quintela M.A. ´ J. Appl. Phys.,**91**, 8903 (2002).

[52] C. Martin, A. Maignan, F. Damay, M. Hervieu, B. Raveau, J. Solid. State.Chem. **134**, 1, 198‑202 (1997).

[53] K. Chahara, T. Ohno, M. Kasai, Y. Kosono, Appl. Phys. Lett. **63**, 1990 (1993).

[54] M. Uehara, S. Mori, C.H. Chen and S.W. Cheong, Nature 399, 560 (1999).

[55] H. Arai, M. Machida, Catal. Today, **10**, 1, 81–94 (1991).

[56**]** V.A. Sadykov, L. A. Isupova, S.F. Tikhov, O.N. Kimkhai: Mat. Res. Soc. Symp. Ser., **386**, 293 (1995).

[57] San Ping Jiang, J. Mater. Sci, **43**,6799–6833(2008).

[58] Minh N Q, J. Am. Ceram. Soc., **76**, 563- 588 (1993).

[59] B. C. H. Steele and A. Heinzel, Nature, **414,** 6861, 345-352 (2001).

[60] Tao Zou, Fen Wang, Yi Liu, Li-Qin Yan and Young Sun, Appl. Phys. Lett. **97**, 092501 (2010).

[61] Daniel Khomskii , Physics, **2**, 20 (2009).

[62] N.A. Hill, J. Phys. Chem. B, **104**, 6694 (2000).

[63] Jing Ma , Jiamian Hu , Zheng Li , and Ce-Wen Nan Adv. Mater., **20**, 1–26 (2011).

[64] W. Eerenstein, N. D. Mathur & J. F. Scott , Nature, **2** ,442, 17(2006).

[65] H. Kuwahara, Y. Tomioka , A. Asamitsu, Y. Moritomo and Y.

Tokura, Science **270**, 961(1995).

[66] G. Q. Zhang, S. J. Luo, S. Dong, Y. J. Gao,1K. F. Wang,and J.-M. Liu, J. Appl. Phys, **109**, 07D901 (2011).

[67] T. Atou et.al, J. Sol.stat. chem. **145**, 639 (1999).

[68] H. Yamada, Y. Ogawa, Y. Ishii, H. Sato, M. Kawasaki, H. Akoh, and Y. Tokura, Science, **305**, 646 (2004).

[69] W. G. Yin, D. Volja, and W. Ku, Phys. Rev. **96**, 116405 (2006).

[70] A. Asamitsu, Y. Moritomo, Y. Tomioka, L. Arima and Y. Tokura, Nature, **373**, 407 (1995).

[71] T. Kimura et al., Nature **426**, 55 (2003).

[72] N. Hur et al., Nature **429**, 392 (2004).

[73] G. Srinivasan**,** Annu. Rev. Mater. Res., **40**, 153-178 (2010).

[74] V. Franco, J. S. Blazquez, B. Ingale, and A. Conde, Annu. Rev. Mater.Res. **42**, 305–342 (2012).

[75] S. Das and T. K. Dey, J. Phys.: Condens. Matter **18**, 7629–7641 (2006).

[76] H. Zeng, C. Kuang, J. Zhang, and M. Yue, Bull. Mater. Sci., **34** (4), 825–828 (2011).

[77] V. K. Pecharsky and K. A. Gschneidner, Jr., Phys. Rev. Lett. **78**, 4494 (1997).

[78] R. D. Shull, V. Provenzano, A. J. Shapiro, A. Fu, M. W. Lufaso, J. Karapetrova, G. Kletetschka, and V. Mikula, J. Appl. Phys. **99**, 08K908 (2006).

[79] F.-x. Hu, B.-g. Shen, J.-r. Sun, Z.-h. Cheng, G.-h. Rao and X.-X. Zhang, Appl. Phys. Lett. 78 ,23, 3675–3677 (2001).

[80] J. Chen, B. G. Shen, Q. Y. Dong, F. X. Hu, and J. R. Sun, Appl. Phys. Lett. **96**, 152501 (2010).

[81] Q. Zhang, J. H. Cho, B. Li, W. J. Hu, and Z. D. Zhang, Appl. Phys. Lett.,**94**, 182501 (2009).

[82] V. Paul-Boncour and T. Mazet, J. Appl. Phys. ,**105**, 013914 (2009).

[83] P. Poddar, J. Gass, D. J. Rebar, S. Srinath, H. Srikanth, S. A. Morrison and E. E. Carpenter, J. Magn. Magn. Mater., **307**, 227–231 (2006).

[84] M.-H. Phan and S.-C. Yu, J. Magn. Magn. Mater. **308**, 325–340 (2007).

[85] K. A. Gschneidner, Jr. and V. K. Pecharsky, Annu. Rev. Mater. Sci. **30**, 387–429 (2000).

[86] X. X. Zhang, J. Tejada, Y. Xin, G. F. Sun, K. W. Wong, and X. Bohigas, Appl. Phys. Lett. **69**, 3596 (1996).

[87] A. Szewczyk, H. Szymczak, A. Wisniewski, K. Piotrowski, R. Kartaszyn-ski, B. Dabrowski, S. Kolesnik, and Z. Bukowski, Appl. Phys. Lett. **77**, 1026(2000).

[88] R. Szymczak, R. Kolano, A. Kolano-Burian, V. P. Dyakonova, and H. Szymczak, Acta Phys. Pol. A, **117**, 203 (2010).

[89] A. Rostamnejadi, M. Venkatesan, P. Kameli, H. Salamati, and J. M. D.Coey, J. Magn. Magn. Mater. **323**, 2214–2218 (2011).

[90] Jeremy J. Ramsden, Nanotechnology An Introduction, Elsevier (2011).

[91] Charles P. Poole. Jr., Frank J. Owens, An introduction to Nanotechnology, John Wiley & sons Inc., New Jersey (2003).

[92] Daniel L. Schodek, Paulo Ferreira, Michael F. Ashby, Nanomaterials, Nanotechnologies and Design: An Introduction for Engineers, Butterworth Heinemann, U.K (2009).

[93] Chris Binns, Introduction to Nanoscience and Nanotechnology, John

Wiley & sons Inc., New Jersey (2010).

[94] Roy S, Guo Y Q, Venkatesh S and Ali N, J. Phys.: Condens. Matter **13**, 9547(2001).

[95].A. Das, M. Sahana, M.S. Hegde et al, Materials Research Bulletin **35**, 651–659(2000).

[96] R.V. Chopdekar, J. Heidler, C. Piamonteze1, Y. Takamura, A. Scholl, S. Rusponi, H. Brune, L.J. Heyderman, and F. Nolting, Eur. Phys. J. B, **86**, 241(2013).

[97] G. Srinivasan, Annu. Rev. Mater. Res.,**40**,153–78(2010).

[98] V.L. Mathe, A.D.Sheikh, G.Srinivasan, J. Mag Mag Mat, **324,** 695–703 (2012).

[99] Peng Tao, Huaihong Guo, Teng Yang, and Zhidong Zhang, J. Appl. Phys., 115, 054305 (2014).

[100] M. M. Ugeda, I. Brihuega, F. Guinea, and J. M. Gomez-Rodrıguez, Phys. Rev. Lett. 104, 096804 (2010).

CHAPTER 2

THEORY

This chapter describes in detail some basic properties of manganites like crystal field effect, Jahn Teller distortion and double exchange/super exchange interactions associated with spin dependent electron transport mechanism. A brief overview of magnetoresistance and spin valves is also provided in this chapter. Significance of monovalent doping in manganites, half metallicity, and theory of magnetoelectric effect are other highlights of this chapter. The principle and theory behind the estimation of magnetic entropy change and adiabatic temperature change are also discussed from a first principle angle.

2.1. Properties of Manganites:

2.1.1. Crystal Field Effect

Perovskite structured manganites possess an octahedral arrangement of oxygen ions with Mn ion at the centre of an octahedron. In an Octahedral complex, the chains of O-Mn-O planes can be assumed to be as directed along the three cartesian axes as shown in Figure 2.2. The O^{2-} ions forms the crystal field enclosing the Mn ions. All the 5 d orbitals of Mn ions will no longer have the same energy as in free ion

as the relative energies of the d orbitals are controlled by the repulsive energy of the oxygen anion complex. The d orbitals, d_{xy},d_{xz},d_{yz} (π bonding orbitals) are oriented in between either of the two cartesian axes (i.e, in the empty space between the oxygen atoms) while the $d_{x^2-y^2}$ and d_{z^2} orbitals (σ bonding orbitals) point towards the axes. As a result, $d_{x^2-y^2}$ and d_{z^2} orbitals face large coulomb repulsion from the oxygen anions and hence their energy will be raised compared to the other three d orbitals and it is called crystal field effect or distortion. The π bonding orbitals after the distortion gives rise to the symmetric class t_{2g} and the σ bonding orbitals as e_g . The energy splitting between the two sets of d orbitals is given by the splitting energy term Δ which equals $\frac{5zq}{3a^5}\langle r^4 \rangle$, zq denotes the charge of Oxygen ion , a is Mn- O distance and r is the distance of the electron to the central Mn ion. The magnitude of Δ varies between 1-2eV [1,2].

2.1.2. Jahn Teller Distortion

The Jahn Teller effect occurs in materials where there is partial electronic occupation in t_{2g} or e_g symmetric classes. This Phenomenon was first proposed by Herman Jahn and Edward Teller in 1937 to explain the instability of a non linear system in a degenerate energy state. They argued that a non linear system in a degenerate energy state will spontaneously distort so as to split its energy states and removes its degeneracy. Different valence states of Mn are shown in figure 2.1.

Consider an Mn^{3+} ion. After the field splitting, 3 electrons of Mn^{3+} occupy the t_{2g} set and one electron in the e_g set which make the

Mn^{3+} ion Jahn Teller active. Two e_g orbitals split raising the energy of one at the expense of the other termed as Jahn Teller distortion followed by the distortion of the octahedra along the z axis. The octahedron elongates along the z axes and compresses along the x and y directions. The elongation and compression profoundly affect the energy states of the d orbitals - d_z^2 will be lowered in energy than $d_{x^2-y^2}$ orbital similarly the d_{xz}, d_{yz} orbitals will have lower energy than d_{xy}. There will be two kinds of energy which comes into consideration at this stage- the lattice strain energy due to distortion and the electronic energy. The single electron of the e_g set occupies the d_z^2 level which lowers the electronic energy outweighing the lattice strain energy thereby lowering the energy of the material structure as a whole. The magnitude of the Jahn Teller distortion is determined by the balance between the lattice strain energy and the electronic energy for attaining energy stabilization. This distortion can affect the properties of the material such as the electrical conductivity and magnetism due to the direct influence of lattice distortion on the electronic configuration and the atomic arrangement [1,2].

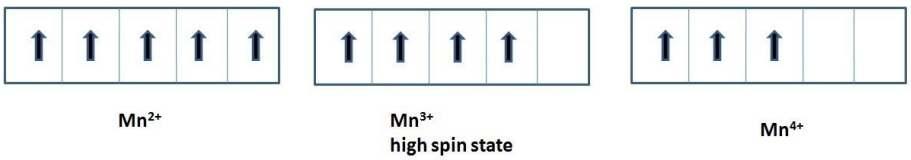

Figure 2.1. d orbital occupancy of different Mn ions

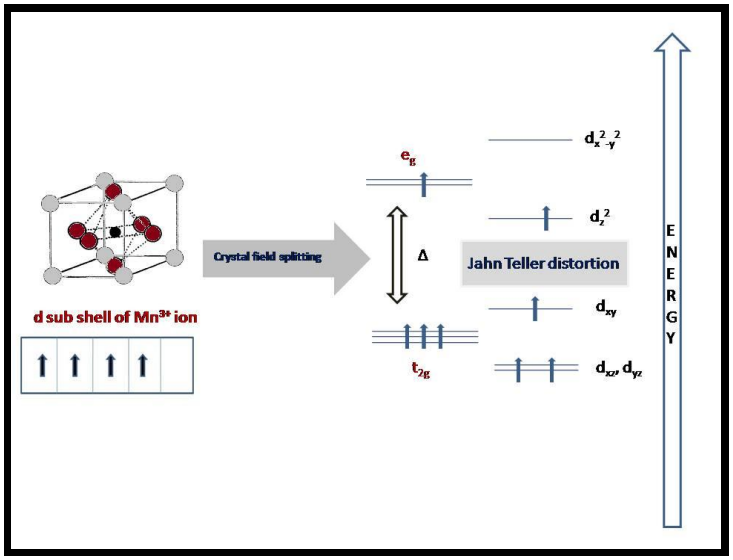

Figure 2.2: Energy levels of d^3Mn ions due to crystal field splitting and Jahn Teller distortion

2.1.3. Double exchange Mechanism

Double exchange mechanism explains the ferromagnetic ordering in mixed valence manganites and was first proposed by Zener. Before the advent of double exchange theory, magnetic interactions between Mn ions in stoichiometric manganites like $LaMnO_3$ were explained based on Mn-O-Mn bonding [3].

When Mn-Mn separation is least, Mn-O bonds are covalent. Since valence electrons of oxygen anion (O^{2-}) are bonded antiparallel, each electron spin couple ferromagnetically via semicovalent bonding with associated Mn ions. This leads to an antiferromagnetic alignment of Mn ions. A second case arises when one Mn-O bond is covalent and counterpart is ionic. In such a case, O^{2-} ion is displaced

towards the Mn ion which is covalently attached to it. Electron spin of O^{2-} couple ferromagnetically to this Mn ion via semicovalent bonding as in the first case. The other electron of O^{2-} participate less in semicovalent bonding and will be coupled antiferromagnetically to the second Mn ion. Thus the net magnetic moment of Mn ions is antiparallel to the O^{2-} moment leading to ferromagnetic alignment between two Mn ions. This explains ferro/antiferro alignments in stoichiometric undoped manganites [3].

When doped manganites were developed, double exchange theory was put forth to explain ferromagnetic ordering. Such a type of magnetic ordering arises from the oxygen mediated coupling of two Mn ions of different valence states. Consider Mn^{3+} and Mn^{4+} ions. There can be two possible configurations having the same energy or the two fold degeneracy in the ground state is given by $\psi 1$ and $\psi 2$.

$$\psi 1: Mn^{3+}\ O^{2-}\ Mn^{4+}$$

$$\psi 2: Mn^{4+}\ O^{2-}\ Mn^{3+}$$

There exist finite probability that an electron which is initially in the d orbital of Mn^{3+} ion is able to transfer to the d orbital of Mn^{4+} ion (converting $\psi 1$ into $\psi 2$) then the degeneracy will be lifted and overall energy of the states will be lowered. An electron transfer from Mn^{3+} to Mn^{4+} occurs as a result of simultaneous double transfer of electron from Mn^{3+} to O^{2-} and then from O^{2-} to Mn^{4+}. Such an electron transfer is possible provided the magnetic moments of the t_{2g} states of two Mn ions are parallel, otherwise Hund's rule would be violated. Hunds rule demands the occupancy of electrons with same spins in the d orbitals of Mn^{3+} and Mn^{4+} ions. A lowered energy state due to double transfer of electrons results in a ferromagnetic ordering between Mn ions and the

mechanism is called double exchange. Spin dependent electron transfer between Mn ions with parallel spin alignment in double-exchange mechanism accounts for both ferromagnetism and metallicity [3-6].

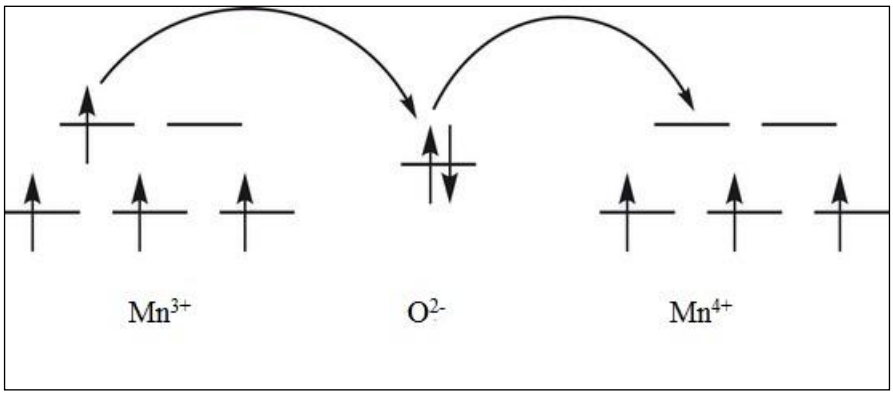

Figure 2.3: Double exchange mechanism between Mn^{3+} and Mn^{4+} ions

Double exchange mechanism between a pair of magnetic ions with general spin directions is governed by the transfer integral't' represented as

$$t = t_0 \cos\left(\Theta/2\right) \qquad 2.1$$

where t_0 is normal transfer integral depending on the spatial wave functions and Θ is the angle between the spin directions of associated Mn ions [4,5].

2.1.4. Super exchange Mechanism

Superexchange mechanism is also an anion mediated indirect exchange mechanism found in transition metal oxides. Super

exchange mechanism in most cases, invokes an antiferromagnetic ordering between same valence states of Mn ions. For two Mn^{2+} ions, it is energetically favorable for the valence electrons on the Mn^{2+} and O^{2-} ions to undergo covalent bonding. The p orbital of O^{2-} ion has filled shell of electrons and for the Mn-O-Mn hybridization to occur, a transfer of electron with a particular spin from the O^{2-} ion onto the Mn^{2+} ion is required followed by the transfer electron of opposite spin to other Mn^{2+} ion. Such a process results in an antiferromagnetic alignment between the Mn^{2+} ions. Figure 2.4 shows the super exchange mechanism between Mn^{2+}-O^{2-}- Mn^{2+} and Mn^{3+}-O^{2-}-Mn^{3+} pairs[1].

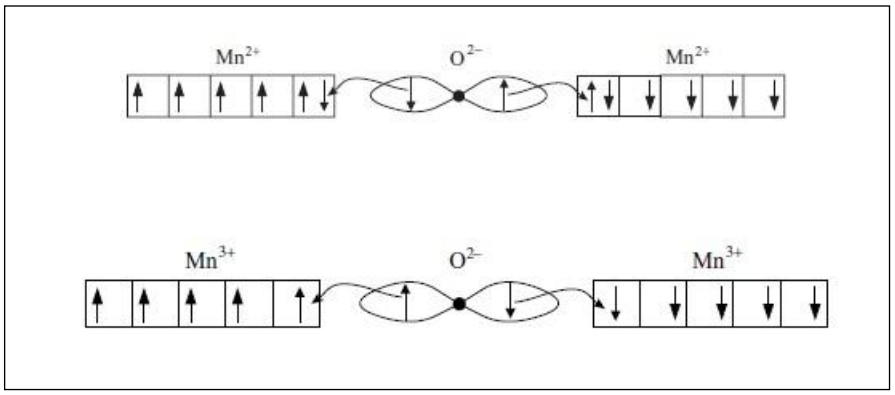

Figure 2.4: Superexchange mechanism between Mn ions [1]

A superexchange mechanism is basically guided by the sign of the exchange integral, J_{ij} in the Heisenberg Hamiltonian which depends on oxygen–metal bond angle and the d electron configuration on the transition metal. It is generally concluded that a 180^0 metal–oxygen–metal angles between identical metal ions with both orbitals either

completely filled or empty lead to antiferromagnetic interactions while of 90^0 angles lead to ferromagnetism.

In super exchange interactions, transfer integral is proportional to cos Θ and magnetic interactions are between orbitally non-degenerate, localized t_{2g} orbitals [3,5].

2.1.5. Colossal Magneto-Resistance (CMR)

Manganites posses the unique property of magnetoresistance which is an appreciable change in resistance of the material upon the application of an external magnetic field. The phenomenon of Colossal magnetoresistance (CMR) was first observed in LaCaMnO films at 77 K as shown in figure 2.5. The term "colossal" applies to very large change in resistance, basically from an insulating to a conducting state, on application of a magnetic field [1,7]. Conventional metals also exhibit magnetorsesisitance but the change in resistance is nearly 5% while in manganites a gigantic decrease in resistance on the application of magnetic field is observed. Spin dependent scattering mechanism of the conduction electrons in metal oxides and suppression of such scattering by magnetic field were the features which led to CMR mechanism.

In CMR materials, decrease in resistivity is of the order of a transition from metal to insulating state which is termed as M-I transition. An additional feature of CMR manganites is that the M-I transition temperature is in the vicinity of magnetic transition from ferromagnetic to paramagnetic state (Curie temperature, T_C). A schematic diagram of two transitions is shown in figure 2.6 [8].

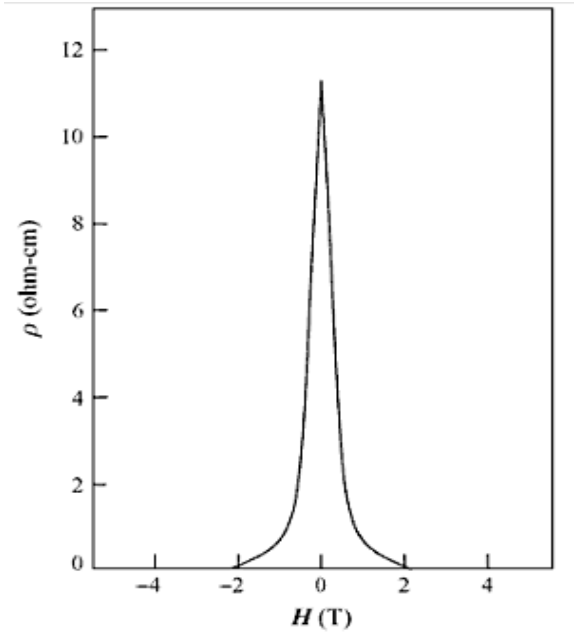

Figure 2.5: Change in resistance with applied magnetic field in La-Ca-Mn-O films at T=77K [1]

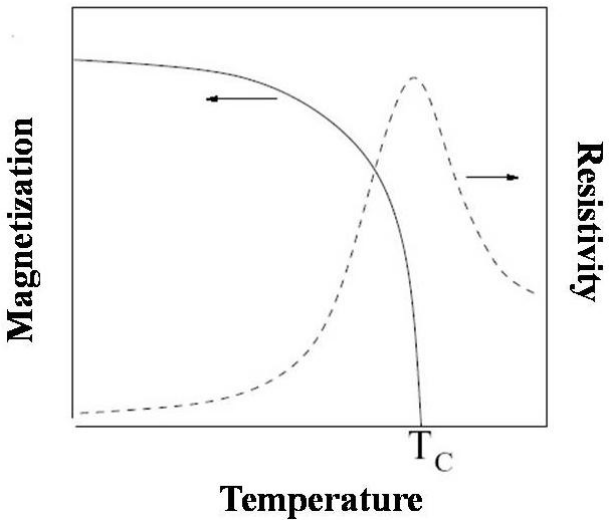

Figure 2.6: M-I transition and T_C

Discovery of CMR led to surge in research in manganites and this resulted in the discovery of Giant magnetoresistance (GMR) in metallic multilayers of Fe/Cr. Nobel Prize in Physics for the year 2007 was awarded to Albert Fert and Peter Grunberg for the discovery of GMR. It has potential application in field sensors, storage devices, and switching devices which is based on two concepts: spin dependent transport and interlayer coupling.

GMR has paved way for the development of spin valves comprising of two magnetic layers with an intermediate non magnetic layer. Thickness of the intermediate layer guides the ferro/ antiferromagnetic alignment of the magnetic layers. In the presence of magnetic field and if the layers are ferromagnetic to each other electrons with compatible spin type of the magnetic layers can travel with less scattering. For an antiferromagnetic alignment, electrons of a particular spin type are strongly scattered by the magnetic layer with opposite spin alignment [1,8]. Thus the same structure functions differently for two types of spin alignment and it forms the heart of a spin valve based on GMR. A typical spin valve is shown in figure 2.7.

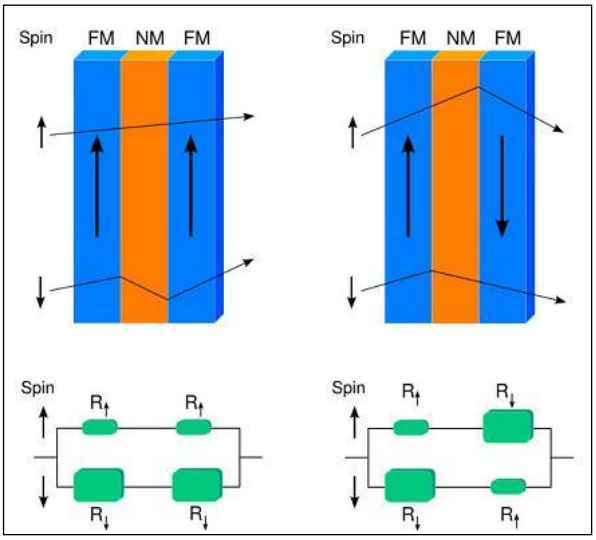

Figure 2.7: A Spin valve

2.1.6. Half Metallicity

It has been observed from the double exchange and the magnetoresistance phenomena that in addition to charge, spin of electrons also play a decisive role in deciding properties of these materials. In normal metals there is equal probability of spin up and spin down electrons so that density of spin up and spin down electrons reaching the Fermi level is equal but manganite like systems favour one type of spin alignment over the other. Thus the material acts as a conductor for one spin type and as an insulator for the other spin type and such materials are called half metallic materials [1,9]. Schematic diagram of density of states in metallic and half metallic materials is shown in figure 2.8.

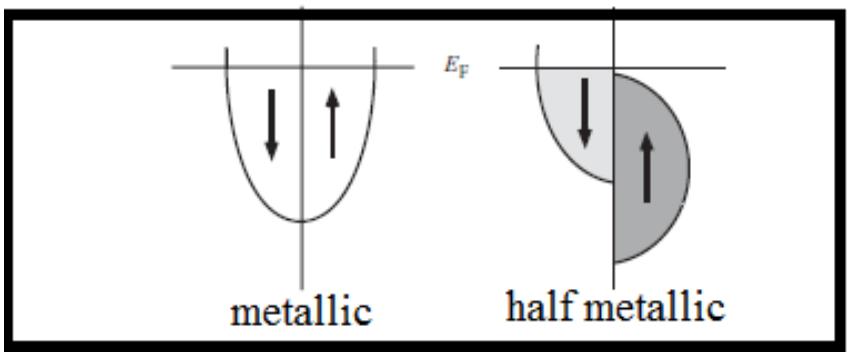

Figure 2.8: Density of states in a metallic and half metallic material [1]

2.2. Doped Manganites: monovalent vs divalent

Manganites in their undoped state are insulators and on substituting A sites or B sites by different elements, they transform to doped manganites exhibiting a wide variety of ordered states like ferromagnetic ordering, charge ordering apart from orbital ordering and antiferromagnetism. In charge ordering (CO), electrons are more localized due to ordering of cations of different charges on specific lattice sites and leads to insulating behaviour of the material. CO was first explained by Wollan and Koehler in rare earth manganites [10].It often competes with double exchange mechanism mediated by electron transport. CO is observed in doped manganites at temperatures below a critical ordering temperature called T_{CO} when there is equal no. of Mn^{3+} and Mn^{4+} ions. Clear evidence for charge ordering was found in $La_{0.5}Ca_{0.5}MnO_3$ using electron microscopy by Chen and Cheong [11,5]

Considering the case of lanthanum manganites, mixed valence states have been obtained with La ions at A sites substituted with divalent ions like (Ca, Sr, Ba, Pb, etc). Thus divalent ion substitution at La

sites lead to hole doped manganites providing a large amount of Mn^{3+} and Mn^{4+} ion in addition to holes to the lattice. Such mixed valence manganites lead to orthorhombically distorted structures with cooperative ordering of Jahn teller distorted octahedra of Mn^{3+}-O_6 [12,13]. An orthorhomic structure of undoped $LaMnO_3$ is shown in figure 2.9. It consists of 20 atoms per unit cell.

Much intense studies on divalent substituted manganites indicated that electron–phonon interaction [14], the charge and orbital ordering [15] and the average sizes of the A cations [16] also play a pivotal role in deciding material properties. Shannon ionic radii (or effective ionic radii) of divalent ions (in pm) like Ca^{2+}, Ba^{2+}, Sr^{2+},Pb^{2+} are 114,149,132 and 133 respectively. Large differences in ionic radii from La^{3+} ions impart a significant change in tolerance factor governing the structure which manifests as a distortion of the crystal lattice. These observations were the stepping stones to find out other alternatives for La site substitutions considering the size of ions unmindful of valencies.

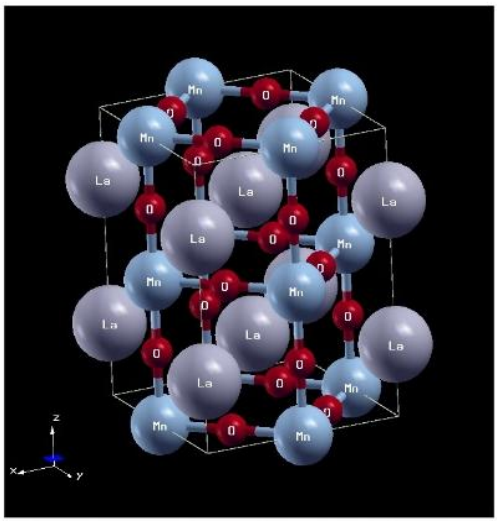

Figure 2.9: Orthorhombic unit cell of $LaMnO_3$

Monovalent ion substitution for La sites were the next major step in that area which immediately gained attention due to the diversity in properties from the divalent substitutions [17-19]. Monovalent ions like Na, K, Ag and Li can be substituted for La sites. It has been found that alkaline earth metal (divalent) doping and alkali metal (monovalent) doping can lead to different effects such as (a) less variation in tolerance factor thereby less distortion of lattice from undoped manganite structure (b) larger random-potential fluctuations experienced by electrons due to the larger difference in valency (c) role of vacancies, oxidation state and stoichiometry of cations/anions in deciding the structural, magnetic and transport properties [18]. A key feature of monovalent ion substitutions are that charge carrier concentration attained is double that is achieved using same amount of divalent substitutions. This implies that twice the number of holes is induced in the lattice by monovalent substitutions in comparison with divalent substitutions [19].

The conversion of Mn^{3+} to Mn^{4+} is explained in divalent and monovalent ion substitutions of $LaMnO_3$. In the case $La_{1-x}Ca_xMnO_3$, 1-x sites of La rare replaced by La. It can be viewed as two structures, $LaMnO_3$ and $CaMnO_3$. In $LaMnO_3$, valency of Mn is 3+ since it donates three electrons along with La^{3+}. In $CaMnO_3$, Ca^{2+} donates two electrons and Mn need to donate 4 electrons to maintain stoichiometry and thus an Mn^{3+} ion is converted to Mn^{4+} ion on single Ca substitution as evident from figure 2.10. Consider the case of sodium substituted for La sites forming the compound $La_{1-x}Na_xMnO_3$ as shown in Figure 2.11. Two adjacent $NaMnO_3$ and $LaMnO_3$ regions in such a material is considered. In $NaMnO_3$, Na donates one electron and Mn donates 4 electron thus

forming Mn^{4+} ion. To maintain stoichiometry, Mn ion in adjacent $LaMnO_3$ donates one electron to the anion in $NaMnO_3$ in addition to donating 3 electrons to the anion in $LaMnO_3$. In this process two Mn^{3+} ions are converted to Mn^{4+} for a single Na substitution.

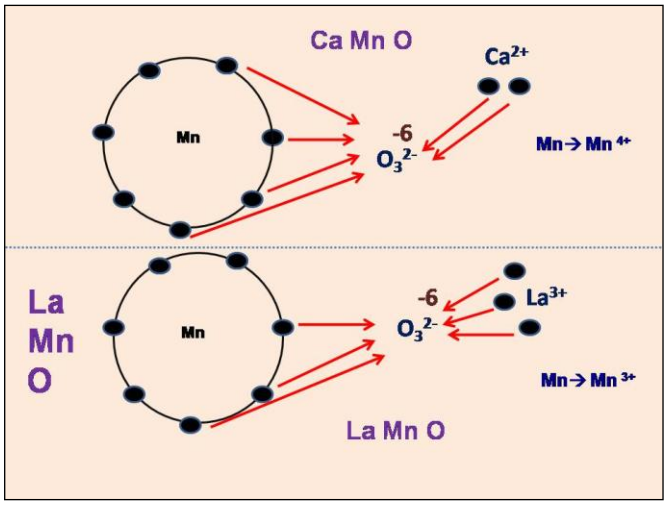

Figure 2.10: Conversion of Mn^{3+} to Mn^{4+} in $La_{1-x}Ca_xMnO_3$

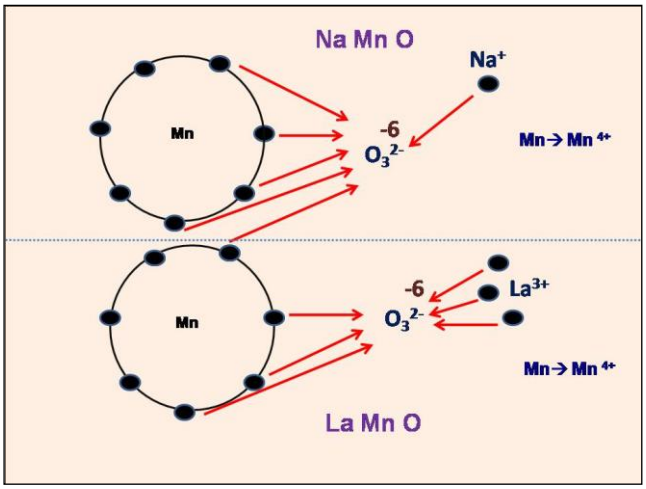

Figure 2.11: Conversion of Mn^{3+} to Mn^{4+} in $La_{1-x}Na_xMnO_3$

Monovalent ions most extensively utilized for substitutions are Na^+(116 pm), K^+(152 pm), Li^+(90 pm) and Ag^+(129 pm). Among them, Na^+ is most preferred for La substitution since its ionic radii is close to La^{3+} ion radii of 117 pm. The substitution produces less distortion of the crystal structure but improved properties due to difference in valence states, increased rate of conversion from Mn^{3+} to Mn^{4+} ions and possibly due to vacancies in lattice [19-22].

2.3. Theory of Magnetoelectric Effect

Magnetoelectric (ME) effect signifies coupling interaction between different order parameters especially electric and magnetic orders. ME effects can be of two types: Direct ME effect and Converse ME effect. Direct ME response is defined as the appearance of an electric polarization *P* upon applying a magnetic field *H*.

$$\Delta P = \alpha \Delta H \text{ or } \Delta E = \alpha_E \Delta H \tag{2.2}$$

where *E* denotes electric field and α_E is ME voltage coefficient. Appearance of a magnetization *M* upon applying an electric field *E* is defined as converse ME effect [23].

$$\Delta M = \alpha \Delta E \tag{2.3}$$

The magnetoelectric effect in a crystal is basically described in Landau theory by writing the free energy F(E,H) of the system in terms of an applied magnetic field H and an applied electric field E . Using Einstein summation convention *F* can be written as

$$-F(E,H) = \frac{1}{2}\varepsilon_0 \varepsilon_{ij} E_i E_j + \frac{1}{2}\mu_0 \mu_{ij} H_i H_j + \alpha_{ij} E_i H_j + \frac{\beta_{ijk}}{2} E_i H_j H_k + \frac{\gamma_{ijk}}{2} H_i E_j E_k + ... \tag{2.4}$$

In eqn. 2.4, first term on the right hand side describes the contribution resulting from the electrical response to an electric field, where ε_{ij} is relative permittivity while second term is the magnetic equivalent of the first term, where μ_{ij} is relative permeability. The third term describes linear magnetoelctric coupling with coupling coefficient given by α_{ij} and it used for the comparison of ME coupling in different systems. Other terms are omitted which represent higher-order magnetoelectric coupling coefficients [24,25].

Magnetoelectric effect can be established in the form electric polarization P_i with respect to magnetic field H_j or as magnetization, M_i with respect to electric field E_j by differentiating F.

$$P_i(H_j) = \alpha_{ij} H_j + \frac{\beta_{ijk}}{2} H_j H_k + \ldots \quad (2.5)$$

$$M_i(E_j) = \alpha_{ij} E_i + \frac{\gamma_{ijk}}{2} E_j E_k + \ldots \quad (2.6)$$

Term α_{ij} is designated as the linear magnetoelectric effect and corresponds to the induction of polarization by a magnetic field or a magnetization by an electric field. Magnetoelectric effect is usually too small to be practically applicable as term αij is limited by the relation

$$\alpha_{ij}^2 \leq \varepsilon_{ii} \mu_{jj} \quad (2.7)$$

In composite materials, ME effect is known as a product tensor property and is a coupled electrical and magnetic phenomenon via elastic interaction first proposed by van Suchtelen in 1972 [26]. Such a

composite ME effect is a result of the product of the magnetostrictive effect (magnetic/mechanical effect) in the magnetic phase and the piezoelectric effect (mechanical/electrical effect) in the ferroelectric one, namely,

$$\text{Direct ME effect} = \frac{magnetic}{mechanical} X \frac{mechanical}{electric}$$

$$\text{Converse ME effect} = \frac{electric}{mechanical} X \frac{mechanical}{magnetic}$$

Thus ME effect in composites is an extrinsic phenomenon depending on the composite microstructure and coupling interaction across magnetic-piezoelectric interfaces [27]. Such a strain-mediated ME effect above room temperature have been exhibited by many bulk composites [28]. In comparison with single-phase multiferroic ME materials which are rare, the large ME response with several orders of magnitude at room temperature can be achieved in the ME composites through this extrinsic phenomena via strain. So ME composites with good coupling coefficient can be helpful in making a four state memory device or smart storage devices a reality.

2.4. Theory of Magnetocaloric Effect

Magnetocaloric effect was termed as the change in magnetic entropy of a magnetic material in the presence and absence of a magnetic field. Entropy of a magnetic material is divided into two: a)

lattice entropy and b) magnetic entropy. On applying and removing magnetic field, there occurs transfer of entropy from lattice to the magnetic phase [29,30]. The concept of magnetic entropy change and magnetocaloric effect stems out from Maxwell's theory of thermodynamics.

Magnetic free energy can be give by

$$A = U(S,M) - TS = A(T,M,N) \tag{2.8}$$

$$dA = -SdT + HdM$$

$$\left(\frac{\partial A}{\partial T}\right)_M = -S; \left(\frac{\partial A}{\partial M}\right)_T = H \tag{2.9}$$

Substituting for the derivatives of A w.r.t T and M, the maxwell's thermodynamic relations can be given by,

$$\left(\frac{\partial S}{\partial M}\right)_T = -\left(\frac{\partial H}{\partial T}\right)_M \tag{2.10}$$

Free energy term can also be written as,

$$F = U - TS - HM = F(T,H) \tag{2.11}$$

$$dF = -SdT - MdH$$

$$\left(\frac{\partial F}{\partial T}\right)_H = -S; \left(\frac{\partial F}{\partial H}\right)_T = -M \tag{2.12}$$

Similarly, Maxwell's relations can be given by,

$$\left(\frac{\partial S}{\partial H}\right)_T = -\left(\frac{\partial M}{\partial T}\right)_H \tag{2.13}$$

Magnetic entropy change (ΔS_M) can be evaluated either from the variation of adiabatic temperature in the presence of magnetic field or from the M-H isotherms at different temperatures. Equation 2.13 in real case can be given by,

$$\left(\frac{\partial S}{\partial H}\right)_T = \mu_0 \left(\frac{\partial M}{\partial T}\right)_H \tag{2.14}$$

The entropy change ΔS_M determining the MCE behaviour can be calculated from the area between the M-H curves multiplied by the reciprocal of the temperature difference between the curves as given by eqn.(2.15).

$$\Delta S_M = \frac{\mu_0}{\Delta T}\left[\int_0^H M_{i+1}(T_{i+1}, H)dH - \int_0^H M_i(T_i, H)dH\right] \tag{2.15}$$

The adiabatic temperature change associated with the entropy change can be given by

$$\Delta T_{ad} = -\mu_0 \int_0^H \frac{T}{C_p}\left(\frac{\partial M}{\partial T}\right)_H dH \tag{2.16}$$

Where C_p denotes specific heat capacity which is considered as independent of magnetic field variations. Magnetic field dependence of C_p for second order phase transition (SOPT) materials is lower than that of first order phase transition (FOPT) materials [29] Considering the insignificant magnetic field dependence of C_p for SOPT materials, eqn.2.16 can be further written in the form

$$\Delta T_{ad} = \frac{T}{C_p}\Delta S_M \tag{2.17}$$

Eqn.2.17 provides approximate values for the indirect estimation of adiabatic temperature change, ΔT_{ad} for different temperatures from the magnetic entropy change and specific heat capacity [31,32].

References

[1] N. A. Spaldin, Magnetic Materials: Fundamentals and Applications, 2nd ed., Cambridge University Press, New York (2011).

[2] Jeremy K. Burdett, Chemical Bonds: A Dialog, John Wiley & sons, England (1997).

[3] C. Zener, Phys. Rev, **82**, 403(1951).

[4] Lev P. Gor'kov, Vladimir Z. Kresin, Physics Reports **400** ,149–208 (2004).

[5] Myron B. Salamon, Marcelo Jaime, Revs. of Mod.Phys **73**,(2001).

[6] Goodenough, J. B., Phys. Rev. **100**, 564(1955).

[7] E. Dagotto, 'Nanoscale Phase Separation and Colossal Magnetoresistance', Springer, Germany (2003).

[8] Y. Tokura, Colossal Magnetoresistive oxides, Gordon and Breach Science , Singapore (2000).

[9] J. M. D. Coey, M. Viret, Adv.Phys., **48**, 2, 167-293(1999).

[10] E. O. Wollan and W. C. Koehler, Phys. Rev., **100**, 545 (1955).

[11] Chen, C. H., and S. W. Cheong, Phys. Rev. B **76**, 4042 (1996).

[12] S. Roy, Y. Q. Guo, S. Venkatesh and N. Ali, J. Phys.: Condens. Matter **13 ,** 9547–9559 (2001).

[13] G. H. Rao, J. R. Sun, K. Barner and N. Hamad, J. Phys.: Condens. Matter **11,** 1523–1528 (1999).

[14] A. J. Millis, P. B. Littlewood and B. I. Shraiman , Phys. Rev. Lett.,**74**, 5144 (1995).

[15] C. H. Chen and S.W. Cheong , Phys. Rev. Lett**. 78,** 4253 (1996).

[16] H. Y. Hwang, S.W. Cheong, P. G. Radaelli, M. Marezio and B.

Battlogg, Phys. Rev. Lett., **75,** 914 (1995).

[17] Y. Kalyana Lakshmi, P. Venugopal Reddy, Phys. Lett. A, **375**, 1543–1547 (2011).

[18] A. I. Tovstolytkin, A. M. Pogorily, D. I. Podyalovskii, V. M. Kalita, A. F. Lozenko, P. O. Trotsenko, S. M. Ryabchenko, A. G. Belous, O. I. V'yunov, and O. Z. Yanchevskii, J. App. Phys, **102**, 063902 (2007).

[19] A. Das, M. Sahana, S.M. Yusuf, L. Madhav Rao, C. Shivakumara, M.S. Hegde, Mater. Res. Bull. **35**, 651–659 (2000).

[20] Newell R. Washburn, Angelica M. Stacya, Alan M. Portis, Appl. Phys. Lett. **70**, 1622, (1997).

[21] M.C. Mozzati, L. Malavasi, C.B. Azzoni, G. Flor, J. Magn. Magn. Mater, 272–276, 1579–1580 (2004).

[22]Y. Kalyana Lakshmi, G. Venkataiah and P. Venugopal Reddy, J. App. Phys.**106**, 023707 (2009).

[23] Jing Ma , Jiamian Hu , Zheng Li , and Ce-Wen Nan Adv. Mater., **20**, 1–26 (2011).

[24] Gerhard, Lukas Leander, Magnetoelectric coupling at metal surfaces, Scientific publishing, Germany (2013).

[25] G. Lawes and G. Srinivasan , J. Phys. Appl.Phys., **44,** 243001(2011).

[26] J. van, Philips Res. Rep., **27** , 28 (1972).

[27] C. W. Nan , Phys. Rev. B, **50** , 6082 (1994).

[28] A. M. Shuvaev, A .A. Mukhin and A. Pimenov, J. Phys.: Condens. Matter, **23,** 113201 (2011).

[29] V. Franco, J. S. Blazquez, B. Ingale, and A. Conde, Annu. Rev.Mater.Res. **42**, 305–342 (2012).

[30] S. Das and T. K. Dey, J. Phys.: Condens. Matter 18, 7629–7641

(2006).

[31] L. M. Wang, Jian-Hong Lai, and Jyh-Iuan Wu, Y.-K. Kuo, C. L. Chang, **102**, 023915 (2007).

[32] A. H. Morrish, The Physical Principles of Magnetism, Wiley, New York, Chap. 3 (1965).

CHAPTER 3

Experimental Techniques

Characterization of materials is an integral part and there are numerous sophisticated characterization tools to study structural, electrical, magnetic, thermal and mechanical properties. This chapter describes the theory and working principle of major experimental techniques utilized for characterization of bulk and thin film samples. A brief description of Pulsed Laser Deposition technique is also provided in this chapter.

Film Deposition Technique

3.1. Pulsed Laser Deposition (PLD)

Pulsed Laser Deposition is a reliable technique for obtaining high quality films. In PLD, high power laser pulses are used to remove the material from the surface of target which will then be deposited on a substrate. The thin films possess exactly the same stoichiometry as the target material and it is a unique characteristic of PLD. Even though laser assisted film growth started years back in the 1960's, origin of the modern PLD technique can be traced to the late 80's when Xindi Wu, Dirk Dijkkamp and T Venkatesan successfully laser deposited a superconducting film of $YBa_2Cu_3O_7$. Since then, laser deposition has been widely accepted for thin film preparation. In a PLD

system, laser pulses melt and ionize material from the target surface placed in one end of vacuum chamber which is termed as laser ablation. Due to ablation, a transient, highly luminous plasma state called plume is produced which spans the region between target and the substrate. Plasma plume is the vaporized material containing ions and electrons which traverses to the substrate placed in the other end of the chamber, gets deposited and thus facilitating thin film growth on the substrate [1,2].

The schematic diagram of a PLD system is shown in figure 3.1. It consists of a large chamber with a rotating target holder (or a carousel) and substrate holder along with a heater. A laser beam is allowed to incident on the target through an SiO_2 window and produces plasma plume between target and substrate. Plume of target material ions hits the surface of substrate and such sputtered species from the substrate and the target material are the source for condensation of particles. When the condensation rate is high, a thermal equilibrium is reached enabling the growth of film on the surface of the substrate [2, 3].

However, deposition process is not simple as explained. There are various factors affecting the deposition conditions such as laser fluence, substrate temperature, target to substrate distance and chamber pressure. In most cases, background gases like nitrogen or oxygen are also used for deposition and the background gas pressure too determines thin film characteristics. Optimization of the deposition parameters is one of the major tasks to be performed in depositing films using PLD. PLD deposition thus goes through four major crucial steps [4, 5]:

- Laser ablation and formation of plasma plume
- Dynamics or movement of Plasma plume guided by coulomb repulsion and recoil from the target surface

- Deposition of the ablated material on the substrate
- Nucleation and growth of thin film on the surface of substrate

Nucleation-and-growth of crystalline thin films on the suface of substrate depends on many factors such as density, energy, degree of ionization, type of target material, and the temperature of the substrate. Growth mechanism is governed by two parameters namely substrate temperature T and the supersaturation Δm. The folloing relation shows the relation between these parameters.

$$\Delta m = kT \ln(R/Re) \tag{3.1}$$

where k is the Boltzmann constant, R is the actual deposition rate, and Re is the equilibrium value at temperature T.

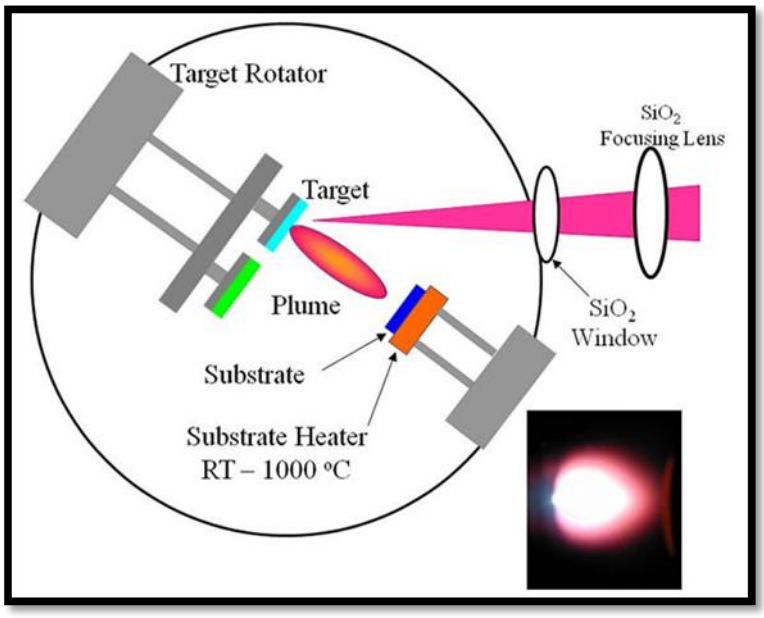

Figure 3.1: Schematic diagram of PLD

PLD has significant advantages over other thin film deposition techniques. They are the following: 1) stoichiometric transfer of material from target to substrate 2) higher deposition rates at moderate laser fluences and the control of film thickness by means of number of laser pulses 3) As laser serves as an external source, entire depsotion process is cleans and does not require any filaments for cleaning 4) deposition occurs in the presence of reactive and inert gases 5) a carousel used for inserting more than one target samples enable multilayer deposition without breaking vacuum for the next deposition. There are some drawbacks for this deposition technique such as 1) smaller area of deposition (~ 1cm^2) makes it unsuitable for industrial usage 2) possibility of having macroscopic globules of ablated material over the substrate surface 3) fundamentals of plasma plume are not understood fully and therefore deposition of novel materials require extensive optimization. Recently modifications have been introduced into PLD systems to obtain high quality films. Raster scan of laser pulses over the target surface and moving the substrate during deposition results in obtaining thin films with uniform thickness and composition. Mechanical velocity filter and techniques like collision of plasma plumes and off axis deposition removes the material particles from the film surface. Thus pulsed laser deposition offers excellent quality stoichiometric films with a good control over the thickness of deposition [2-6].

Analytical Tools and Techniques

3.2. X-Ray Diffraction (XRD)

X -Ray Diffraction (XRD) is the most widely used analytical technique for structural determination of powdered bulk/ nanomaterials as well as thin films, their surfaces and interfaces. X ray diffraction is based purely on diffraction phenomenon and will generate information of the phase of the material from the orderly arrangement of atoms without individually identifying each atom. Thus XRD is a generic tool for studying the crystallinity of the materials, their symmetry groups, and unit cell dimensions directly from diffraction patterns. X-rays are high energy electromagnetic radiation having energies ranging from about 200eV to 1 MeV and wavelength close to 1 Å [7].

An X-ray diffractometer consists of mainly three basic components: X-Ray source, specimen or sample stage and X-ray detector as shown in figure 3.2. Sample to be analysed is spread on a flat non diffracting glass slide and is exposed to the x-ray beam. The most commonly used target material for X-ray diffraction is Cu. If an element in the sample has an atomic number slightly below that of the target metal, the X-rays will be strongly absorbed leading to decrease in intensity of the diffracted beam. The XRD patterns of the samples were recorded on the X-ray diffractometer (Rigaku Dmax-C) using Cu Kα radiation (λ=1.5418 Å), which has energy of 8.04 keV [7, 8].

When a collimated beam of X-ray with a wavelength of 1.5406Å is incident on a specimen it is diffracted by the crystalline planes in the specimen according to the Bragg's law as given by equation 3.2.

W.H. Bragg and his son Sir W.L. Bragg developed this equation connecting crystalline planes and diffraction angle in the year 1913[8].

$$n\lambda = 2dSin\theta \tag{3.2}$$

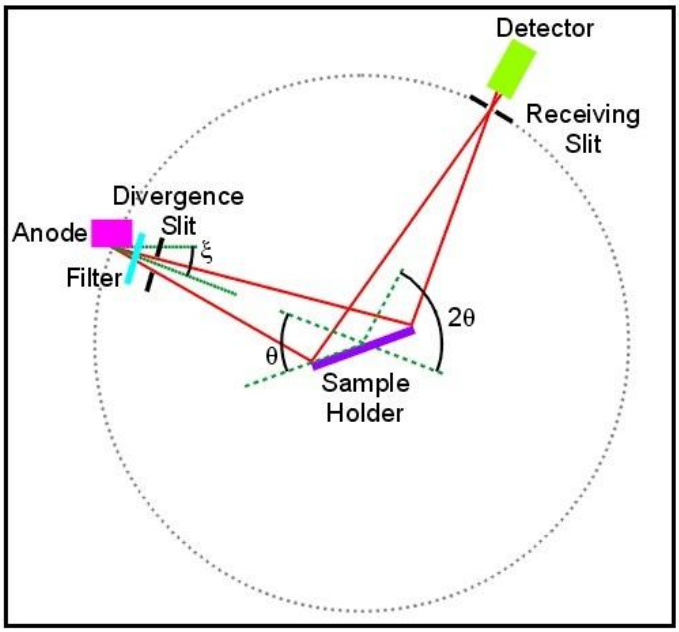

Figure 3.2: Schematic diagram of X-ray diffractometer

Where λ is the wavelength of the X-radiation, *n* is an integer, *d* is the spacing between atomic planes in the crystalline planes and θ is known as diffraction angle. The intensity of the diffracted x-rays can be measured and plotted as a function of diffraction angle 2θ. Lattice

parameters can be calculated with the help of a computer programme or by employing refinement methods like Rietveld.

Apart from the determining the crystal planes, XRD can also be utilized for determining crystallite size, strain effects and porosity. XRD is an initial study to evaluate the structural quality of the synthesised materials [7-9].

3.3. Rietveld Refinement

Rietveld refinement is a technique used for performing fine structure refinement using X-ray diffraction or neutron diffraction in characterizing the crystalline samples. It utilizes the diffraction data of peak reflections vs angle values in evaluating various material characteristics like lattice parameters and space group. Rietveld method was first devised by Hugo rietveld and uses a least squares approach to refine a theoretical line profile to match with measured profile. The method was first reported for the diffraction of monochromatic neutrons with reflection-position expressed in terms of Bragg angle 2θ. Same terminology is widely used for refinement although alternative scales such as x-ray energy or neutron time-of-flight are also in practice. Refinement parameters like fundamental lattice vectors, angle between them, positions and occupancy of ions are varied and the theoretical profile is made to match with the measured profile. Thus principle of the rietveld refinement involves minimizing a function M which is the difference between a calculated profile y (calc) and the observed data y(obs) [10].M can be given by the relation as follows:

$$M = \sum_i w_i \{ y_i^{obs} - \frac{1}{c} y_i^{calc} \}^2 \quad (3.3)$$

where w_i is the statistical weight and c is the scaling factor such that $y^{calc} = c\, y^{obs}$. The introduction of this technique is a significant step forward in the diffraction analysis of powder samples as it relies on strongly overlapping reflections and gives accurate values of lattice parameters [11].

3.4. Scanning Electron Microscope (SEM)

The Scanning Electron Microscope (SEM) is an electron microscope utilizing electrons similar to optical microscope utilizing visible light. Large depth of field, which allows more of specimens to be in focus at one time, is the prime advantage of SEM over optical microscope In fact SEM supplants optical microscope for closely analyzing material surface and features. It is a starting tool for material analysis that images the sample surface by scanning it with a high-energy beam of electrons in a raster scan pattern. It gives a magnified image of the sample surface and the resolution of SEM approach a few nm and it can operate at magnifications easily adjustable from about 10 X - 30000 X. Electrons while scanning interact with the atoms of the sample and produces signals that contain information about the sample's surface topography, composition and other properties such as electrical conductivity [12].

The principle images produced in the SEM are from three main sources: secondary electrons, backscattered electrons and elemental X-rays. Secondary and backscattered electrons are conventionally

separated according to their energies. Electrons undergo elastic as well as inelastic scattering from the sample. Higher energy electrons are primary electrons that have been scattered without loss of kinetic energy (i.e., elastically) by the nucleus of an atom and backscattered electrons (BSEs) are considered to be the electrons that exit the specimen with an energy greater than 50 eV, including Auger electrons [13].

The geometry of SEM is shown in figure 3.3. An electron gun produces electrons of high energy which is accelerated by an anode. The beam is defocused by a series of magnetic lenses. Each lens has an associated defining aperture that limits the divergence of the electron beam. The top lenses are called condenser lenses, and are often operated as if they were a single lens. By increasing the current through the condenser lens, the focal length is decreased and the divergence increases. The lens therefore passes less beam current on to the next lens in the chain. The beam next arrives at the final lens-aperture combination. The final lens does the ultimate focusing of the beam onto the surface of the sample. The sample is attached to a specimen stage that provides x and y motion, as well as tilt with respect to the beam axis and rotation about an axis normal to the specimen's surface**.** The two dimensional map of the signal yields a SEM image [12]. The main applications of SEM are in surface topography and elemental mapping.

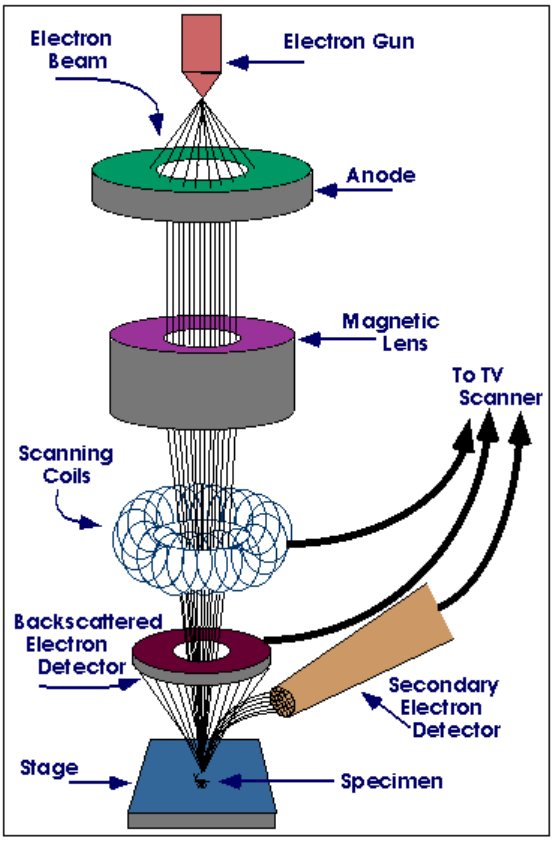

Figure 3.3: Geometry of SEM

3.5. Energy Dispersive X-ray Spectroscopy (EDS)

Energy dispersive X-ray spectrometer analyses characteristic X-ray radiation emitted from the specimen when the electron beam interact with the specimen. EDS is used for the compositional analysis of samples. Upon exposing the samples to high energy electron beams, various atoms present in the sample emit characteristic X-rays which can be observed as several distinct peaks on

an energy scale. The intensities of the peaks can be compared with the peaks of a standard sample to obtain the relative amounts of each atomic species, whereby accurate composition of the sample can be determined [12, 13].

3.6. Atomic Force Microscopy (AFM)

Atomic Force Microscopy is an extensively used imaging technique and maps surface property on an atomic or nanometre scale. In an AFM, spatial position of probing tip is controlled by piezoelectric transducers with high precision to place it relative to sample for scanning the surface. Gerd Binning, Calvin Quate and Christoph Gerber are credited for the discovery of Atomic Force Microscopy in 1986. Force acting between the atoms on tip and sample surface is picked up and is utilized for imaging. AFM tip experiences primarily inter-atomic forces: the very short range Born repulsive forces for 0.1nm and the longer range Van der Waals forces up to 10 nm. Van der Waals forces decay rapidly on moving away from the surface and become negligible for 100-500 nm above the surface where long-range electric - magnetic and capillary forces are prevalent [14]. Figure 3.4 shows tip –surface distance vs tip-surface force.

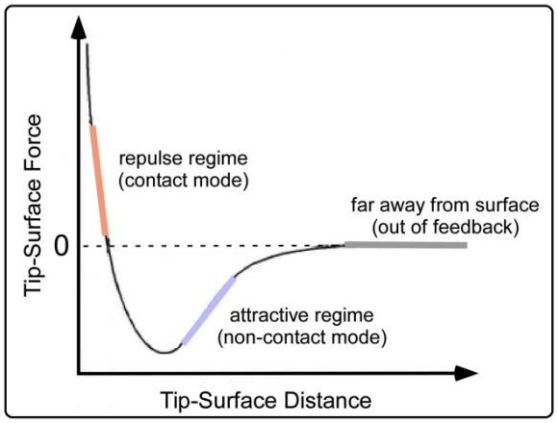

Figure 3.4: Tip –surface distance vs tip-surface force in AFM

Van der Waals (VdW) are attractive forces acting between the atoms are strong enough to move macroscopic objects like AFM cantilevers. As the scanning tip further approaches the sample and the electronic wave functions of the atoms at the tip and sample atoms start to overlap, strong repulsive forces arise also called Born repulsive forces. The underlying principle of AFM is the interactions between the sample and the probe tip which result in a deflection in cantilever.

Geometry of an AFM is shown in figure 3.5. It consists of piezoelectric scanner like arrangement on which sample is mounted, a cantilever with probe tip, laser and a photodiode. Position of the sample surface with respect to the tip along x, y and z directions is determined by a piezoelectric scanner. A set point is defined for the movement of the sample in the *z*-direction, during *x*-*y* scanning, Beam from laser is positioned as to be reflected off the back of the cantilever, *via* a mirror, and fed to a position-sensitive photo detector or photodiode. The laser

beam functions as an optical lever arm and a three dimensional map is constructed which is closely related to the topography of the surface [15].

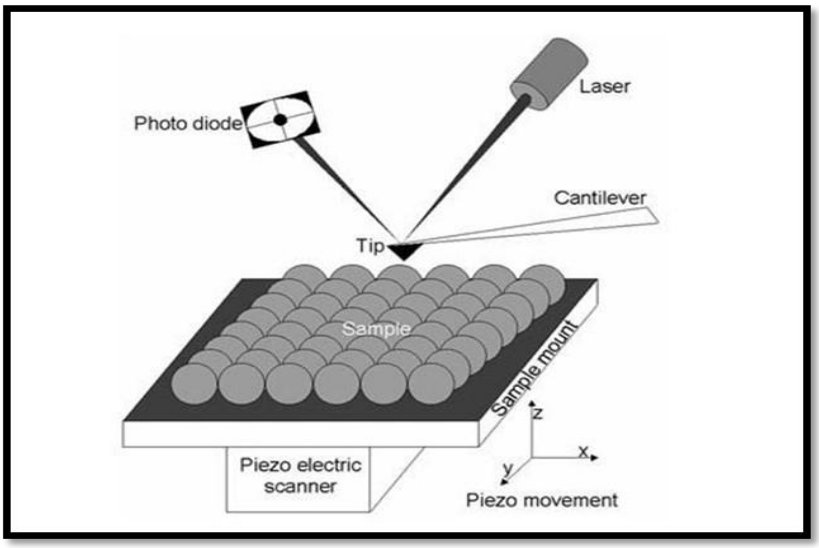

Figure 3.5: Geometry of AFM

The oscillation of the cantilever is governed by the equation of motion for a damped harmonic oscillator with forced oscillation. The oscillation frequency is therefore,

$$W_0 = \sqrt{\frac{k}{m}} \tag{3.4}$$

where k is spring constant of the cantilever and m is mass. The interaction between tip and sample in AFM changes the spring constant of cantilever as given by eqn. 3.5.

$$k_{eff} = k - \frac{\partial F}{\partial z} \tag{3.5}$$

where F is the force and z is the distance between interacting molecules. The resonance frequency is then shifted and the shift can be given by

$$\Delta w_0 = -\frac{w_0}{2k}\frac{\partial F}{\partial z} \tag{3.6}$$

The Van der waals potential, VdW potential between two interacting molecules is given by

$$U_{VdW} = -\frac{C_1}{z^6} \tag{3.7}$$

Born repulsive interaction expressed as potential is given by

$$U_{rep} = \frac{C_2}{z^{12}} \tag{3.8}$$

Total intermolecular potential is the sum of attractive and repulsive force is

$$U = \frac{C_2}{z^{12}} - \frac{C_1}{z^6} \tag{3.9}$$

where C_1 and C_2 are coefficients for attractive and repulsive interactions respectively.

VdW potential between the spherical tip end and the plane surface is expressed as,

$$U_{VdW} = -\left(\frac{AR}{6z}\right) \tag{3.10}$$

where A is the radius of the sphere and R is Hamaker constant.

An AFM operates in three different modes like contact mode, tapping mode and non contact mode. In contact mode, AFM, also known as repulsive mode, an AFM tip makes soft "physical contact" with the sample. The sharp probe tip which is of a pyramidal-shaped etched silicon nitride tip, is attached to the cantilever with a low spring constant, typically between 0.06 N/m and 0.6 N/m. Contact force causes deflection

in cantilever in accordance with the crest and troughs on surface as it traces the tip across the sample. In tapping mode, the silicon probe tip oscillates at a frequency near to the resonance frequency as it rasters across the sample surface. A suitable height from the sample surface is always maintained by the cantilever and in turn, amplitude of oscillation is lowered by the interactive forces whenever the tip approaches surface. Tapping mode does not provide much atomic resolution but appears to be advantageous considering the less damage done to sample surface. In non contact mode, the tip does not touch the sample surface. Long range forces acting between the tip and sample reduce the resonance frequency which in turn maintains a constant amplitude of oscillation or frequency by adjusting the tip to sample distance. This distance is used to generate the topographical image of the sample surface without damaging the sample surface [16, 17].

Magnetic Force Microscopy (MFM) is a characterization tool close to AFM where the scanning tip is coated is coated with a ferromagnetic film. MFM images the spatial variation of magnetic forces on scanning the sample surface and contains information of the distribution of magnetic domains on the sample surface.

An advantage of AFM is that it is applicable for studying all types of surfaces, conducting, semiconducting and insulating since it functions on interatomic forces other than diffraction or electron bombardment.

3.7. Magnetic characterization

3.7.1. Vibrating Sample Magnetometer

Vibrating Sample Magnetometer or VSM is used to measure the magnetic properties of the material and the idea of VSM based on Faradays's law of induction was put forth by Simon Foner at Lincoln Laboratory, MIT in 1955.

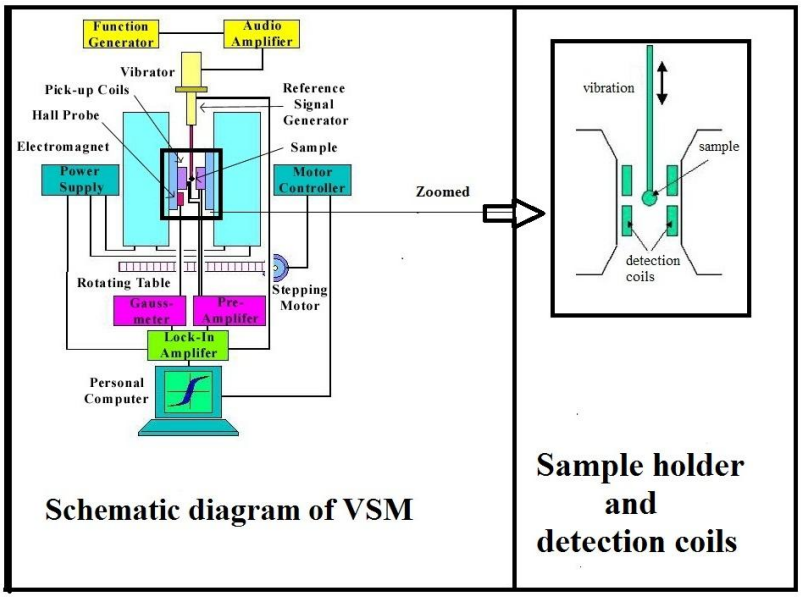

Fig.3.6: Geometry of VSM

Faraday's Law of induction, which tells us that a changing magnetic field will produce an electric field. This electric field can be measured and provides information about the changing magnetic field. A VSM is used to measure the magnetic behaviour of magnetic materials. Using VSM the hysteresis loop parameters namely saturation magnetisation (M_s), coercive field (H_c), remanence (M_r) and squareness ratio (M_r/M_s) can be derived. The schematic of a vibrating sample magnetometer is given in figure 3.6.

In a VSM, the sample to be studied is placed in a constant magnetic field. If the sample is magnetic, this constant magnetic field will magnetize the sample by aligning the magnetic domains or the individual magnetic spins, with the field. The stronger the constant field, the larger the magnetization. The magnetic dipole moment of the sample will create a magnetic field around the sample, sometimes called the magnetic stray field. As the sample is moved up and down, this magnetic stray field change as a function of time and can be sensed by a set of pick up coils. A transducer converts a sinusoidal ac drive signal provided by a circuit located in the console in to a sinusoidal vertical vibration of the sample rod and the sample is thus made to undergo a sinusoidal motion in a uniform magnetic field. Coils mounted on the pole pieces of the magnet pick up the signal resulting from the sample motion.

The alternating magnetic field will cause an electric field in the pickup coil as according to Faradays law of induction, the current will be proportional to the magnetization of the sample. The greater the magnetization, larger will be the induced current. The induction current is amplified by a transimpedence amplifier and a lock-in amplifier. The various components are interfaced via a computer. Controlling and monitoring software, the system can tell you how much the sample is magnetized and how magnetization depends on the strength of the constant magnetic field. For particular field strength, the corresponding signal received from the probe is translated into a value of magnetic moment of the sample. When the constant field varies over a given range, a plot of magnetization versus magnetic field strength is generated.

Principle and theory involved in VSM

When a sample is placed in a magnetic field 'H' it will respond with a magnetic induction 'B'

$$B_{sample} = \mu_0[H + \frac{m}{v}] \tag{3.11}$$

where m/v represents magnetic moment per unit volume, i.e., magnetization of the sample.

Thus in free space, $B_{sample} = gm$, where g is a proportionality constant depending on position of the point in space and is magnetic moment.

Total magnetic induction at a point in space is given by

$$B_{space} = B_{ext} + B_{sample} = B_{ext} + gm \tag{3.12}$$

where B_{ext} is the magnetic induction of free space due to magnetic field.

When the sample is moved near a pickup coil, a voltage is induced in the coil:

$$V = -NO\frac{dB_{space}}{dt} = -NO\frac{d}{dt}(B_{ext} + gm) \tag{3.13}$$

Where N is the the no. of turns of the coil and O is a constant depending on the geometry of the coil. Note that when the external field B_{ext} is varied, the pickup coils do not pick up the change due to the fact that the coil pairs are wound in opposite directions.

Since g is not a contant but is a function of time, if the sample is in sinusoidal motion, V can be given by,

$$V = -NO\frac{dg}{dt}m \Rightarrow -NOh\frac{dAe^{\omega t}}{dt}m \tag{3.14}$$

where h is a proportionality constant and A is related to amplitude of the wave. –Noh is substituted by a proportionality constant k. Taking the derivative of eqn. 3.6,

$$V = k\omega Ame^{wt} \tag{3.15}$$

It can be seen that a voltage 'V', proportional to the magnetic moment, 'm' is induced in the coil. A VSM uses an electromechanical driver (voice coil) to move a vertical drive rod with a small amplitude A, and frequency ω mounted on the drive rod of the sample holder S, and a small permanent magnet or small coil with a constant dc excitation current of constant magnitude as reference magnetic moment *R.* Pick-up coils near *R* will have an induced voltage

$$V_R = k_R \omega Am_R e^{wt} \tag{3.16}$$

where $'k_R\ '$ is a constant depending on coil geometry, and 'm_R' is the constant magnetic moment of reference R. $'V_R\ '$ is in the millivolt range and easily measured by a rms voltmeter. Similarly, the sample pick-up coils will see a voltage

$$V_S = k_S \omega Am_S e^{wt} \tag{3.17}$$

An RMS-to-dc conversion is performed on both $'V_R\ '$ and $'V_s'$ by the RMS voltmeter and lock-in amplifier, respectively. The ratio of these two dc voltages is then taken by a digital multimeter (DMM) which has ratio capabilities. Taking the root-mean-square average of the previous two equations, it is seen that the dependence on frequency ω and drive amplitude 'A', cancel and the DMM output is

$$V_{out} = Km_s \tag{3.18}$$

Where k is a proportionality contant which has absorbed k_R, K_S, m_R as well as any amplifications of the reference and sample by

lock in amplifier. The output voltage, V_{out} is equivalent to kvM, and the magnetization can be evaluated [18, 19]. A block diagram of VSM with RMS voltmeter, DMM and lock in amplifier is shown in figure 3.7.

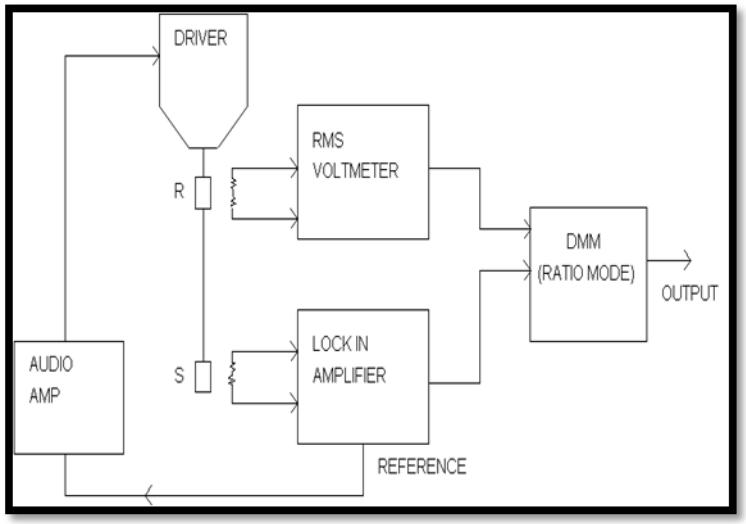

Figure 3.7: Block Diagram of VSM.

3.7.2. SQUID Magnetometer

A SQUID (Superconducting Quantum Interference Device) is a device made out of two superconductors separated by thin insulating layers so as to form two Josepson junctions. A schematic of SQUID is shown in figure 3.8. SQUID magnetometers are developed to measure small magnetic fields of the order of 10^{-14} T with low noise levels. It is a highly sensitive device and is capable of measuring changes in magnetic field of even one flux quantum (h/2e).

In a SQUID device, electrons move simultaneously in both directions since there are two Josephson junctions. When a constant bias

current is applied to the SQUID device, the voltage oscillates with the change in phase at two junctions. Such a change in phase is caused by change in magnetic flux. Number of oscillations corresponds to change in flux. Thus working principle of SQUID is that when the sample is moved through the superconducting magnetic coils, a flux change is induced in the pickup coils. SQUID basically is a flux-to-voltage transducer. Flux-to-voltage characteristic has increased the demand of SQUID for detecting small magnetic field, current, voltage, inductance and magnetic susceptibility. SQUIDs have been used for a variety of testing purposes that demand extreme sensitivity including engineering, medical, and geological equipment including mineral exploration and earthquake prediction.

It is to be noted that highly magnetic sample should be moved only slowly through the coils without exceeding the maximum slewing rate of the electronic system [17, 20].

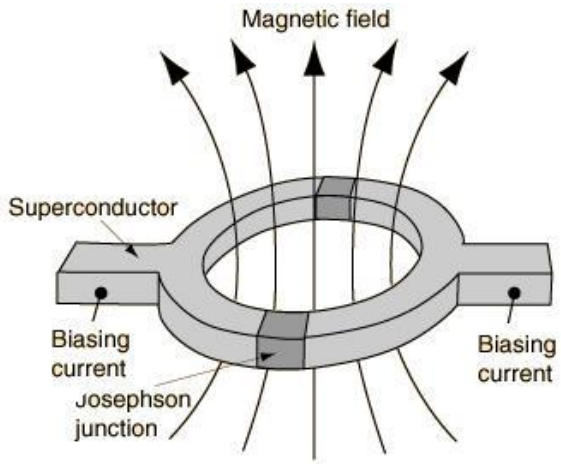

Fig. 3.8: Schematic of a SQUID

3.7.3. Field Cooled (FC) and Zero Field Cooled (ZFC) Measurements

Zero field cooled (ZFC) and Field cooled (FC) measurements are temperature dependent magnetization measurements for analyzing various magnetic interactions. In an ZFC measurement, sample is cooled to very low temperatures close to 5 K or 10 K in the absence of magnetic field. It is cooled from very high temperatures usually much above the T_C or T_B (Curie temperature and Blocking temperature) respectively for ferromagnets and superparamagnets. On reaching lowest possible temperature, a small magnetic field is applied. Magnetization values are recorded on heating the sample at a constant rate. In ZFC, at low temperature and in the zero applied magnetic field, sample is in equilibrium state and exhibits no net magnetization. Reason is as follows: when sample is cooled, magnetic moments tend to align along the preferred crystal directions lowering the magnetocrystalline energy. Since orientation of one crystallite differs from the other, net moment is zero. When a small magnetic field is applied, equilibrium state is broken due to Zeeman energy, but the magnetic moments will be locked in their respective orientation and no substantial change in magnetization will be observed since system cannot attain an equilibrium state at such low temperatures. As the sample is heated, more thermal energy is available and more moments will be aligned in the direction of magnetic field thus minimizing the Zeeman energy. Thus sample attains an equilibrium state through a relaxation process as temperature goes up. Eventually at a particular temperature, the net magnetization of the system reaches a maximum where maximum number of moments will have aligned with the external field. On further increasing temperature,

thermal energy will exceed Zeeman energy and the moments will be randomized leading to decrease in magnetization as per Curie's law. In FC measurements, sample is cooled to lower temperatures in the presence of magnetic field and measurements are carried out as sample is heated to high temperatures.

In both FC and ZFC measurements, applied magnetic field should be smaller than the anisotropy field so as to get information of competing magnetic interactions. Also, there is divergence in FC and ZFC curves. This is because, in ZFC, spins corresponding to each particle tend to align with different crystalline axes and will be frozen in that state at low temperatures while in FC, spins from each particle will tend to align with the easy crystalline axis that is closest to the applied field direction and remain frozen in that direction at low temperature. FC and ZFC measurements are considered as most sensitive magnetic measurements for analyzing a close inspection of magnetic behaviour [17, 21].

3.8. Heat Capacity Measurements using PPMS

Heat Capacity option of a basic PPMS helps to control environmental variables, such as the temperature and magnetic field and perform the heat capacity measurement with specialized components.
Major components of a heat capacity system include:

- Specialized heat capacity pucks and sample frame
- Precision electronics to control the measurement and gather the raw data
- P640 High-Vacuum system to thermally isolate the sample
- sample-loading station that allows convenient sample preparation

- Associated software that automatically performs data analysis

The heat capacity puck utilizes the standard PPMS 12-pin format for electrical connections, and it provides a small microcalorimeter platform for mounting the sample. Samples are mounted to this platform by standard cryogenic grease. The sample platform is suspended by eight thin wires that serve as the electrical leads for an embedded heater and thermometer along with a good thermal connection between the sample platform and the puck. An additional thermometer embedded in the puck provides a highly accurate determination of the puck temperature, and a thermal shield aids in maintaining stable sample temperature and uniformity. To ensure that heat is not lost via exchange a sample chamber pressure near 0.01 mbar is maintained.

A single heat capacity measurement consists of several distinct stages. First, the sample platform and puck temperatures are stabilized at some initial temperature. Power is then applied to the sample platform heater for a predetermined length of time, causing the sample platform temperature to rise. When the power is terminated, the temperature of the sample platform relaxes toward the puck temperature. The sample platform temperature is monitored throughout on both heating and cooling, providing (with the heater power data) the raw data of the heat capacity calculation [22].

3.9. X-Ray Photoelectron Spectroscopy (XPS)

X-Ray Photoelectron Spectroscopy also called Electron Spectroscopy for Chemical Analysis (ESCA) is a method for

characterizing the top few atomic layers at the surface of a solid. ESCA can not only give the elemental composition of a surface (C, O, N, etc.) but can also provide insights into the chemical bonding at the surface. It utilizes photo-ionization and analysis of the kinetic energy distribution of the emitted photoelectrons to study the composition and electronic state of the surface region of a sample. X-rays with a photon energy of 200-2000 eV called soft X-rays are generally used in XPS to examine core-levels. In XPS the photon is absorbed by an atom in a molecule or solid, leading to ionization and the emission of a core (inner shell) electron. The kinetic energy distribution of the emitted photoelectrons (i.e. the number of emitted photoelectrons as a function of their kinetic energy) can be measured using any appropriate electron energy analyser and a photoelectron spectrum can thus be recorded. Figure 3.9 shows the photoelectron emission process involved in XPS.

The process of photoionization can be considered as follows.

$$A + h\nu \rightarrow A^{+} + e- \qquad (3.19)$$

Conservation of energy then requires that :

$$E(A) + h\nu = E(A^{+}) + E(e-) \qquad (3.20)$$

Since the electron's energy is present solely as kinetic energy (KE) this can be rearranged to give the following expression for the KE of the photoelectron:

$$KE = h\nu - (E(A^{+}) - E(A) \qquad (3.21)$$

The final term in brackets, representing the difference in energy between the ionized and neutral atoms, is generally called the binding energy (BE) of the electron which leads to the following commonly quoted equation :

$$KE = h\nu - BE \quad (3.22)$$

In addition, Φ is the work function of the solid when KE is counted near surface, however, KE is detected by analyzer then Φ is the work function of analyzer. Considering the work function Φ, KE relation changes to

$$KE = h\nu - BE - \Phi \quad (3.23)$$

Intensity of photoemission is proportional to the intensity of photons and kinetic energy of photoemission is inversely proportional to binding energy. Since each element has unique set of core levels, KE's can be used to fingerprint the element. There will be no photoemission for $h\nu < \phi$ and from levels with $BE + \phi > h\nu$.

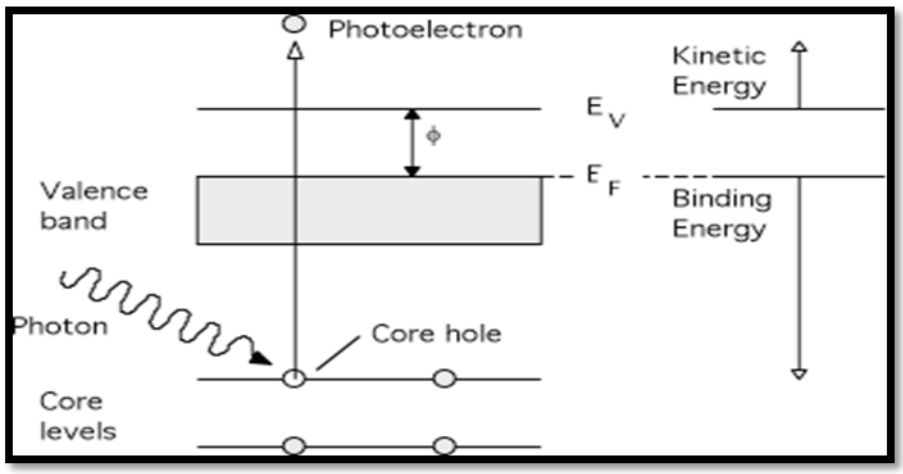

Figure 3.9: Photoelectron emission in XPS

Experimental Details

The basic requirements for a photoemission experiment are:

1. a source of fixed-energy radiation (an x-ray source for XPS or, typically, a He discharge lamp for UPS (Ultraviolent Photoelctron Spectroscopy))
2. an electron energy analyser (which can disperse the emitted electrons according to their kinetic energy, and thereby measure the flux of emitted electrons of a particular energy)
3. a high vacuum environment (to enable the emitted photoelectrons to be analysed without interference from gas phase collisions)

Such a system is illustrated schematically in figure 3.10.

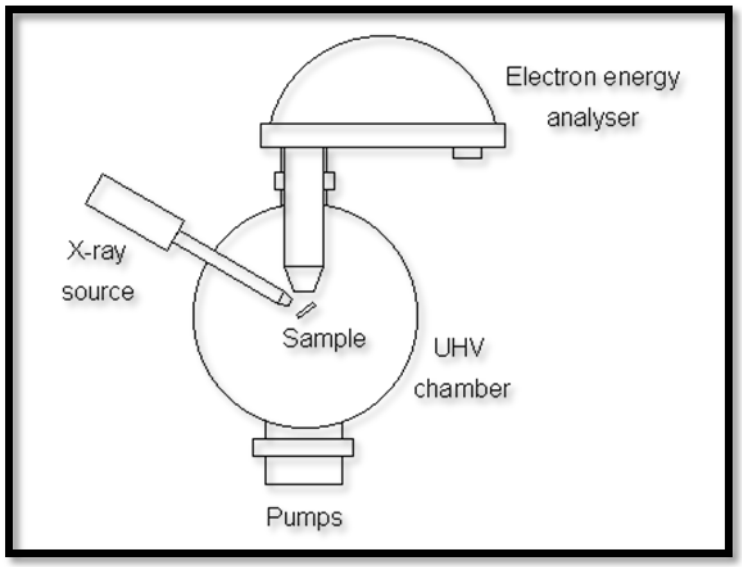

Figure 3.10: XPS Instrumentation

There are many different designs of electron energy analyser but the preferred option for photoemission experiments is a concentric hemispherical analyser (CHA) which uses an electric field between two hemispherical surfaces to disperse the electrons according to their kinetic energy.

An XPS is capable of qualitative analysis of detecting all elements from ^{3}Li to ^{103}Lr **(**Except H and He) and the detection limits range from 0.1 to 1.0 atom%. It also performs quantitative analysis giving the relative elemental composition of the surface [23,24] .

3.10. Ferromagnetic Resonance (FMR)

Ferromagnetic resonance (FMR) is a spectroscopic technique used to probe the magnetization of ferromagnetic materials. If a magnetic field is applied on a series of magnetic moments, they will tend to line up parallel to the field, since it will minimize their magnetostatic energy. If, in this configuration, the magnetic moments are taken out from this equilibrium stage, they will try to go back to it through the torque produced by the magnetic field. In a real ferromagnetic system, a damping term must be added to this "equation of motion", to describe correctly the behaviour of the magnetic moments involved. Landau Lifshitz Gilbert (LLG) equation describes such a damped motion of a magnetic moment about the direction of an external magnetic field. If a varying force perpendicular to magnetic field, H is applied over the magnetic moment (like a radio frequency (RF) electromagnetic signal), it can make the moment to precess about the equilibrium direction. Besides, if this force has a frequency similar to the precessional frequency of

magnetization, M called ω_0; a maximum of energy absorption by the ferromagnetic sample will be observed. This is when ferromagnetic resonance take place, and all magnetic moments will be oscillating in phase. The ferromagnetic resonance of this type by means of sweeping external magnetic field is termed as conventional resonance and applies only to materials with single domain magnetization configuration.

Conventional FMR cannot be applied for materials with complex domain configuration since sweeping of magnetic field results in change of magnetization configuration. Thus frequency is made to sweep instead of magnetic field and is achieved using a network analyzer. A Vector Network Analyzer (VNA) is connected to a high bandwidth waveguide. VNA serves as source and the detector of the sinusoidal high frequency signal. It sweeps the frequency of the outgoing signal across a specified range. The signal excites the magnetization but the energy is transferred to sample only near the resonance frequency of the system. Phase shifting of the signal at resonance causes destructive interference with the incident wave resulting in a decrease of amplitude of transmitted signal detected by VNA. Such an FMR technique is called Network Analyzer-Ferromagnetic Resonance (NA-FMR).

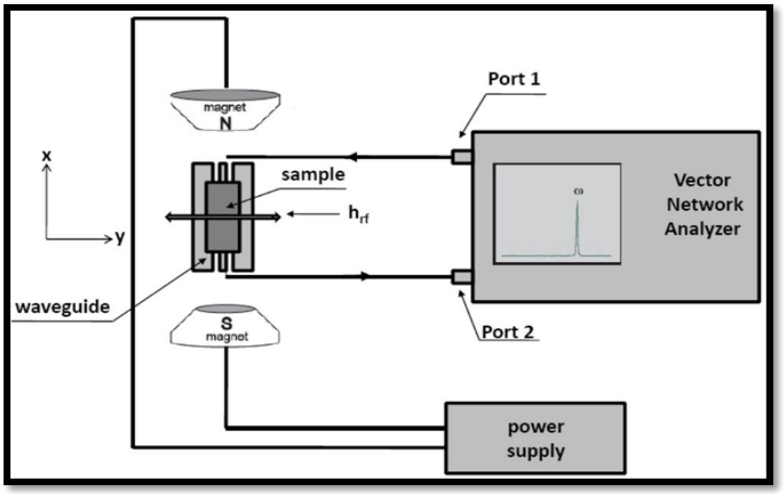

Figure 3.11: NA-FMR Set up

Figure 3.11 shows NA-FMR measurement set up. The sample is placed on the central conductor of a coplanar waveguide (CPW). The CPW will excite the sample with a time dependent electromagnetic signal ranging from a few MHz to GHz. Input and output signals from the CPW are sent and received in a VNA. In a two terminal VNA, S_{21} is a complex number defined as the ratio of the received voltage in port 2 and the input voltage in port 1. It is the S_{21} parameter which is measured. A frequency sweep like this will be carried out at several external magnetic fields, for example from 2250 to -2250 Gs. These magnetic fields will be created by a pair of Helmholtz coils (1345 Oe/A). The current through the coils is supplied by a current source [25,26]. FMR is perceived to be an excellent method for studying spin waves and nature of magnetic domains.

3.11. Ferroelectric Loop Tracer

A ferroelectric loop or P-E loop for a device is a plot of the charge or polarisation (P) developed, against the field applied to that device (E) at a given frequency. The significance of this measurement can be easily understood by examining the P-E loops for some simple linear devices. The P-E loop for an ideal linear capacitor is a straight line whose gradient is proportional to the capacitance since current leads voltage by 90^0 and thus integral of current with time which is charge is in phase with voltage. In a resistor, charge and current being in phase, P E loop is circular in shape. Ferroelectric materials possess regions with uniform polarization called ferroelectric domains. Within a domain, all the electric dipoles are aligned in the same direction. A very strong field could lead to the reversal of the polarization in the domain, known as domain switching. The polarization reversal can be observed by measuring the ferroelectric hysteresis.

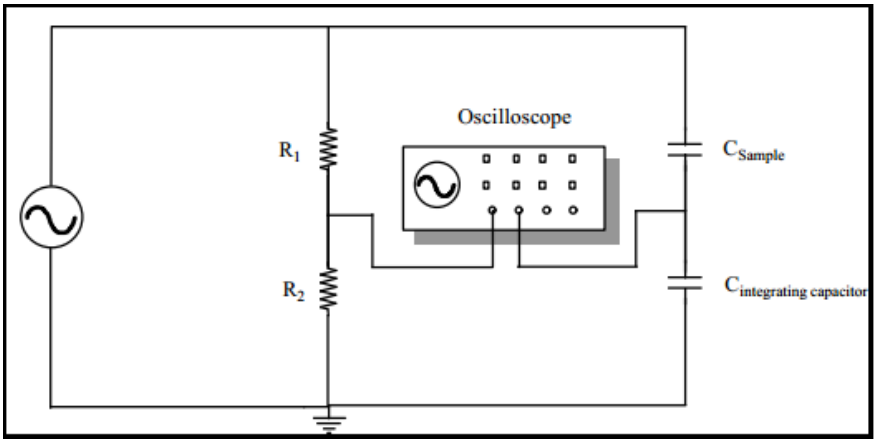

Figure 3.12: Sawyer Tower circuit for P-E loop measurement

Working principle of Ferroelectric loop tracer is based on conventional Sawyer Tower circuit as shown in figure 3.12. A high voltage oscillator produces an adjustable sinusoidal output from 0 to 350V (RMS). The frequency is variable in a small range around 30Hz. The oscillator output is applied to the dielectric sample kept in a temperature-controlled oven. Due to the large amplitude of the alternating source, the dielectric material exhibits a hysteresis loop similar to that observed in a ferro-magnetic material under the influence of an alternating magnetic field. The loop can be displayed on a CRO with the help of a circuit, which basically monitors the charge flow through the sample and plots it against the voltage applied on it [27]. P-E loop is the characteristic of a ferroelectric response.

References

[1] Venkatesan, T., and Steven M. Green, The industrial physicist, **2**, 3, 22-24, (1996).

[2] Andor, an Oxford Instruments company, http://www.andor.com/learning-academy/pulsed- laser-deposition-an-introduction-to- pulsed-laser-deposition.

[3] Yves Pauleau, Chemical Physics of Thin Film Deposition Processes for Micro- and Nanotechnologies, Kluwer Academic publishers, Netherlands (2002).

[4] C. Barry Carter, M. Grant Norton, Ceramic Materials: Science and Engineering, Springer, New York (2007).

[5] Milton Ohring, Materials Science of Thin Films, 2nd edn., Academic press, Santiago, USA (2002).

[6] John Venables, Introduction to Surface and Thin Film Processes, Press Syndicate of the University of Cambridge, United Kingdom (2000).

[7] Scintag, Inc., Chapter 7, Basics of X-ray diffraction, www.scintag.com.

[8] Kittel, C. Introduction to solid state physics, John-Wiley &Sons, New York (1997).

[9] C. Suryanarayana, M. Grant Norton, X-Ray Diffraction: A Practical Approach, Plenum press, Springer, New York (1998).

[10] H. M. Rietveld J. Appl. Crystallogr., **2** (2), 65–71 (1969).

[11] Full Prof manual, http://www.psi.ch/lns-diffraction/MacEN/fullprof-manual.pdf.

[12] C. Richard Brundle, Charles A. Evans Jr., Shaun Wilson, Encyclopedia of Materials Characterization, surfaces, Interfaces, thin

films, Manning Publications Co.Reed Publishing, USA (1992).

[13] Watt, M. The principle and practise of electron microscopy, Cambridge Uni. Press, Cambridge (1997).

[14] Greg Haugstad, Atomic Force Microscopy: Understanding Basic Modes and Advanced Applications, John Wiley & sons, New Jersey (2012).

[15] Binning, G.; Quate, c. F.; Gerber, C. Phy. Rev. Lett., **56,** 9,930 (1986).

[16] W. Richard Bowen, Nidal Hilal, Atomic Force Microscopy in Process Engineering: An Introduction to AFM for improved processes and products, Butterworth Heinmann, USA (2009).

[17] T.N. Narayanan, Ph.D. thesis, Department of Physics, Cochin University of Science and Technology (2010).

[18] Swapna S. Nair, Ph.D. thesis, Department of Physics, Cochin University of Science and Technology (2006).

[19] Simon Foner, Rev. Sci. Instrum. **30**, 548 (1959).

[20] John Clarke, Alex I. Braginski, The SQUID Handbook: Fundamentals and Technology of SQUIDs and SQUID systems, John Wiley & sons, Germany (2004).

[21] David J. Sellmyer, Yi Liu, D. Shindo, Handbook of Advanced magnetic materials, volume 1: Advanced magnetic materials Nanostructural effects, Tsinghua university press, Springer

[22] PPMS, Quantum Design, California, Rev 8.04, http://www.qdusa.com/sitedocs/productBrochures/heatcapacity-he3.pdf

[23] John. C. Vickerman, Surface analysis – the principal techniques, John Wiley & Sons (1997).

[24] Casa XPS software manual, Casa Software Ltd.(2008) www.casaxps.com.

[25] G. Srinivasan, Ann. Rev. Mater. Res., **40**,153 (2010).

[26] Practical session: Ferromagnetic resonance, www.uam.es/personal.../guion_FMR_ingles.pdf

[27] M. Stewart & M. G. Cain, Ferroelectric Hysteresis, Measurement & Analysis, NPL Report CMMT(A) 152 (1999).

CHAPTER 4

On Magnetic Ordering in Sodium Substituted Hole doped Lanthanum Manganites

This chapter deals with the synthesis and characterization of bulk samples of sodium substituted lanthanum manganites. Lanthanum manganites with sodium concentrations varying from 50 to 90 percent in steps of 10 percent were prepared using modified citrate gel method. These samples are subjected to structural studies using X-ray Diffraction and fine structure refinement using Rietveld method. Magnetic characterization of the samples are carried out using Vibrating Sample Magnetometer, and Magnetization versus Temperature measurements including Field cooled and Zero Field cooled measurements using SQUID magnetometer. Surface analysis of samples is carried out using X-ray Photoelectron Spectroscopy. Ferromagnetic resonance studies are also carried out to probe the frequency dependence of magnetization.

Sethulakshmi et al., (submitted to JOURNAL OF MAGNETISM AND MAGNETIC MATERIALS)

4.1. 1ntroduction

Manganites are perceived as a store house of rich and fascinating physics where charge, spin and lattice degrees of freedom play decisive role and there exists close correlation between them. Structural, magnetic as well as electric transport properties and their interdependence make manganites suitable for potential applications. A variey of interesting phenomena like colossal magneto – resistance (CMR), metal - insulator transition, dielectric response, ferro/antiferro magnetic ordering, coexistent magnetism, charge ordering or spin glass state has been exhibited by manganites. It is established that substitutions at A sites (in $AMnO_3$) by divalent or trivalent ions render mixed valence states of Mn ions and charge carriers in the crystal lattice. Most of the properties are entangled to these charge carriers which is a unique feature of manganites [1-3].

There are numerous investigations carried out on $AMnO_3$ systems with A sites substituted with trivalent rare earth elements like La, Pr, Nd, or Gd and divalent substitutions like Ca, Sr, Pb or Ba. Lanthanum manganites with lanthanum (La) ions for A sites are one of the prominent members of these series. Properties of these materials are dependent on the nature of substitution, their concentration and are also influenced by temperature dependent structural phase transitions [4-7]. In addition to divalent and trivalent substitutions, monovalent ion for La sites in manganites is another way of inducing mixed valency for manganese ions forming hole doped manganites. Reports exist in literature pertaining to

magnetic behaviour in $La_{1-x}Na_xMnO_3$ (LNMO) series with lower substitution levels of Na. However no reports could be found dealing with higher substitutions of Na beyond 40 percent. It is from this particular observation that we find compositions with Na substitutions from 50 to 90 percent will be of interest to the scientific community.

One of the difficulties in synthesizing these compositions is the upkeep of Na stoichiometry beacause of its volatility at high temperatures and hence their substitution leads to the formation of vacancies at lanthanum and oxygen sites in the lattice [8-16]. These vacancies also play a crucial role in determining the material properties including magnetic ordering. Preparation technique adopted for LNMO series plays a significant role in maintaining the desired composition of series. Hence adoption of an appropriate preparative technique which will maintain stoichiometry assume significance.

4.2. Method of Synthesis

Sodium substituted lanthanum manganite sample series ($La_{1-x}Na_xMnO_3$ with x=0.5, 0.6, 0.7, 0.8 and 0.9) were prepared using modified citrate gel method. Stoichiometric amounts of the precursors namely lanthanum oxide, manganese nitrate and sodium carbonate were dissolved in de - ionized water and an adequate amount of citric acid was added. An appropriate amount of nitric acid was added to the solution to convert all the constituents to nitrates and was heated at a temperature of 80^0C with continuous stirring; the solution boiled, frothed, turned dark and caught fire giving a spongy dark powder. The resultant powder was then fired at a temperature of 1100^0C for several hours. The synthesis was

carried out for Na composition ranging from 50 percent to 90 percent in steps of 10. Five samples were synthesized and the samples are coded as LNMO5, LNMO6, LNMO7, LNMO8 and LNMO9 corresponding to 50, 60, 70, 80 and 90 percent Na concentrations respectively.

4.3. Characterization

4.3.1. Structural Characterization using XRD and Rietveld Refinement

X-ray Diffraction (XRD) pattern of the synthesized bulk samples of LNMO series is shown in figure 4.1. XRD pattern correspond to distorted orthorhombic structure and the peaks are indexed in the figure 4.1. The characteristic peak of perovskite is observed at 2θ angle of 32^0. It may be noted here that monovalent ion substutution can result in distorted perovskite as suggested by Shimura et.al [17]. Orthorhombic structure is exhibited by higher Na substituted compositions of lanthanum manganites and is usually in a mixed state with rhombohedral phase for heavily doped samples [8]. Peaks are more clearly defined in LNMO5 sample and as Na concentration is increased, structural distortion is enhanced as indicated by the decreased intensity of peaks and shift in peak positions. Structural distortion is maximum for 90 percent substituted sample.

All the samples were subjected to rietveld refinement and the best fit is obtained for the LNMO5 sample. Rieteveld refinement for LNMO5 sample is depicted in figure 4.2. Rietveld refinement pattern for LNMO6 to LNMO9 samples are shown in figures 4.3(a), 4.3(b), 4.4(a) and 4.4(b) respectively which indicates that distortion increases with increase in Na concentration. All samples possess pbnm spacegroup and

with undoped lanthanum manganites with a = 5.5367 Å, b =5.7473 Å, and c = 7.6929 Å [18], a and b lattice parameters have contracted while there is an elongation along the c direction maintaining the relation $c/a < \sqrt{2}$ of O' orthorhombic for all the compositions of LNMO series.

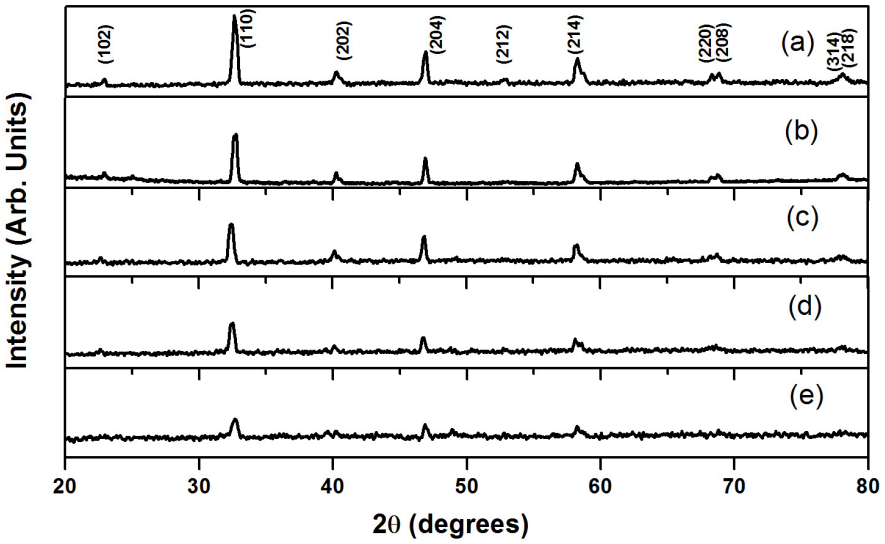

Figure 4.1: XRD patterns of LNMO samples

(a) LNMO5 (b) LNMO6 (c) LNMO7 (d) LNMO8 and (e) LNMO9

Variation of lattice parameters and unit cell volume with Na concentration is not systematic. Unit cell volume evaluated from the lattice parameters decreased for LNMO7 compared to LNMO6 and then increased for LNMO8 and LNMO9. The change in unit cell volume and lattice parameters in LNMO series can be attributed to structural changes due to a) difference in ionic radius of Mn^{3+} and Mn^{4+} and b) oxygen stoichiometry or presence of vacancies [12]. Variation of lattice parameters namely a, b and c with Na substitution is shown in figure 4.5 and parameters are tabulated in table 4.1.

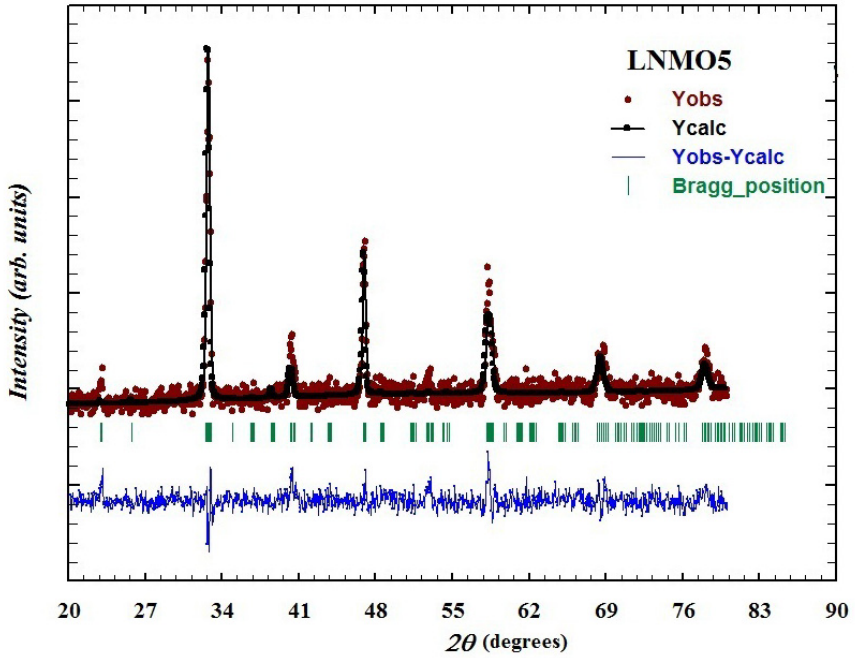

Figure 4.2: Rietveld refinement performed on LNMO5

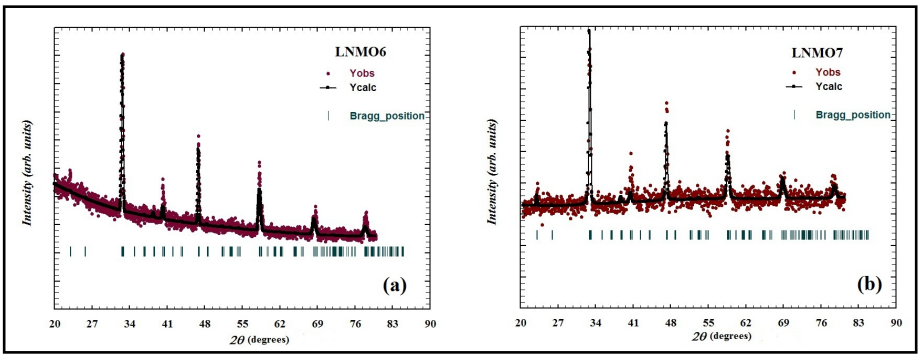

Figure 4.3: Rietveld refinement performed on (a) LNMO6 and (b) LNMO7

.

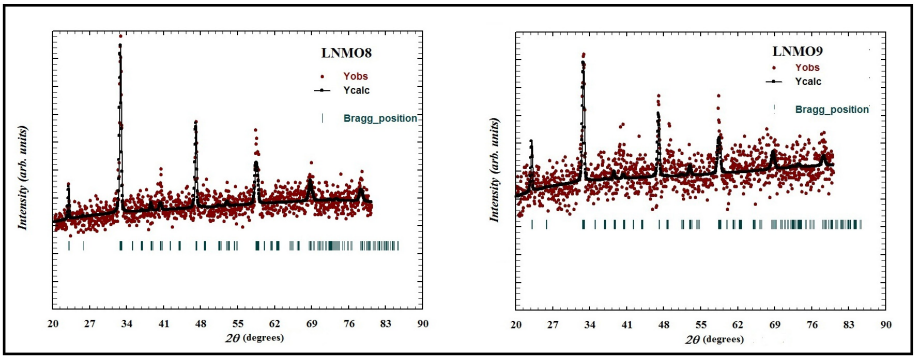

Figure 4.4: Rietveld refinement performed on (a) LNMO8 and (b) LNMO9

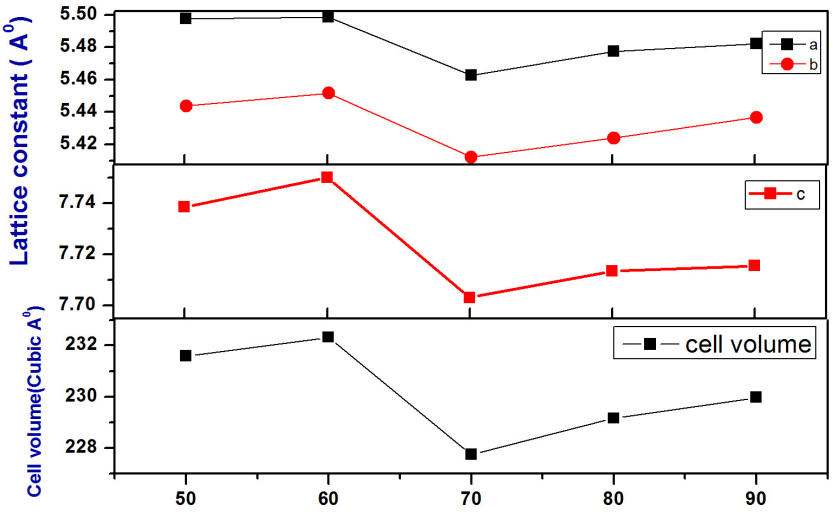

Figure 4.5: Variation of lattice parameters and cell volume with Na concentration. LNMO5 values are shown inside circle.

Sample code	Lattice parameters (A^0)			c/a	Unit cell volume (Cubic A^0)
	a	b	c		
LNMO5	5.4976± 0.0025	5.4436± 0.0025	7.7385± 0.0039	1.408	231.58
LNMO6	5.4986± 0.0014	5.4517± 0.0014	7.7501± 0.0022	1.409	232.32
LNMO7	5.4627± 0.0036	5.4121± 0.0035	7.7031± 0.0051	1.410	227.73
LNMO8	5.4774± 0.0047	5.4238± 0.0046	7.7135± 0.0065	1.408	229.15
LNMO9	5.4822± 0.0113	5.4366± 0.0109	7.7155± 0.0144	1.407	229.95

Table 4.1:. Table showing the lattice parameters and cell volume from rietveld refinement

4.3.2. Magnetic Characterization using VSM and FC/ZFC

Magnetic characterization at room temperature (at 300 K) using VSM (figure 4.6) showed that all samples exhibit a ferromagnetic ordering with nominal coercivity close to 10 Oe. LNMO recorded the highest saturation magnetization (M_S) of 34.4 emu/g. Since an orthorhombic unit cell of manganite system have four formula units, M_S

can be represented in bohr magnetons and the corresponding bohr magneton equivalent in LNMO5 is 1.37 μ_B/Mn. M-H isotherms with M_S in terms of emu/g and μ_B/Mn is depicted in figure 4.6(a) and 4.6(b) respectively. It is found that saturation magnetization decreased with increase in Na concentration and the lowest M_S of 0.34 μ_B /Mn is observed for LNMO9 sample. Saturation magnetization values of LNMO samples are shown in table 4.2.

It is observed from Field Cooled (FC) and Zero Field Cooled (ZFC) curves (figure 4.7) that in the low temperature region, both FC and ZFC curves of LNMO5 are found to be decreasing with decrease in temperature. Figure 4.8 shows FC ZFC curves for LNMO6 to LNMO9 samples. Bifurcation in FC and ZFC curves at low temperature and the small cusp like behaviour in ZFC near 300 K is observed in all samples, similar to LNMO5. At lower temperatures, FC plot for LNMO6 and LNMO7 are almost linear indicating ferromagnetic behaviour. However, for LNMO8 and LNMO9, FC plots appear to be deviating from the pattern followed by LNMO6 and LNMO7. There are earlier reports on doped lanthanum manganite systems where ZFC magnetization deviates from FC magnetization at low temperatures and such a trend of vanishing ZFC is indicative of a magnetic inhomogeneity possibly due to the presence of oxygen vacancies [19]. It is also observed that difference between the magnetization in FC and ZFC curves or magnetic inhomogeneity is found to be increasing with increase in Na concentration on approaching low temperatures. Magnetic property in manganites is closely associated with double exchange and superexchange mechanism between different valence Mn ions mainly Mn^{3+} and Mn^{4+}. Magnetic inhomogeneity can manifest either as a

coexistent antiferromagnetism (AFM) or resulting out of a spin glass behaviour. AFM spin interaction is expected between Mn^{3+} - O - Mn^{3+} or Mn^{4+} - O - Mn^{4+} pairs in LNMO. On first observation, it can be said that as Na concentration increases Mn^{4+} ion content also increases favouring antiferromagnetic alignment.

Thus ferromagnetism found in these compounds may have contributions arising from double exchange mechanism as well as from vacancy induced magnetic interactions which need to be investigated.

Yet another reason for the decreased double exchange ferromagnetic behaviour is the decreased mobility of e_g electrons [20] which can be due to two phenomena. LNMO samples possess pbnm spacegroup rather than the conventional R3c group as investigated earlier and for pbnm spacegroup, lattice distortion from MnO_6 octahedra deformation causes bending of Mn-O-Mn bond angle.

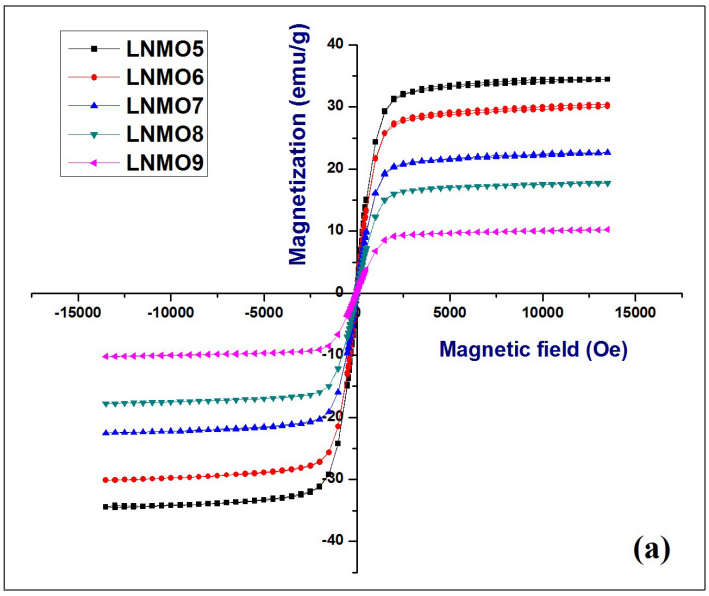

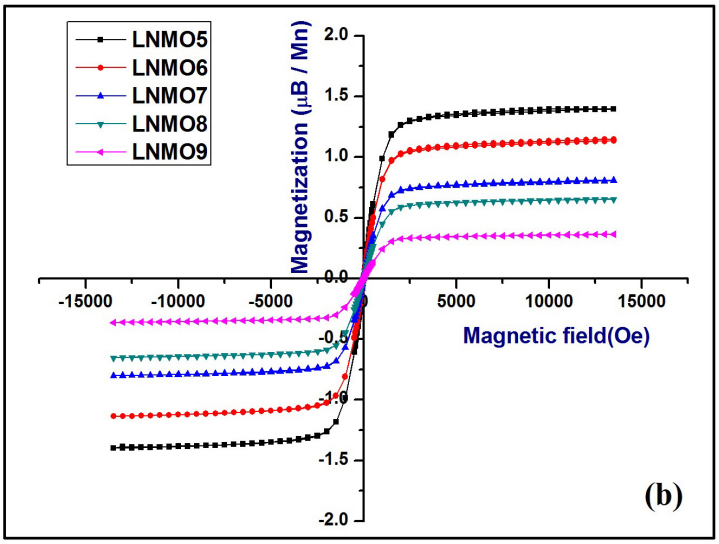

Figure 4.6: Ferromagnetic behaviour in LNMO samples at 300 K (a) Magnetization in emu/g (b) Magnetization in μ_B/Mn

Sample	M_S (emu/g)	M_S (μ_B/Mn)
LNMO5	34.4	1.37
LNMO6	29.5	1.08
LNMO7	22.4	0.76
LNMO8	17.6	0.62
LNMO9	10.1	0.34

Table 4.2: Table showing saturation magnetization values in LNMO samples

Bending of Mn-O-Mn bond angle results in narrowing of bandwidth which results in weak double exchange mechanism. Secondly, oxygen vacancies can result as point defects in lattice which act as trapping centers of charge carriers resulting in decreased mobility of e_g

electrons . Variation of ionic radii of La^{3+} and Na^{+} ions at A sites and high voltaility of monovalent ions are reported to have significant influence in oxygen stoichiometry and can also lead to vacancies in the lattice [21]. Oxygen vacancies also alter magnetic and structural properties of the material [16]. Thus it is to be assumed that the role of oxygen vacancies increases with increase in Na concentration**.** Hence it is reasonable to assume that the magnetism exhibited by LNMO series is a result of the co-existence of ferro/antiferro magnetic phase with dominant double exchange mechanism**.**

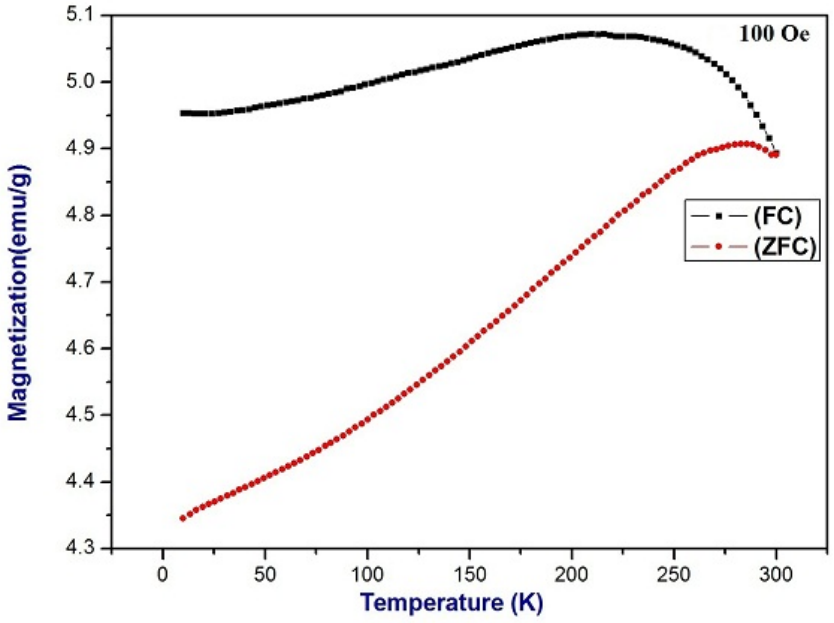

Figure 4.7: FC ZFC curves for LNMO5 sample

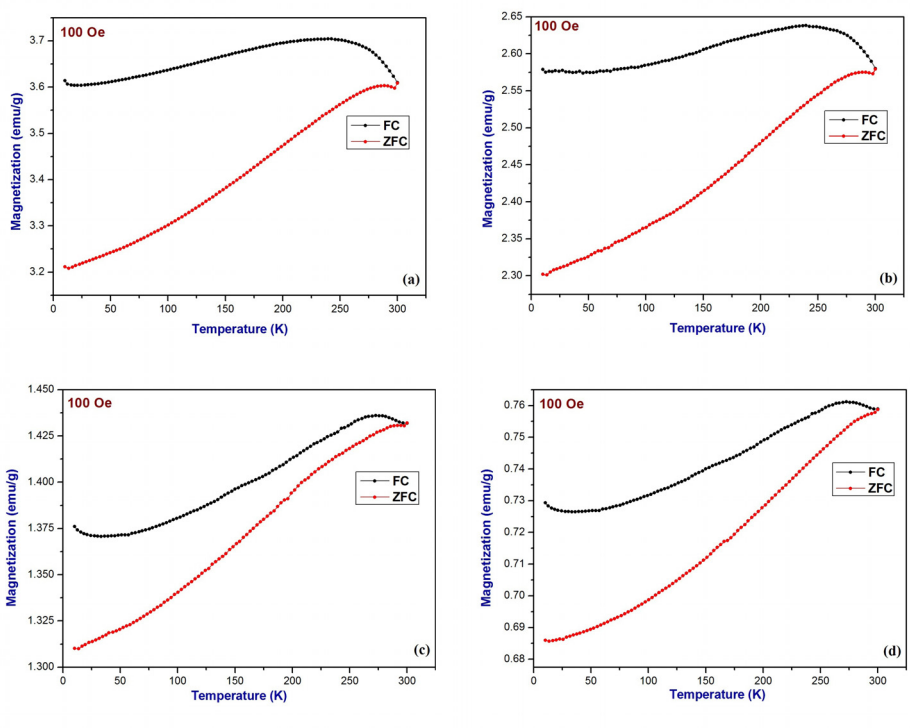

Figure 4.8: FC ZFC curves for different concentrations of Na in LNMO. (a) LNMO6 (b) LNMO7 (c) LNMO8 (d) LNMO9

For a thorough understanding of the magnetic nature, surface analysis techniques like X-ray Photoelectron Spectroscopy was utilized to determine valence states of Mn ions and their concentration.

4.3.3. Surface Analysis using XPS

X-ray Photoelectron Spectroscopy (XPS) is an ideal tool for ascertaining the surface structure and composition where the sensitivity extends to a few monolayers on the surface. Figure 4.9 deals with XPS survey scan of the representative element of the series, LNMO5, plotted with Binding energy (in eV) versus Intensity and

transitions corresponding to Na 1s, O 1s, La 3d, La 4d and Mn 2p are found in the recorded spectrum. Choosing LNMO5 as the representative sample of the series is justified by the fact that it is found to be possessing higher saturation magnetization as compared to other samples. For a thorough interpretation of the XPS data, a slow scan of the most intense peaks is recorded. The surface stoichiometry is also estimated from the XPS analysis and the ratio of La^{3+} and Na^{+} ions is found to be 1:1.

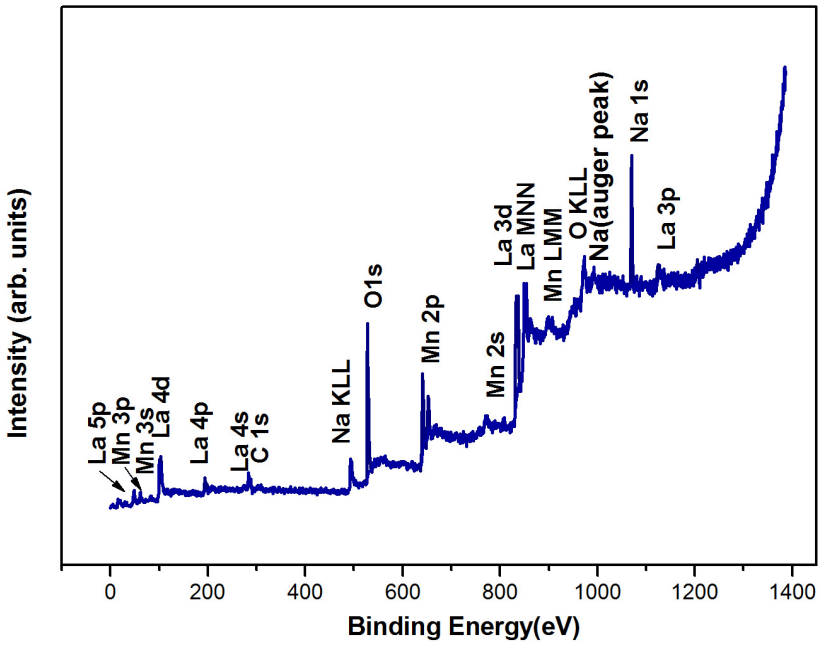

Figure 4.9: XPS survey scan of LNMO5

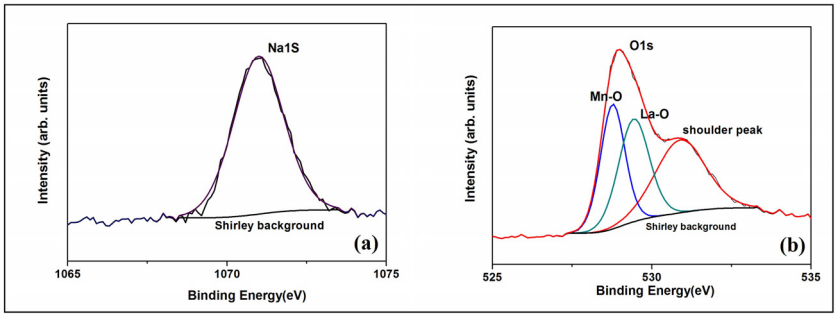

Figure 4.10: (a) Na 1s XPS spectrum (b) O 1s XPS spectrum of LNMO5

Figure 4.10(a) shows the XPS peak of Na in the higher binding energy side at 1070.98± 0.4eV with FWHM (full width at half maximum) of 1.85. The presence of single peak indicates that the Na ions exist only in single oxidation state of +1. Auger peak of Na KLL is at 495.27± 0.2 eV as shown in figure 4.9. An accurate interpretation of the oxygen peaks in manganites is rather difficult since the literature presents a lot of contradicting arguments [22, 23]. With the best fit adopted, oxygen peaks corresponding to O1s can be resolved into three components as shown in figure 4.10(b). Two major peaks observed at 528.77±0.2eV and 529.43±0.2eV applies to the earlier results on manganites system and are attributed to the bonding of oxygen ions with La and Mn ions simultaneously (i.e., La-O and Mn-O components respectively) [24,25]. Shoulder peak at 530.88±0.4eV is associated with contamination on the surface such as hydroxides. Peaks observed in the range of 830 eV – 860 eV is identified as peaks of doublets of La 3d: $La3d_{3/2}$ and $La3d_{1/2}$. Doublets find further splitting as reported earlier for various La compounds such as oxides, hydroxides and borates and are resolved into two peaks each necessitating a total of four peaks for a perfect Lorentzian - Gaussian curve fitting. For perfect fitting, two

parameters are chosen: (1) Area ratio of $La3d_{3/2}$ to $La3d_{5/2}$ peaks is fixed to be 2:3 which is the theoretical ratio for degeneracy between the two spin orbit components of 3d obitals (2) Full width at half maximum (FWHM) of both peaks are in the range 2.3 to 2.6.

Doublet splitting finds safe and clear explanation due to the presence of hole in La 3d configuration as well as from the impact of oxygen ligands [26]. Hole in La 3dcore level lowers the energy of 4f orbital below the Fermi level. Thus Lanthanum ions with configuration $3d^9 4f^0 L$ where L represents oxygen ligand acquires a final state configuration $3d^9 4f^1 \underline{L}$ when the empty f orbital accepts an electron from the lower energy valence p orbital of oxygen ligand with $\underline{L}$ denoting hole in the valence state of oxygen anion due to the transfer of electron to f orbital. Hence doublet structure in $3d_{5/2}$ and $3d_{3/2}$ with an energy gap of 16.8eV accounts for two configurations $3d^9 4f^0 L$ (lower BE peak) and $3d^9 4f^1 \underline{L}$ (higher BE satellite). For $La3d_{5/2}$, lower BE peak corresponding to $3d^9 4f^0 L$ is observed at 833.74±0.8eV and higher BE satellite corresponding to $3d^9 4f^1 \underline{L}$ is observed at 837.57±1.1eV as shown in figure 4.11. The aforementioned peak distribution for the two states of La holds also for La $3d_{3/2}$ with peak at lower binding energy 850.45±0.9eV as $3d^9 4f^0 L$ and 854.29±1.5eV as $3d^9 4f^1 \underline{L}$ state [27, 28]. In addition, La 4d peaks with $La4d_{5/2}$ peak at 101.54±1.1eV with satellite peak at 106.63±1.1eV and $La4d_{3/2}$ peak at 104.46±0.8eV as shown in figure 4.12 is also in good agreement with earlier results [29,30].

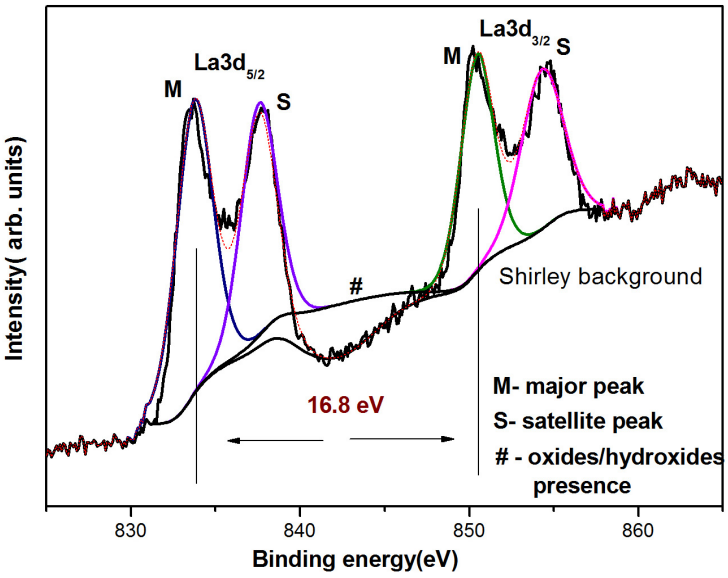

Figure 4.11: La3d XPS spectrumof LNMO5

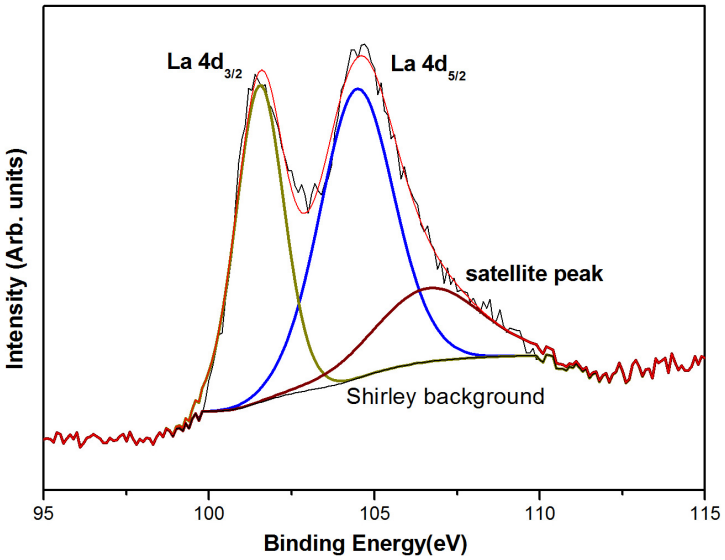

Figure 4.12: La4d XPS spectrumof LNMO5

Manganese peak analysis is the central part of the XPS analysis in manganites as magnetism owes its origin to the oxidation states of Mn. Binding energy range of 640-660 eV corresponds to Manganese 2p peaks.

In curve fitting, following two parameters are chosen:

(1) Area ratio of $Mn2p_{1/2}$ to $Mn2p_{3/2}$ peaks is fixed to be 1:2 corresponding to theoretical ratio for degeneracy between the two spin orbit components of p obitals

(2) A range of 3.0 to 3.2 is applied to FWHM.

Mn2p doublet peaks corresponding to $Mn2p_{1/2}$ and $Mn2p_{3/2}$ are observed with an energy gap of 12 eV [31]. Peak fitting of Mn2p peaks gives a signature of mixed valence state. $Mn2p_{3/2}$ peaks are resolved into two: one at 641.98±0.9eV and other at 644.53±2.1 eV as shown in figure 4.13. Separating the peaks for different valence states of Mn is a tedious task as most of the peaks overlap. But from an analysis of the results published so far it is observed that Mn^{2+} peaks are at lower binding energy than $Mn^{3+}$and Mn^{4+} states, and the Mn^{3+} peaks are assigned with a specific binding energy value of 641.7 eV [32-35]. In our results, peak at 641.98±0.9eV is confirmed to be due to Mn^{3+} ions and thus peak at 644.53±2.1 eV is due to Mn^{4+} ions.

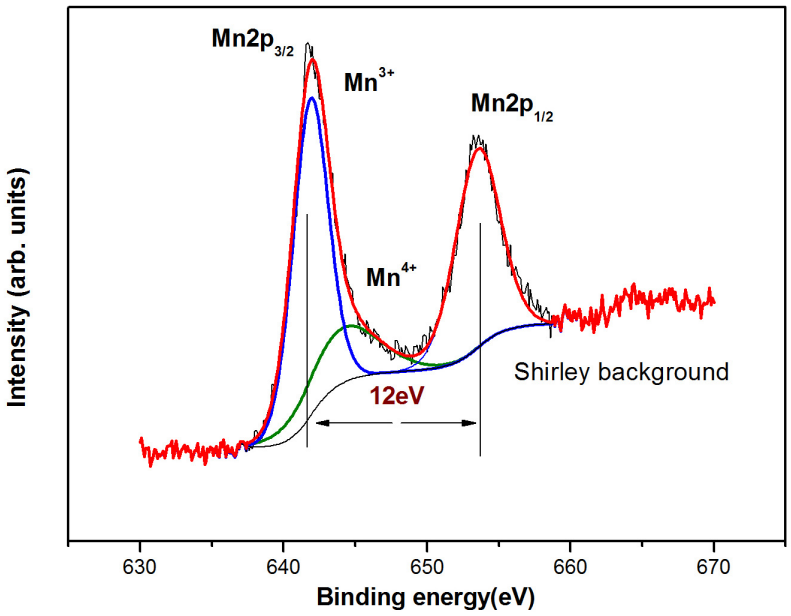

Figure 4.13: Mn2p XPS spectrumof LNMO5

From a detailed analysis of XPS spectra of the LNMO series, $2p_{1/2}$ and $2p_{3/2}$ peaks of Mn ions are analysed to determine the valence states of Mn and their concentration. Figure 4.14 shows Mn 2p peaks of the remaining members of the sample series. i.e from LNMO6 to LNMO9 and it is observed that Mn^{4+} peak is dominating with increase in Na concentration at the expense of Mn^{3+} peak . The concentration of Mn^{3+} and Mn^{4+} ions in LNMO5 to 9 samples are tabulated in table 4.3. It can be seen that amount of Mn^{3+} ions is larger than Mn^{4+} ions for LNMO5 and LNMO6; thereon ratio of Mn^{4+}/Mn^{3+} increases with Na substitution. For LNMO7 and LNMO8 Mn^{4+}/Mn^{3+} ratio reaches close to 0.5 and further Na substitution corresponding to sample LNMO9 results in Mn^{4+} ions exceeding Mn^{3+} ions. Mn^{4+}/Mn^{3+} ratio observed in LNMO sample series is shown in Table 4.4. The observed Mn^{4+}/Mn^{4+} ratio of the series are

different from the expected values. It is known that undoped lanthanum manganite consists of Mn ions with +3 oxidation state and is an AFM insulator. Substituting La sites with Na ions results in the conversion of some of Mn^{3+} ions to Mn^{4+} ions**.** Replacement of Na for La could result in the formation of Mn^{4+} ions and more than 50 percent replacement imply that most of the ions are Mn^{4+} . But XPS spectra of LNMO5 shows larger contribution of Mn^{3+} ions which suggests that Na is not capable of fully replacing 50 percent La sites even though ratio of La: Na is 1:1 in the compound and hence a small fraction of Na remains in the material as Na itself or in oxide form as evident from the XPS spectra of Mn and Na ions. These are clear evidences suggesting the presence of oxygen vacancies. There are earlier reports dealing with La-Na MnO_3 systems indicating that larger Na substitution can lead to vacancies in La and O^{2-} sites. But a systematic decrease in magnetization with Na substitution provides the information that with increase in Na concentration there is indeed increase in La substitution by Na even though the desired level of substitution is not reached**.** Thus LNMO represent an excellent system showing dependence of structural and magnetic properties on monovalent content, mixed valence ions and oxygen vacancies.

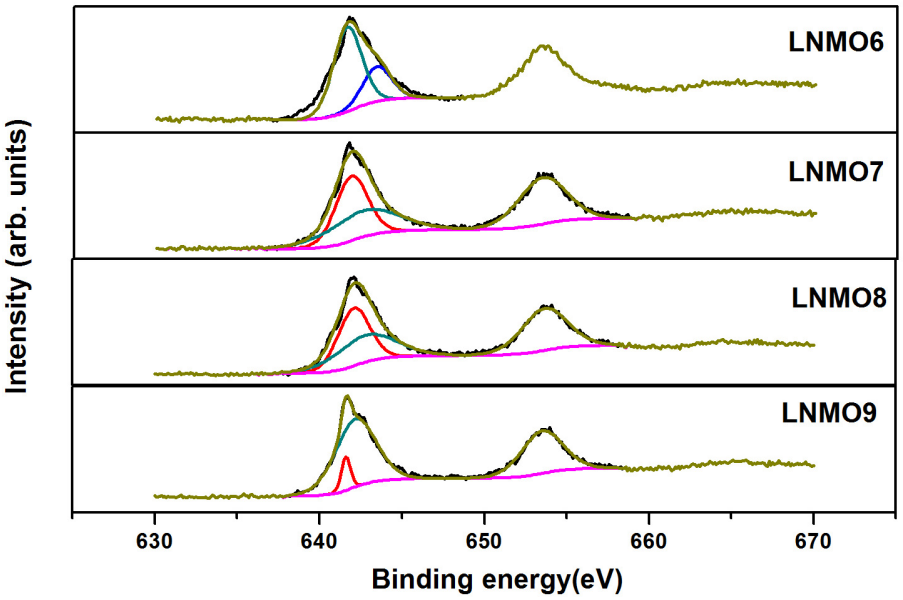

Figure 4.14: Mn 2p peaks in LNMO6, LNMO7, LNMO8 and LNMO9

Sample Name	Mn^{3+} concentration	Mn^{4+} concentration
LNMO5	0.895	0.105
LNMO6	0.879	0.121
LNMO7	0.699	0.301
LNMO8	0.697	0.303
LNMO9	0.428	0.572

Table 4.3: Table showing concentration of Mn^{4+} and Mn^{3+} ions in LNMO samples

Sample	Mn^{4+}/Mn^{3+} ratio
LNMO5	**0.117**
LNMO6	**0.138**
LNMO7	**0.431**
LNMO8	**0.435**
LNMO9	**1.336**

Table 4.4: Table showing Mn^{4+}/Mn^{3+} ratio of LNMO samples

Hence it can be estalished that magnetic inhomogeneity is present in LNMO as coexisting ferromagnetic and antiferromagnetic phases. Ferromagnetism dominates for lower Na concentrations in $LaMnO_3$ but on increasing Na concentration, antiferromagnetism is preferred. Magnetization of ferromagnetic materials can be analyzed using ferromagnetic resonance (FMR) studies which records the response of magnetization with respect to frequency. Thus samples in LNMO series were subjected to FMR studies.

4.3.4. Ferromagnetic Resonance Studies

Ferromagnetic resonance spectroscopy is an excellent characteristic tool for ferromagnetic materials. Magnetization arising from the magnetic domains precesses at about a particular frequency due to the torque provided by the external magnetic field. The precession frequency is dependent on the macroscopic magnetization of the sample, its orientation and magnetic field strength. In ferromagnetic resonance studies incorporated with network analyzers, the complex reflection

coefficient through the scattering matrix denoted by S11 is plotted against frequency. Such an FMR spectrum for LNMO series is indicated in figure 4.15. In the absorption spectra of pure ferromagnetic materials, generally two modes are present: acoustic and optic. In the case of LNMO samples, only a broad absorption around 6.5GHz with an approximate line width of 1.7 GHz is observed. Perfect ferromagnetic behaviour is reflected as a clear and sharp absorption at a particular frequency. Thus broad absorption and larger line width indicate magnetic inhomogeneity [36]. Thus FMR studies establish that LNMO samples are not purely ferromagnetic. This observation compliments with our early findings using VSM and XPS

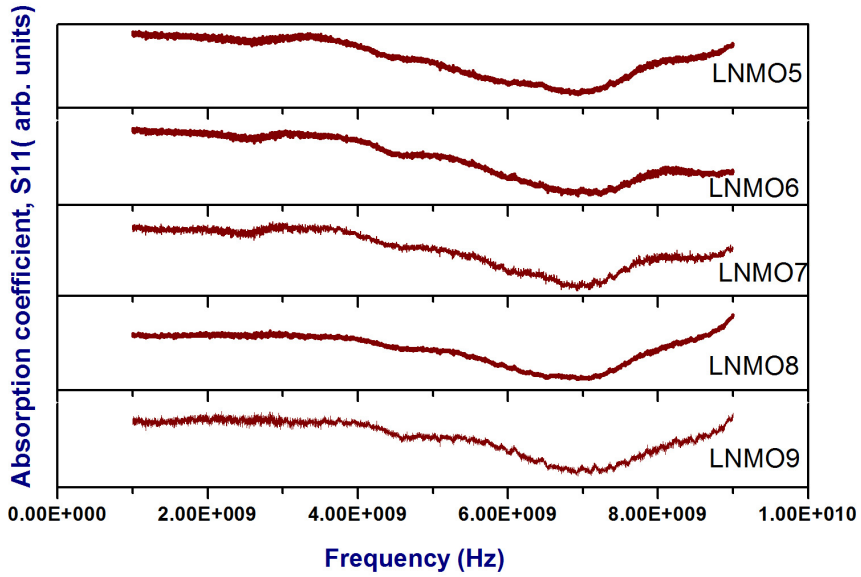

Figure 4.15: FMR spectra of LNMO samples

Conclusion

Sample series corresponding to 50 to 90 percent Na substitutions for La sites for LNMO were synthesized using modified citrate gel method and the structural characterization using XRD showed that all samples exhibited distorted orthorhombic structure with pbnm spacegroup. Lattice parameters evaluated from Rietveld refinement were utilized to evaluate cell volume and variation of cell volume with Na substitution was observed. All samples were found to be ferromagnetic at 300 K and the saturation magnetization decreased with increase in Na substitution. Magnetization vs temperature analysis corresponding to FC and ZFC plots was a proof for the coexistent antiferromagnetic behaviour with ferromagnetic ordering. Competing ferro/ antiferro magnetism were dependent on the ratio of Mn^{3+}/Mn^{4+} ions and the XPS analysis showed that Mn^{3+}/Mn^{4+} ratio decreased with increase in Na concentration. For the terminal sample in the series, LNMO9, it was found that Mn^{4+} ratio exceed Mn^{3+} and the antiferromagnetism dominates or have an upper hand over ferromagnetism. Disparity between the theoretical and calculated ratio of Mn^{4+}/Mn^{3+} indicate that desired Na substitution is not taking place even though stoichiometry is maintained. But change in properties with increase in Na content is indicative of increase in Na contribution at La sites. A significant and systematic reduction in saturation magnetization is an evidence for the dominating antiferromagnetic ordering over ferromagnetism as Na concentration is increased. In effect, Magnetic ordering in Na doped Lanthanum manganites have contributions from double exchange/ super exchange

meachanisms and vacancy induced interactions from Lanthanum and oxygen site deficiencies. Ferromagnetic resonance studies also confirm the presence of a mixed magnetic phase in LNMO series.

References

[1] M. B. Salamon and M. Jaime, Rev. Mod. Phys.,**73**, 3 (2001).

[2] E.Pollert, S. Krupicka, and E. Kuzmicova, J. Phys. Chem. Solids, **43**,12, 1137-1145(1982).

[3] J.Volger , Physica **20**, 49-66 (1954).

[4] R.Von Helmholt, J.Wecker, B.Holzapfel, L.Schultz, , and K.Samwer, Phys. Rev. Lett.,**71**,14 (1993).

[5] K.Chahara, T.Ohno, M.Kasai, , and Y.Kozono, Appl. Phys. Lett. **63**, 1990 (1993).

[6] J. M. D. Coey, M. Viret, Adv.Phys., **48**, 2, 167-293 (1999)

[7] H. Arai, M. Machida: Catal. Today **35**, 27 (1997).

[8] S.Roy , Y.Q. Guo, S. Venkatesh and N.Ali , J. Phys.: Condens. Matter **13**, 9547 (2001).

[9] R. Thaljaoui, W. Boujelben, M. Pekała, K. Pekała, A. Cheikhrouhou, J Supercond. Nov. Magn**, 26**, 1625–1630 (2013).

[10] A. Das, M. Sahana, S.M. Yusuf, L. Madhav Rao, C. Shivakumara, M.S. Hegde, Mater. Res. Bull. **35**, 651–659 (2000).

[11] Y. Kalyana Lakshmi, P. Venugopal Reddy, Phys. Lett. A **375**, 1543–1547(2011).

[12] Y. Kalyana Lakshmi, G. Venkataiah and P. Venugopal Reddy, J. App. Phys.**106**, 023707 (2009).

[13] M.C. Mozzati, L. Malavasi, C.B. Azzoni, G. Flor, J. Magn. Magn. Mater, 272–276, 1579–1580 (2004).

[14] G. H. Rao, J. R. Sun, K. B¨arner and N. Hamad, J. Phys.: Condens. Matter **11,** 1523–1528 (1999).

[15] Newell R. Washburn, Angelica M. Stacya, Alan M. Portis, Appl. Phys. Lett. **70**, 1622(1997).

[16] A. I. Tovstolytkin, A. M. Pogorily, D. I. Podyalovskii , V. M. Kalita, A. F. Lozenko, P. O.Trotsenko, S. M. Ryabchenko, A. G. Belous, O. I. V'yunov and O. Z. Yanchevskii, J. Appl. Phys. **102**, 063902 (2007).

[17] Tetsuo Shimura, Toshimasa Hayashi, Yoshiyuki Inaguma, and Mitsuru Itoh, J. Solid State Chem, **124,** 250–263 (1996).

[18] J. Rodríguez-Carvajal, M. Hennion, F. Moussa and A. H. Moudden Phys. Rev. B, 57 (6) R3189 (1998).

[19] Lorenzo Malavasi, Maria Cristina Mozzati, Carlo B. Azzoni, Gaetano Chiodelli, Giorgio Flor, Solid State Commun, **123**, 321–326 (2002).

[20] Y. Kalyana Lakshmi, G. Venkataiah, M. Vithal, P. Venugopal Reddy,_Physica B, **403**, 3059–3066 (2008).

[21] S. L. Ye, W. H. Song, J. M. Dai, K. Y. Wang, S. G. Wang, and J. J. Dua, Y. P. Sun, J. Fang, J. L. Chen, and B. J. Gao, J. Appl. Phys., **90**, 6 (2001).

[22] J. Liang and H.-S. Weng, Ind. Eng. Chem. Res. **32**, 2563-2572 (1993).

[23] S. Ponce, M. A. Peña, and J. L. G. Fierro, Appl. Catal., B **24**, 193-205 (2000).

[24] O. I. Klyushnikov, V. V. Sal'nikov, and N. M. Bogdanovich, Inorg. Mater., **38**, 12,1284-1289(2002).

[25] Elke Beyreuther, Stefan Grafström, and Lukas M. Eng et al, Phys. Rev. B, **73**, 155425 (2006).

[26]. L. Perkins, M. Trenary, T. Tanaka, S. Otani , Surf. Sci, **423**, L222–L228 (1999).

[27] E. Talik , A. Novosselov , M. Kulpa , A. Pajaczkowska, J. Alloys Compd, **321**, 24– 26 (2001).

[28] Andrei Novosselov, Ewa Talik, Anna Pajaczkowska, J. Alloys Compd, **351**, 50-53(2003).

[29] M.F. Sunding, K. Hadidi, S. Diplas, O.M. Løvvik, T.E. Norby, A.E. Gunnaes, J.Electron. Spectrosc. Relat. Phenom. **184**, 399- 409 (2011).

[30] Wei-Yean Howng and R J. Thorn, Chem. Phys. Lett, **56**, 3 (1978).

[31] S. W. Han, J. D. Lee and K. H. Kim et al, J. Korean Phys. Soc. **40**, 3, 501-510 (2002).

[32] A. Santoni, G. Speranza, M. R. Mancini, F. Padella, L. Petrucci and S. Casadio, *J*. Phys.: Condens.Matter **11**, 3387–3393 (1999).

[33] P. Wang, L. Yao, M. Wang, W. Wu, J. Alloys Compd, **311**, 53–56(2000).

[34] S. Mickevicius, V. Bondarenka, S. Grebinskij,) Acta Phys. Pol., A **113** (2008). No. 3, Proceedings of the 13th International Symposium UFPS, Vilnius, Lithuania 2007

[35] L. Wang and J. Gao, J. Appl.Phys, **105**, 07E514 (2009).

[36] Bijoy K. Kuanr, M. Buchmeier, Daniel E. Bu¨rgler, and P. Gru¨nberg, J. Appl. Phys., 91,10 (2002).

CHAPTER 5

Estimation of Transition Temperature and Magnetic Entropy Change in Sodium Substituted Lanthanum Manganites

Magnetic measurements can be utilized for deducing various parameters dealing with structure, thermodynamics and magnetic moments. In this chapter, magnetic isotherms are utilized to generate Arrott plots for estimating the nature of magnetic transition in sodium substituted lanthanum manganites. Arrott plots are also utilized for predicting approximate magnetic transition temperature in these samples. Variation of transition temperature with sodium substitution is discussed in this chapter. Isotherms for a wide range of temperature are used to estimate magnetic entropy change in manganites. Adiabatic temperature change is evaluated from values of specific heat capacity and entropy change. Variation of entropy change with temperature and sodium substitution is also described in detail.

***Sethulakshmi et al., APPLIED PHYSICS LETTERS* 104, 092407 (2014)**

Sethulakshmi et al., (submitted to MATERIALS RESEARCH BULLETIN)

5.1. Introduction

Magnetic refrigeration is based on the phenomena of magnetocaloric effect (MCE) and the materials exhibiting such phenomena are called MCE materials. Reversible temperature change of a magnetic material in the presence or absence of magnetic field is defined as magnetocaloric effect. When a magnetic field is applied to a magnetic material, domains align ferromagnetically decreasing the magnetic entropy but providing a release of thermal energy leading to increase in temperature. Alternately, upon removal of the magnetic field, domains are oriented randomly which leads to cooling of the magnetic material. This type of temperature tunability does not require any compressor gas nor is toxic thereby providing an eco friendly system [1].

Lanthanum manganites (LMO) with ABO_3 structure and its derivatives have secured a prominent position in the MCE phenomenon as they possess high magnetic moments and are ferromagnetic in nature. Ferromagnetic (FM) to paramagnetic (PM) transition at high temperatures often coupled with metal-insulator transition in doped manganites directed the focus towards magnetic entropy studies and it has been proved successful [2, 3]. In $La_{0.67}Ca_{0.33}MnO_3$ ΔS_M of 1 $J.Kg^{-1}K^{-1}$ and that of 2 $J.Kg^{-1}K^{-1}$ was observed in $La_{0.87}Sr_{0.13}MnO_3$ under a field of 10 KOe [4, 5]. Highest ΔS_M of 8 $J.Kg^{-1}K^{-1}$ at around 250 K was found in $La_{0.7}Ca_{0.3}MnO_3$ under 2 T magnetic field [6]. Recently a ΔS_M of 5.15 $J.kg^{-1}K^{-1}$ corresponding to a magnetic field of 5 Tesla was reported for $La_{0.67}Sr_{0.33}MnO_3$ at 370 K [7]. Efforts are on to effectively utilize the tunability of magnetic properties of doped manganites in MCE for

developing manganites with high entropy values near room temperature. A possible concern in manganites is that their specific heat is higher and hence adiabatic temperature variation is smaller, but higher Curie temperature well above room temperatures can be of help as the adiabatic temperature change is proportional to temperature [7].

MCE behaviour for divalent and trivalent substitutions in manganites have already been discussed and reported [8]. The present work deals with above fifty percent monovalent ion Sodium (Na^{+}) substitution for La^{3+} sites in Lanthanum manganites (LMO) as no reports could be found pertaining to higher concentrations of Na at La sites possibly due to loss of Na during sintering process. Thus sodium doped lanthanum manganites (LNMO) are virgin compounds and hence evaluation of magnetic entropy change and associated adiabatic temperature change are of interest to scientific community.

Magnetic entropy change (ΔS_M) can be evaluated either from the variation of adiabatic temperature in the presence of a magnetic field or from the M-H isotherms at different temperatures. In this work, the second method using M-H isotherms was employed as adiabatic temperature measurement in manganites is rather difficult as stated earlier. Magnetic entropy change can be evaluated from the difference in area between the isotherms governed by equations 2.14 and 2.15 as described in chapter 2.

5.2. Method of Synthesis

Sodium substituted lanthanum manganite samples, $La_{1-x}Na_xMnO_3$ with x=0.5, 0.6, 0.7, 0.8 and 0.9 were synthesized using modified citrate gel method. Synthesis details are described in chapter 4.

5.3. Magnetic characterization

5.3.1. Magnetic isotherms and Arrott plots

Pre characterized samples belonging to the series LNMO ($La_{1-x}Na_xMnO_3$ with x=0.5, 0.6, 0.7, 0.8 and 0.9) were subjected to Magnetization vs. Magnetic field studies (i.e., M-H isotherms). M-H isotherms with magnetization expressed in Am^2/Kg for magnetic field variation ($\mu_0 H$) up to 5 Tesla for the temperature range 200 K to 300 K with a step of 20 K of LNMO5 is shown in figure 5.1. A saturation magnetization (M_s) of 54 Am^2/Kg is observed at 200 K and on increasing temperature to 300 K, M_s decreases steadily to 34 Am^2/Kg.

From M-H isotherms, Banerjee criterion has been utilized to determine the nature of magnetic transition in LNMO5. Thermodynamic theory for phase transitions first developed by Landau and Lifshitz [9,10] was later applied in ferromagnets for magnetic transitions near Curie point by Ginzburg as governed by the equation: $\alpha M + \beta M^3 = H$ where α and β are constants incorporating thermodynamic variables and magnetization [11].

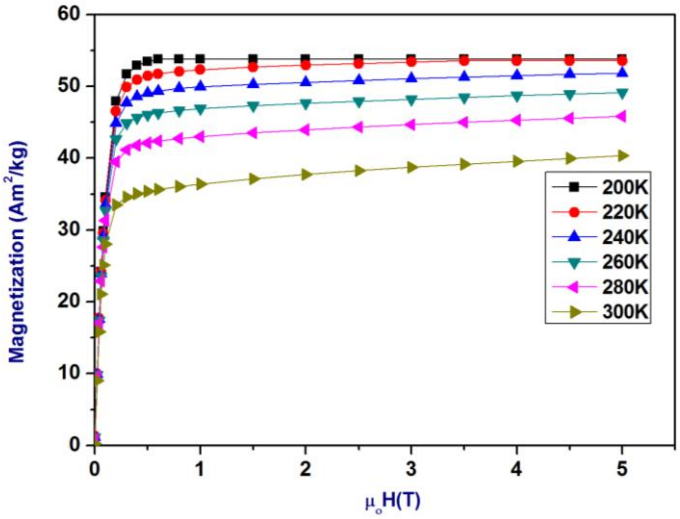

Figure 5.1: M-H isotherms of LNMO5 in the temperature range of 200 K to 300 K

Bean and Rodbell [12] suggested a theory for First order phase transition (FOPT) materials and later Banerjee combined all these existing theories into one and proposed a criterion for distinguishing between First order phase transition (FOPT) and Second order phase transition (SOPT) [13]. In order to test this criterion, Arrott plots are drawn with $\mu_0 H/M$ versus M^2 in the temperature range of 200 K to 300 K within the magnetic field range of 5 T. Arrott plots for LNMO5 sample is indicated in figure 5.2 where 5.2(a) shows Arrott plots in the temperature range of 200 K to 300 K. It is observed that Arrott plots are approaching a linear behaviour parallel to one another with increase in temperature. Thus positive slope of the curves confirm that the magnetic transition is of second order and the magnetic transition is above 300 K [13]. For a detailed investigation of the magnetic phase in manganites, M-H isotherms for the temperature range 303 K to 393 K with small steps of 10

K are analyzed for the maximum magnetic field of 1.35 T and Arrott plots plotted from these isotherms shows a parallel behaviour as observed in figure 5.2(b).

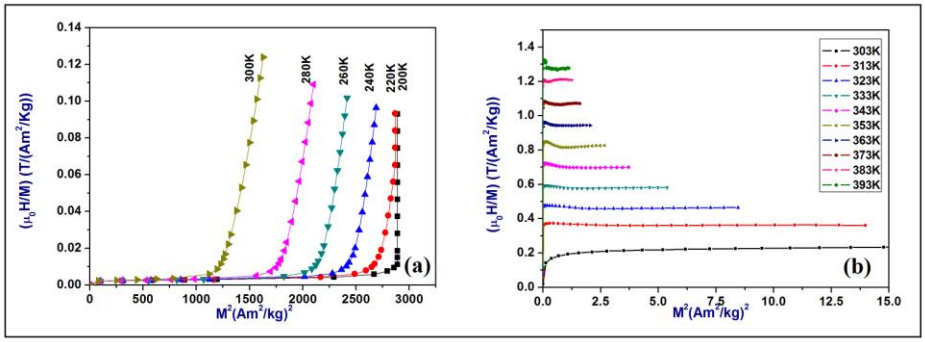

Figure 5.2: Arrott plots of LNMO5 (a) in the temperature range of 200 K to 300 K (b) in the temperature range of 303 K to 393 K

Arrott plots can also be utilized for determining the magnetic ordering temperature (T_C) range. From arrott plots depicted in figure 5.3 (figure 5.2(b) zoomed) for LNMO5, a linear line from the origin which is 45^0 inclined to both x and y axes are taken as reference line and the nearest curve for which the slope is less than the reference line is taken as T_C. Since the straight line in the case of LNMO5 is between 323 K and 333 K curves, only T_C range can be determined and it is within 323 K - 333 K. Magnetization vs. Temperature analysis of LNMO5 also shows transition temperature at 334 K as indicated in figure 5.4 which confirms the result.

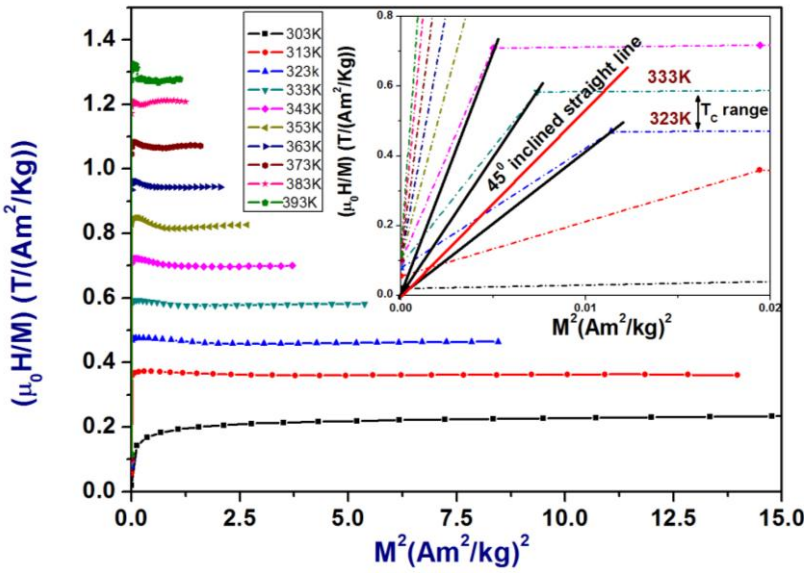

Figure 5.3: Determination of T_C of LNMO5 from M – H Isotherms using Arrott plots. T_C is found to be between 323 K and 333K

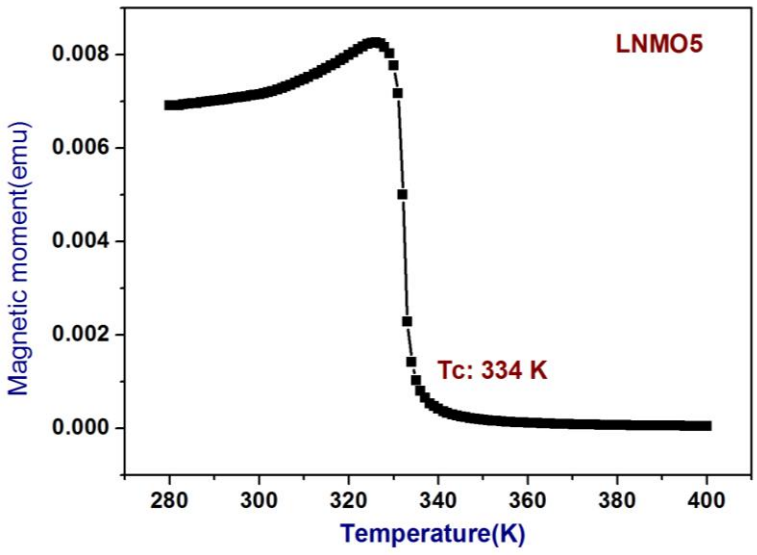

Figure 5.4: Magnetization vs. Temperature plot of LNMO5 in the temperature range of 280 K to 400 K at 30 Oe magnetic field

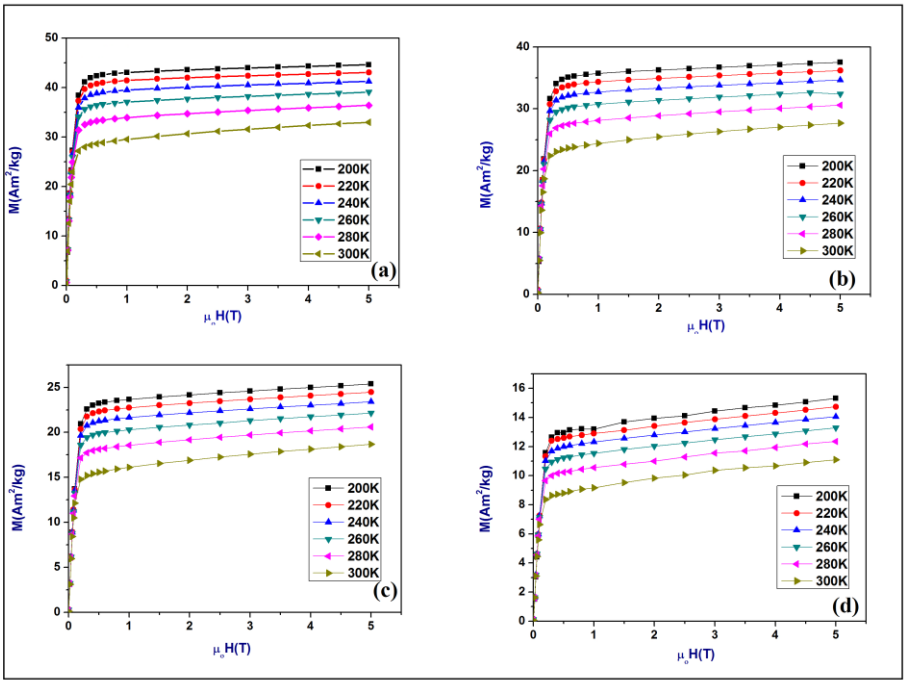

Figure 5.5: M-H Isotherms for LNMO samples. (a) to (d) LNMO6 to LNMO9

M-H isotherms of other members of the LNMO series from LNMO6 to LNMO9 is shown in figure 5.5. From the isotherms in the temperature range of 200 K to 300 K, it could be seen that all samples are ferromagnetic with a magnetic ordering temperature above 300 K. Arrott plots for LNMO6, LNMO7, LNMO8 and LNMO9 samples in the temperature range of 200 K to 300K and 303 K to 393 K are shown in figures 5.6, 5.7, 5.8 and 5.9 respectively. Similar linear behaviour is observed for all the samples of LNMO indicating a second order phase transition with a transition temperature above 300 K.

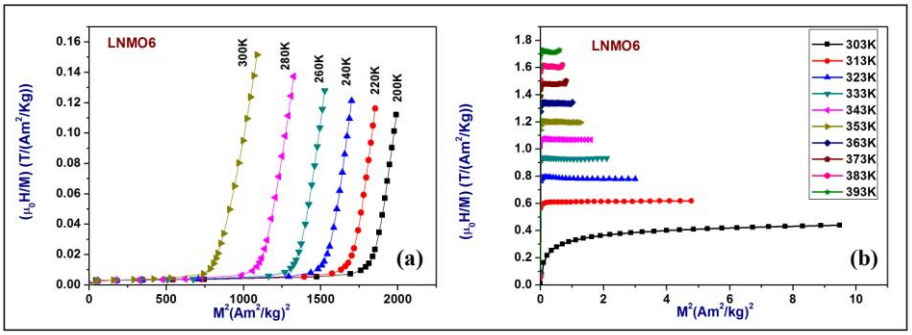

Figure 5.6: Arrott plots of LNMO6 (a) in the temperature range of 200 K to 300 K (b) in the temperature range of 303 K to 393 K

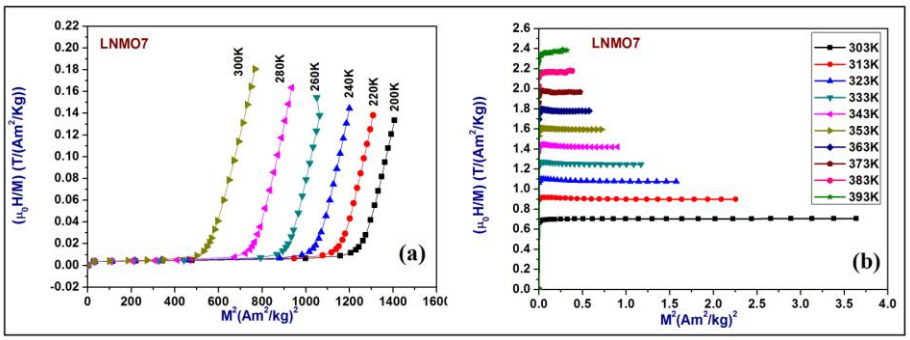

Figure 5.7: Arrott plots of LNMO7 (a) in the temperature range of 200 K to 300 K (b) in the temperature range of 303 K to 393 K

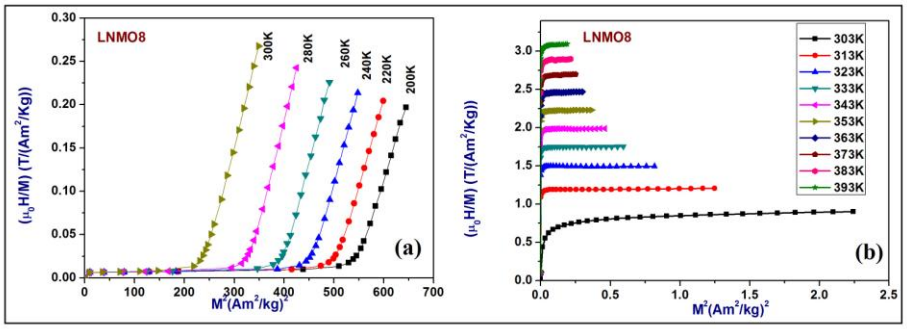

Figure 5.8: Arrott plots of LNMO8 (a) in the temperature range of 200 K to 300 K (b) in the temperature range of 303 K to 393 K

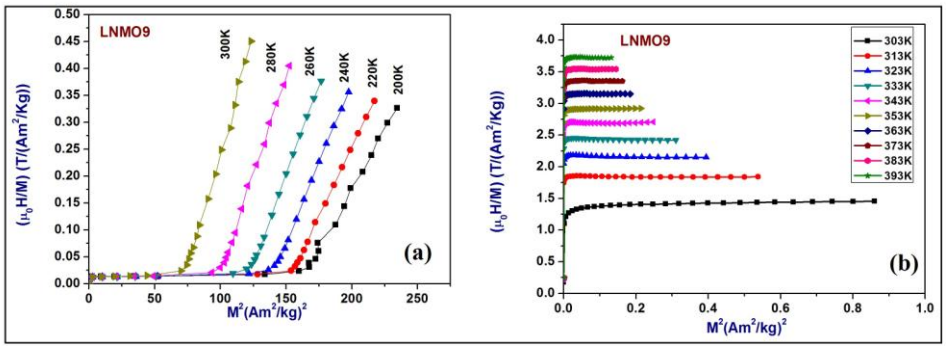

Figure 5.9: Arrott plots of LNMO9 (a) in the temperature range of 200 K to 300 K (b) in the temperature range of 303 K to 393 K

Evaluation of T_C in the case of LNMO6 is shown in figure 5.10. Since the curve below the reference line is of 323 K T_C is around 323 K. Magnetization vs. Temperature analysis also indicates T_C at around 323 K as seen in figure 5.11.

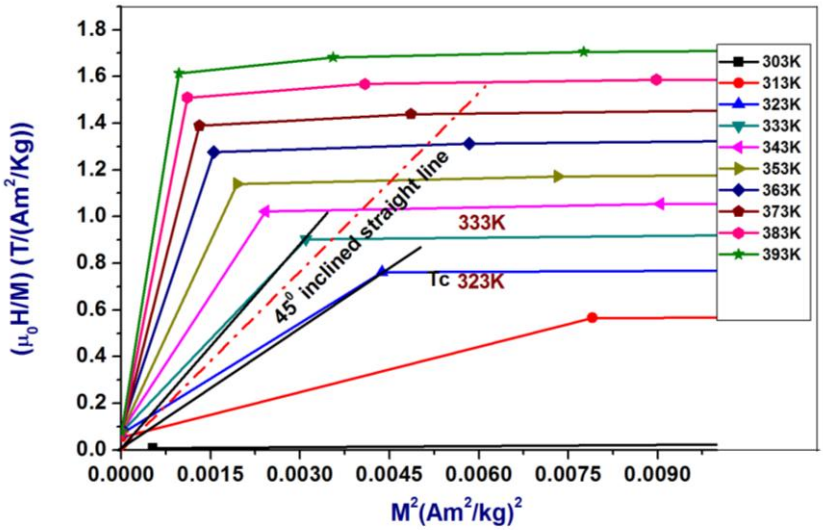

Figure 5.10: Determination of T_C range from M – H Isotherms of LNMO6; T_C is found to be at 323 K

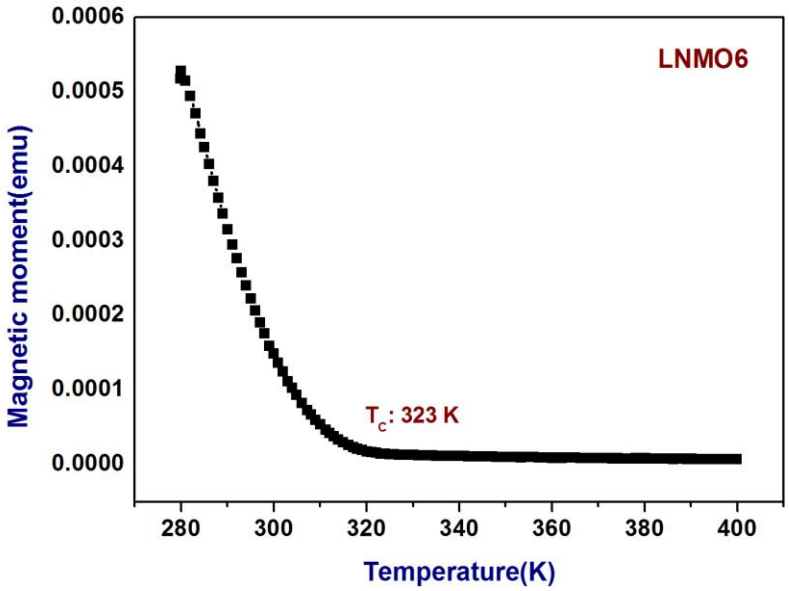

Figure 5.11: Magnetization vs. Temperature plot of LNMO6 in the temperature range of 280 K to 400 K at 30 Oe magnetic field

In the case of Arrott plots for LNMO7, the reference line passes between the two curves, 323 K and 313 K and hence in this case, only T_C range can be defined which is found to be between 313 K and 323 K (Figure 5.12 (a)). In the case of LNMO8 also, T_C is between 313 K and 303 K (Figure 5.12 (b)) and in LNMO9 T_C is found to be at 303 K (Figure 5.13). Although accurate estimation of T_C from Arrott plots is difficult, it can be established that there is considerable variation of T_C with Na doping. T_C is found to be decreasing with increase in Na doping as observed in monovalent substituted manganites [14]. Approximate T_C ranges are depicted in table 5.1.

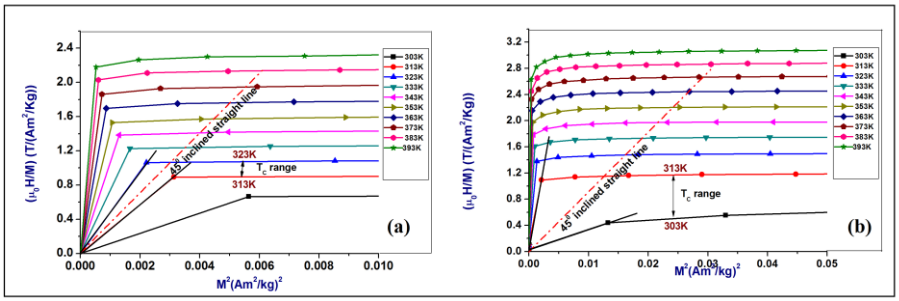

Figure 5.12: Determination of T_C range from M – H Isotherms of (a) LNMO7; T_C range is found to be between 323 K and 313 K (b) LNMO8; T_C range is found to be between 303 K and 313 K

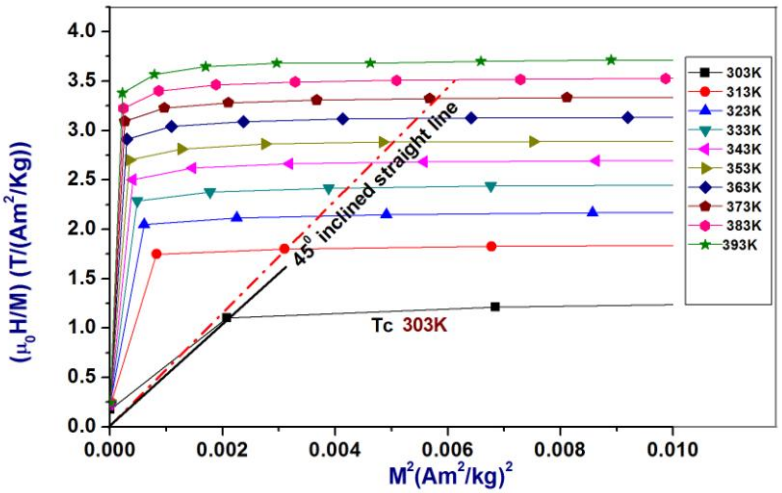

Figure 5.13: Determination of T_C range from M – H Isotherms of LNMO9; T_C at 303 K

Sample	T_C or T_C range (K)
LNMO5	**334**
LNMO6	**323**
LNMO7	**323-313**
LNMO8	**313-303**
LNMO9	**303**

Table 5.1: Table showing T_C range in LNMO samples

5.3.2. Estimation of Magnetic entropy change

For LNMO5, two sets of M-H isotherms, first one in the low temperature range of 200 K to 300 K and the second one within the range of 303 K to 393 K are utilized for calculating magnetic entropy. After determining the area between the adjacent curves from isotherms, magnetic entropy change, ΔS_M is evaluated using eqn (2.15) as given in chapter 2 [negative sign of entropy is excluded][10,11]. ΔS_M evaluated for dH (or ΔH) values of 0.5 T, 1 T, 2 T and 5 T from 200 K to 300 K is depicted in figure 5.14 [Inset]. It is observed that magnetic entropy increases with increase in dH thus establishing a linear dependence of entropy with magnetic field and a maximum entropy change of 1.5 $J.Kg^{-1}K^{-1}$ is found at 290 K for an applied magnetic field of 5 T. ΔS_M is also

found to be increasing with increase in temperature in the region of 200 K to 300 K. In order to determine the temperature range within which ΔS_M is maximum, second set of isotherms in the temperature range 303 K to 393 K dealing with small magnetic fields is considered. Also small steps of 10 K give more precise values of ΔS_M near transition temperature. Entropy values corresponding to magnetic fields of 0.5 T, 1 T, 1.15T, 1.25 T, 1.35 T has been plotted and the maximum entropy change of 0.12 $J.Kg^{-1}K^{-1}$ is observed for 1.35T for a temperature of 308 K in the case of LNMO5. Further, ΔS_M decreases with increase in temperature as evident from figure 5.14. Although two sets of isotherms consider two different field variations, it can be confirmed that the entropy approaches maximum values in the room temperature range.

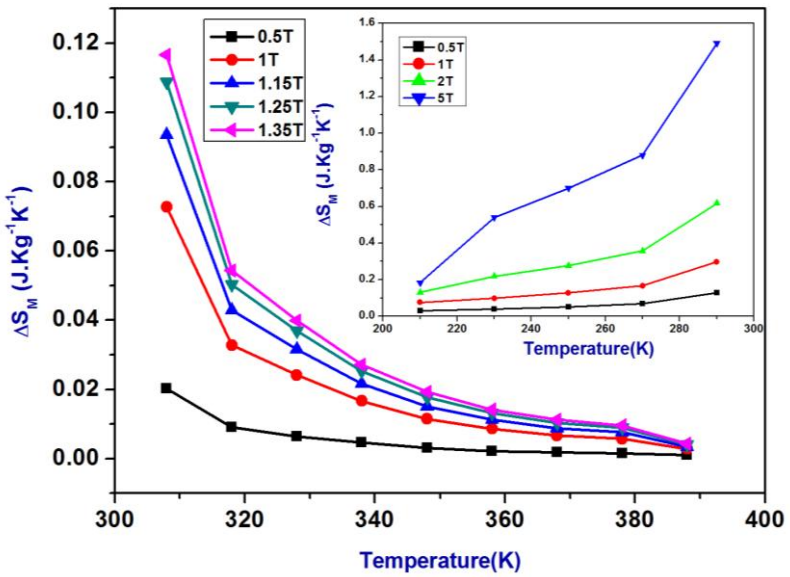

Figure 5.14: Variation of Magnetic entropy change (ΔS_M) for LNMO5 sample (a) in the temperature range of 303 K to 393 K (inset) in the temperature range of 200 K to 300 K

Magnetic isotherms of LNMO 6 to LNMO 9 were also analyzed and the magnetic entropy variation is estimated. Calculated ΔS_M (absolute values, i.e., sign of entropy are not considered) values for LNMO6 are shown in figure 5.15 (a) and (b). From figure 5.15 (a) it is observed that ΔS_M increases with an increase in temperature reaching a maximum of 1 $J.Kg^{-1}K^{-1}$ at 290 K and the entropy change increases with increase in external magnetic field. Entropy values for 0.5 T, 1 T, 2 T and 5 T follows a decreasing trend for a particular temperature. From figure 5.15(b), it can be found that ΔS_M is found to be decreasing from 308 K and reaches a minimum at 388 K. Thus the entropy variation is maximum in the temperature range of 250 K to 320 K. Entropy change at 308 K for 1.35 T magnetic fields is found to be 0.082 $J.Kg^{-1}K^{-1}$. Similarly, ΔS_M values for LNMO7 is also determined and is shown in figure 5.16 (a) for 0.5 T, 1 T, 2 T and 5 T in the temperature range of 200 K to 300 K which also shows a decreasing trend with increase in temperature with a maximum ΔS_M of 0.82 $J.Kg^{-1}K^{-1}$ for 5 T magnetic field. For LNMO7, a maximum ΔS_M of 0.028 $J.Kg^{-1}K^{-1}$is observed for 1.35 T as analyzed from isotherms in the high temperature range 303 K to 393 K (figure 5.16(b)). LNMO8 and LNMO9 recorded a maximum ΔS_M of 0.55 $J.Kg^{-1}K^{-1}$ and 0.32 $J.Kg^{-1}K^{-1}$ respectively for 5 T magnetic fields (figure 5.17 (a) and figure 5.18 (a)). In the high temperature range LNMO8 and LNMO9 possessed a ΔS_M of 0.033 $J.Kg^{-1}K^{-1}$ and 0.015 $J.Kg^{-1}K^{-1}$ for 1.35 T magnetic field (figure 5.17(b) and 5.18 (b)) respectively.

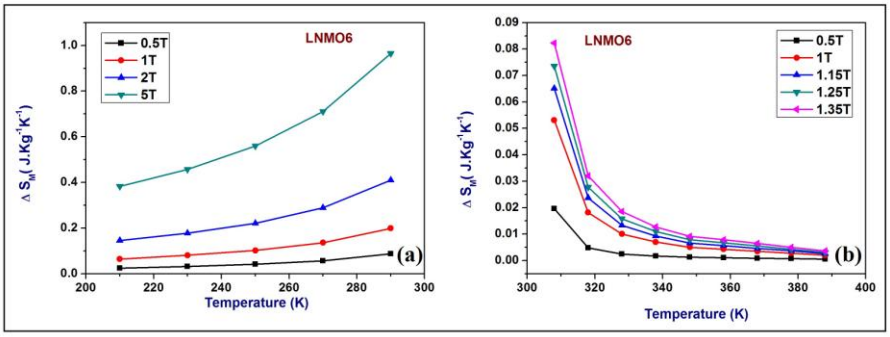

Figure 5.15: Variation of Magnetic entropy change (ΔS_M) for LNMO6 sample (a) in the temperature range of 200 K to 300 K (b) in the temperature range of 303 K to 393 K

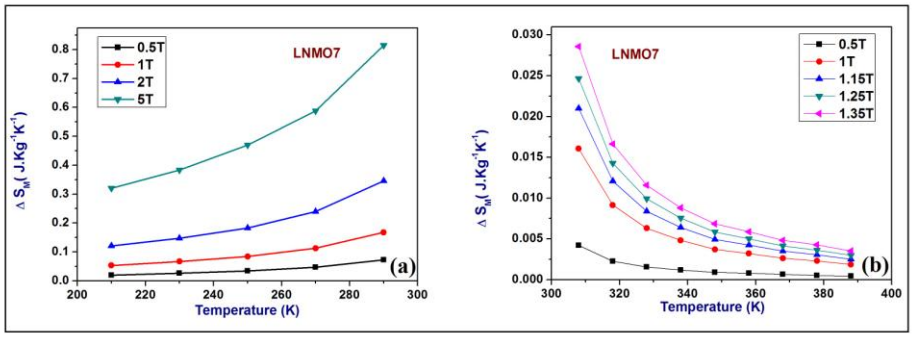

Figure 5.16: Variation of Magnetic entropy change (ΔS_M) for LNMO7 sample (a) in the temperature range of 200 K to 300 K (b) in the temperature range of 303 K to 393 K

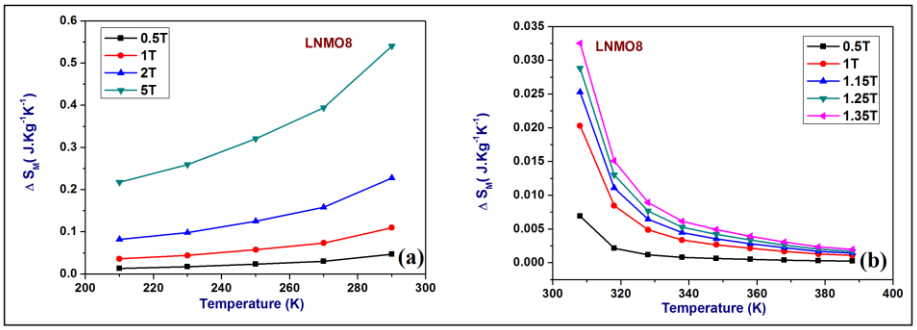

Figure 5.17: Variation of Magnetic entropy change (ΔS_M) for LNMO8 sample (a) in the temperature range of 200 K to 300 K (b) in the temperature range of 303 K to 393 K

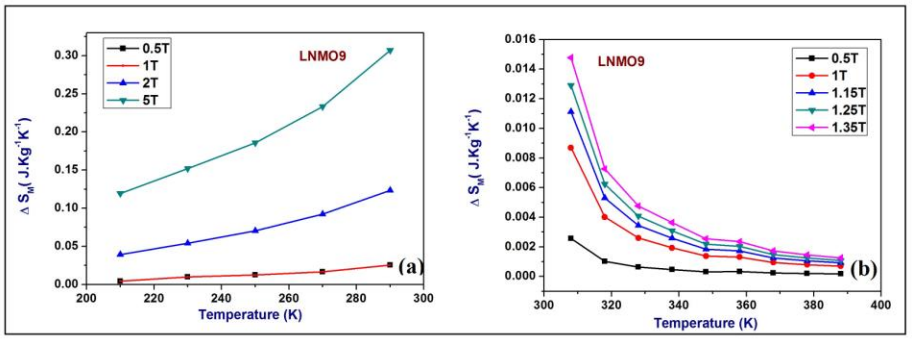

Figure 5.18: Variation of Magnetic entropy change (ΔS_M) for LNMO9 sample. (a) in the temperature range of 200 K to 300 K (b) in the temperature range of 303 K to 393 K

A comparison of magnetic entropy change in LNMO series at 5T and 1.35 T magnetic fields are shown in figure 5.19 and figure 5.20 respectively. It is evident that maximum magnetic entropy is obtained for

LNMO5 which has the highest magnetization in the series. Magnetic entropy change decreases with increase in Na concentration

.

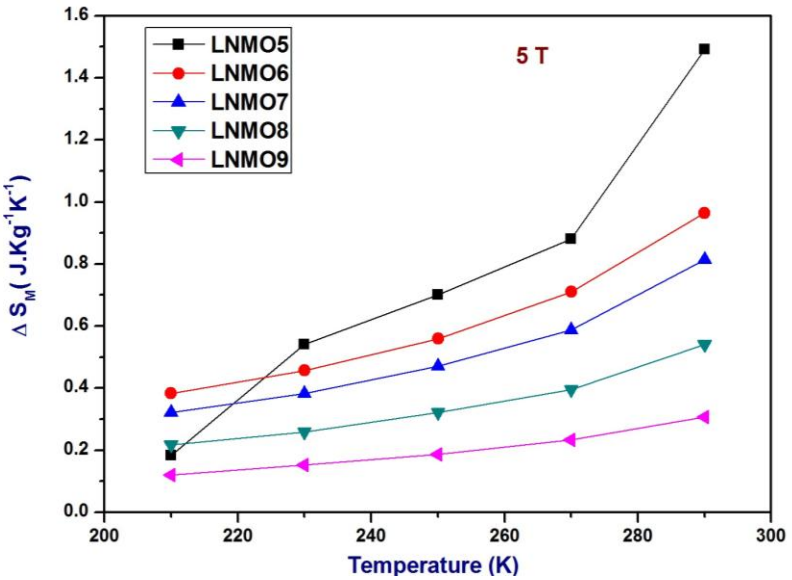

Figure 5.19: Magnetic entropy change (ΔS_M) in LNMO series at 5 T

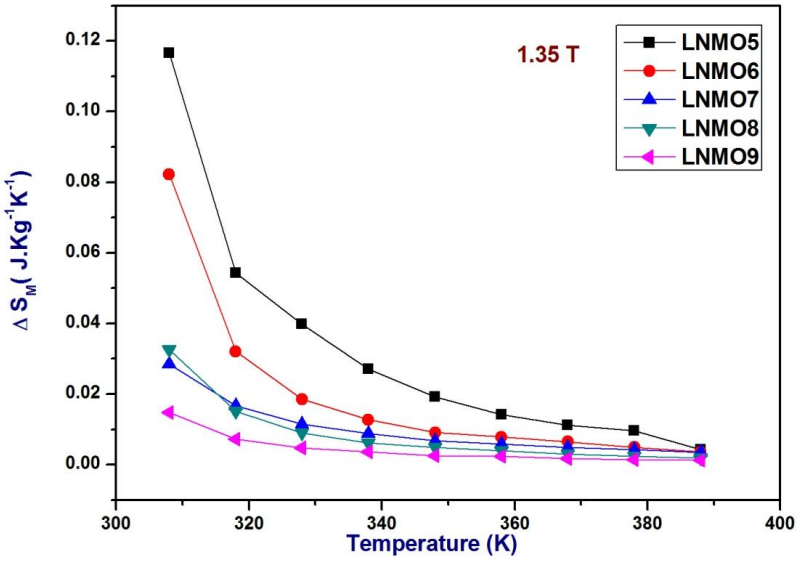

Figure 5.20: Magnetic entropy change (ΔS_M) in LNMO series at 1.35 T

5.3.3. Heat Capacity Measurements and Estimation of Adiabatic Temperature Change

Heat capacity (C_p) measurement in manganites assumes importance and can be utilized for the estimation of ΔT_{ad} as governed by equation 2.16 in chapter 2. Evaluation of ΔT_{ad} from measured C_p values are more accurate rather than relying on earlier reported results of C_p. Heat capacity of LNMO5 having the highest magnetic entropy change is plotted as a function of temperature and the measurements have been carried out for temperatures below 300 K as indicated in figure 5.21. Magnetic field dependence of C_p for second order phase transition (SOPT) materials is lower than that of first order phase transition FOPT materials. It is known that magnetic field dependence of C_p for SOPT material is insignificant. Variation of C_p with and without magnetic fields is similar in the case of LNMO5 as indicated in figure 5.21. Heat capacity is found to have direct dependence on temperature and C_p approached highest value of 660 $J.Kg^{-1}K^{-1}$ at 300 K.

C_p values are then used to evaluate the adiabatic temperature change (ΔT_{ad}) associated with manganite system as given by eqn. (2.16) and ΔT_{ad} values are plotted with respect to temperature. It is found that ΔT_{ad} increases with increase in temperature and a maximum temperature change of 0.62 K is observed at 280 K as indicated in figure 5.22. Variation of ΔT_{ad} against temperature plot is linear which is a promising result as far as MCE applications are concerned. Increase in ΔT_{ad} close to room temperatures and preferably near transition

temperature is indicative of the potential of this material for room temperature refrigeration.

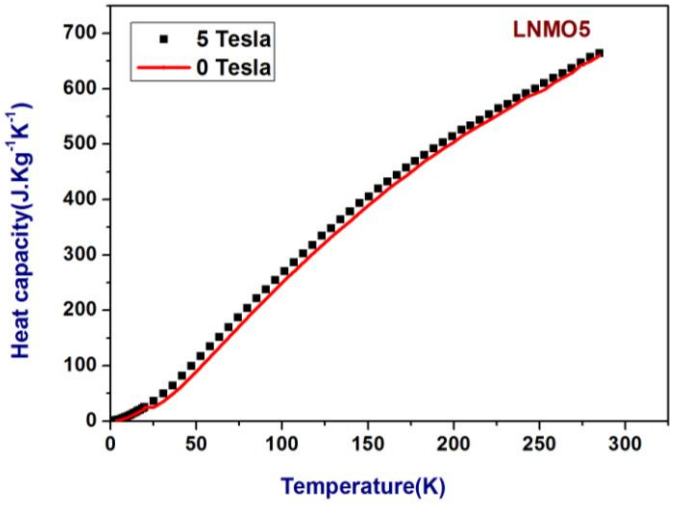

Figure 5.21: Heat capacity (C_p) Vs Temperature of LNMO5 sample for T < 300 K

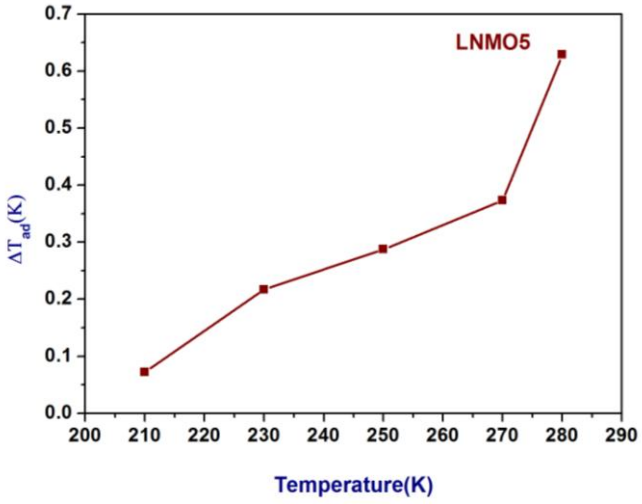

Figure 5.22: Adiabatic temperature change (ΔT_{ad}) of LNMO5 sample

Chapter 5

Conclusion

In conclusion, magnetic isotherms were utilized to estimate transition temperature and the magnetic entropy change for samples belonging to the series of sodium substituted lanthanum manganites, LNMO5 to LNMO9. Arrott plots generated from these isotherms indicated a second order phase transition. M-H isotherms at higher temperatures were also utilized to determine approximate T_C or range of T_C and it was found that T_C shifted to low temperatures with increase in concentration of sodium. An appreciable change in magnetic entropy was observed for the samples and the entropy variation is dependent on magnetic field and temperature. From the entropy values of LNMO65to LNMO9, it can be pointed out that entropy change increases with increase in magnetization while it exhibits maximum entropy change in the temperature range of 250 K to 320 K. Maximum entropy variation is observed for sample with lower Na content which is LNMO5. Magnetic entropy change of 1.5 $J.Kg^{-1}K^{-1}$ was observed at 290 K for ΔH of 5T while 0.12 $J.Kg^{-1}K^{-1}$ was observed for 1.35 T at 308 K for LNMO5. Heat capacity of LNMO5 was also determined and C_p was evaluated to be 660 $J.Kg^{-1}K^{-1}$ at 300 K. Adiabatic temperature change was evaluated from C_P and ΔS_M values and was found to be increasing with increase in temperature with a maximum of 0.62 K at 280 K. Thus magnetic entropy studies on monovalent sodium substituted lanthanum manganites provided higher values of entropy for a wide range of temperature close to room temperature and are highly beneficial from an application perspective.

References

[1] V. Franco, J.S. Blazquez, B. Ingale, and A. Conde, Annu. Rev. Mater. Res., **42**, 305–42 (2012).

[2] M.-H. Phan, S.-C. Yu, J. Magn. Magn. Mater., **308**, 325 – 340 (2007).

[3] K. A. Gschneidner, Jr. and V. K. Pecharsky, Annu. Rev. Mater. Sci., **30**, 387-429 (2000).

[4] X. X. Zhang, J. Tejada, Y. Xin, G. F. Sun, K. W. Wong, and X Bohigas, Appl. Phys. Lett., **69**, 3596 (1996).

[5] A. Szewczyk, H. Szymczak, A. Wisniewski, K. Piotrowski, R. Kartaszyn-ski, B. Dabrowski, S. Kolesnik, and Z. Bukowski, Appl. Phys. Lett., **77**, 1026 (2000).

[6] R. Szymczak, R. Kolano, A. Kolano-Burian, V.P. Dyakonov*a* and H. Szymczak, Acta Physica Polonica A, **117**, 1, (2010).

[7] A. Rostamnejadi , M. Venkatesan , P. Kameli , H. Salamati , J. M. D. Coey , J. Magn. Magn. Mater, **323**, 2214–2218 (2011).

[8] Manh-Huong Phana, Seong-Cho Yub, J. Magn. Magn. Mater., **308** , 325–340 (2007).

[9] L. D. Landau, JETP, **7**, 19 (1937); **7**, 627 (1937).

[10]M. Lifshitz, JETP, **11**, 269, 1941.

[11] V. L. Ginzburg, JETP,**17**, 833, 1947.

[12]C. P. Bean and D. S. Rodbell, Phys. Rev. **126**, 104 (1962**).**

[13] S. K. Banerjee, Phys. Lett., **12**, 1 (1964).

[14] Y. Kalyana Lakshmi, G. Venkataiah, M. Vithal, P. Venugopal Reddy, Physica B **403**, 3059–3066 (2008).

CHAPTER 6

Evaluation of Magnetic and Magnetocaloric parameters in Sodium Substituted Lanthanum Manganite Thin films deposited on Si Substrates

This chapter deals with studies carried out on LNMO samples deposited by pulsed laser deposition on silicon substrates. Their structure and compositions are also discussed in this chapter. It also deals with room temperature magnetic hysteresis measurements and the variation of magnetic entropy change with temperature above and below 300 K. Variation of magnetic entropy change with sodium concentration in thin films of LNMO series is also presented in this chapter . Surface morphology of the films is evaluated from SEM and AFM images.

6.1. Introduction

Investigations on manganite thin films accelerated after the CMR/ GMR discovery and with the advancement of thin film techniques [1]. Compared to bulk materials, thin film forms of these materials can find applications in the field of sensors, micro electro mechanical systems (MEMS), memory and spintronic devices. Pulsed laser deposition (PLD),

molecular beam epitaxy (MBE), RF sputtering and spin coating are commonly used to obtain high quality thin films. Among them, PLD, MBE and sputtering are the best methods for obtaining good films especially of oxides with high structural perfection. Films deposited using PLD have an added advantage of being stoichiometric with the target bulk material and hence the exact composition of bulk can be maintained in thin films also [2-5].

Doped lanthanum manganite thin films with Sr and Ca substitutions have been investigated largely and there exist reports in literature correlating their electric transport with magnetic properties [5-7]. An extensive study carried out on the bulk samples of Lanthanum manganites with monovalent ion (sodium) substitutions ranging from 50 to 90 percent revealed that they exhibit mixed magnetic phase with dominant ferromagnetic ordering. It could be interesting to deal with thin film analogues of these materials since only a few reports are seen in the literarure. It is found that saturation magnetization decreases with increase in Na concentration for bulk samples of LNMO. Magnetic measurements in thin films could be carried out to determine the saturation magnetization values and the variation of magnetization with Na concentration in thin films.

It has been found that samples belonging to the series ($La_{1-x}Na_xMnO_3$ with x= 0.5, 0.6, 0.7, 0.8 and 0.9) are stoichiometric and exhibit excellent magnetic and magnetocaloric parameters suitable for applications. The composition corresponding to LNMO5 is found to be promising since it exhibited fairly reasonable ΔS_M values at reasonable applied magnetic fields of 1.35 T and 5T. Investigations on the thin film forms of these compositions form the backbone for any further study

especially in realizing their application potentials. This chapter deals with the preparation of thin film samples of LNMO with Na concentration varying from 50 to 90 percent deposited on Si substrates. Their structural and magnetic properties are evaluated and the entropy change and relative cooling power are also estimated and correlated.

6.2. Experimental

Bulk powder samples belonging to the series LNMO ($La_{1-x}Na_xMnO_3$ with x= 0.5, 0.6, 0.7, 0.8 and 0.9) were synthesized using the citrate gel method. The details are described in chapter 4. Cylindrical pellets of radius 10mm were used as targets for thin film deposition. Thin films of sodium substituted lanthanum manganites were prepared employing pulsed laser deposition technique. For this, a laser beam from a KrF laser with a wavelength of 248nm and a repetition rate of 10Hz was used as the source. Laser pulses were allowed to hit the target placed at a distance of 4.5cm from the substrate holder where a silicon substrate is affixed. The deposition was carried out for two different thicknesses, 100 nm and 300 nm for each sample in the series of LNMO. Thin films are coded as SiLNMO5, SiLNMO6, SiLNMO7, SiLNMO8, and SiLNMO9. Thin film deposition was also carried out on chromium – gold (chrom gold) sputtered silicon substrates with a view to using them for electrical measurements. Thin films of two members on the extreme end of the LNMO series deposited on Si/ CrAu substrate are coded as Si/CrAu-LNMO5 and Si/CrAu-LNMO9. In the case of metal oxides, thin film deposition is usually carried out in the background of gases like nitrogen or oxygen maintained at a suitable pressure [8, 9]. Oxygen atmosphere

was preferred for the present case under a pressure of 0.33 mbar.The method of preparation of thin films using Pulsed laser deposition is described in chapter 3. Optimized deposition parameters are tabulated in table 6.1.

Parameters	Magnitude
Laser fluence	**2 J/cm^2**
Target to substrate distance	**4.5cm**
Oxygen pressure	**0.33 mbar**
Substrate temperature	**700 ^{0}C**
Thickness	**300nm, 100nm**

Table 6.1: PLD deposition parameters

6.3. Characterization

6.3.1. X-Ray Diffraction

Structural characterization of these samples was carried out using X-ray diffraction studies. XRD pattern of a representative sample of the series representative sample of the series, $La_{1-x}Na_xMnO_3$ with x= 0.5, 0.6, 0.7, 0.8 and 0.9), LNMO5 for 100nm thickness (SiLNMO5) within the 2θ range of $20^0$to 40^0 is depicted in figure 6.1. From the XRD pattern, with Si contribution subtracted, it is observed that the characteristic peak of perovskites is observed at a 2θ angle of 32^0 corresponding to (110) plane [ref.Chapter 4]. The inset figure shows the XRD pattern of LNMO5

film deposited on Si substrate showing the characteristic peak of silicon at 60^0.

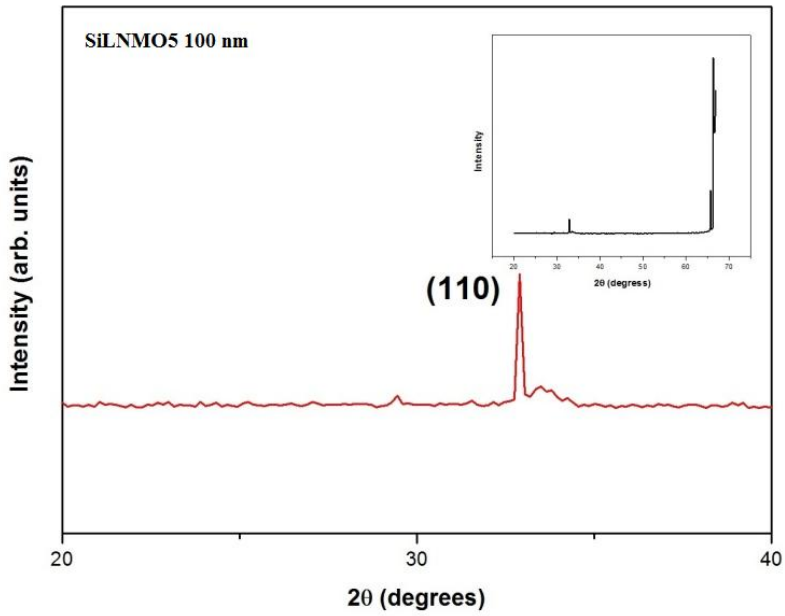

Figure 6.1: XRD pattern of SiLNMO5 100nm film

6.3.2. Scanning Electron Microscopy

Surface morphology of thin films deposited on Si substrate was examined using scanning electron microscopy (SEM). Figures 6.2(a) and 6.2(b) show SEM images of LNMO5 film deposited on Si and Si/ CrAu substrates. The etched part and deposited film part can be clearly seen in both images. Etching was carried out using a Si piece kept on the side of the substrate during the deposition which could be helpful in drawing out contacts for electrical measurements. Figures 6.3(a) and (b) depicts thin film surface of samples belonging to the extreme end of the

series, LNMO5 and LNMO9. Both the SEM pictures indicate that particles appear spherical in nature.

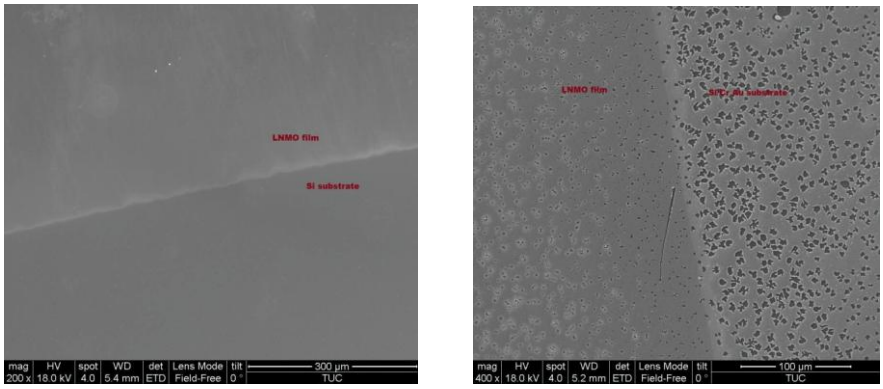

(a) **(b)**

Figure 6.2: SEM image of (a) SiLNMO5 (b) Si/ CrAu-LNMO5

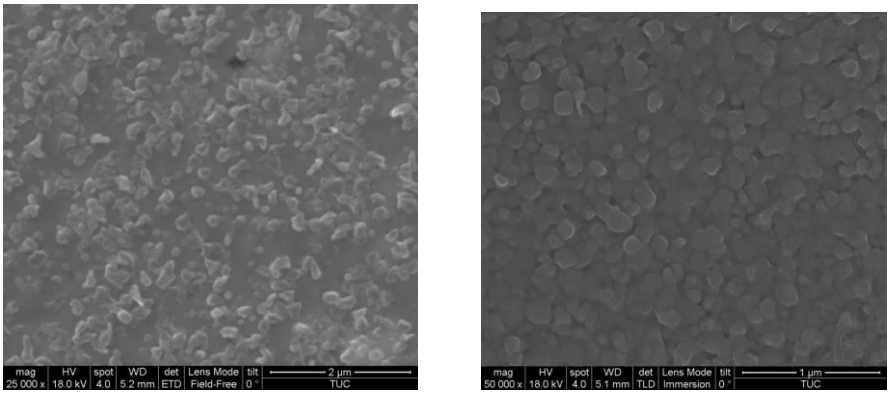

(a) **(b)**

Figure 6.3: SEM image of (a) SiLNMO5 (b) Si/ CrAu-LNMO9

6.3.3. Energy Dispersive Spectroscopy

Energy Dispersive Spectroscopy (EDS) analysis of the samples in the LNMO series was utilized to determine the composition of the samples. EDS spectra of SiLNMO5 and etched part of SiLNMO5 are indicated in figures 6.4 (a) and (b) respectively. From the EDS data given in table 6.2, it can be inferred that thin film contains all the desired elements La, Na, Mn and O in the required ratio. EDS spectrum of etched part shows only the presence of silicon and no other impurities are detected.

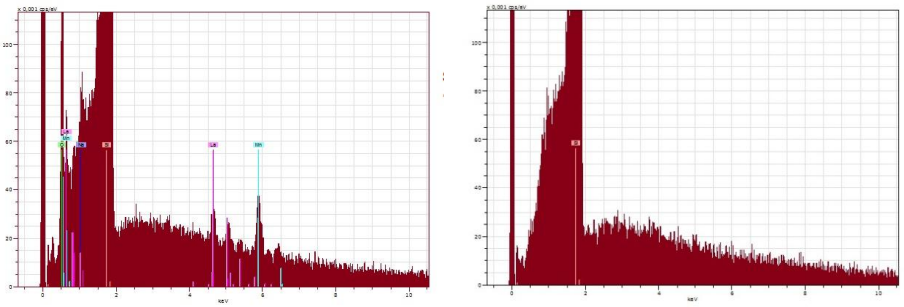

(a) **(b)**

Figure 6.4: EDS spectrum of (a) Si- LNMO5 (b) etched part of Si-LNMO5

Element	Atom C (wt.%)	Error
O 8 K-series	10.8	0.9
Na 11 K-series	0.21	0.0
Si 14 K-series	88.01	3.5
Mn 25 K-series	0.74	0.1
La 57 L series	0.24	0.1
	100%	

Table 6.2: EDS data of Si-LNMO5

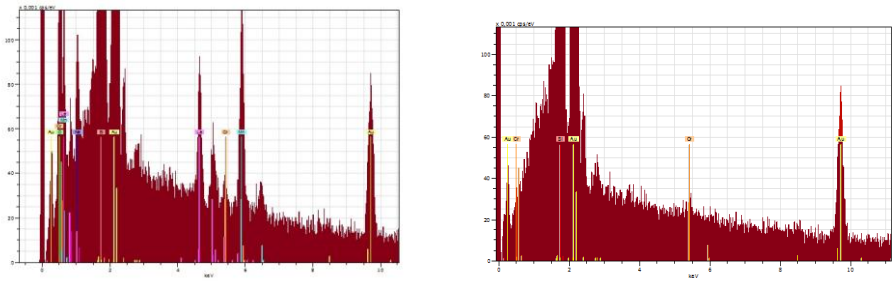

(a) **(b)**

Figure 6.5: EDS spectrum of (a) Si/CrAu-LNMO5
(b) etched part of Si/CrAu-LNMO5

Element	Atom C (wt.%)	Error
O 8 K-series	32.24	2.0
Na 11 K-series	1.25	0.1
Si 14 K-series	50.85	1.6
Cr 24 K-series	0.19	0.0
Mn 25 K-series	3.93	0.2
La 57 L-series	1.66	0.2
Au79 L-series	9.88	1.8
	100%	

Table 6.3: EDS data of Si/Cr Au-LNMO5

Figures 6.5(a) and (b) show Si/CrAu-LNMO5 film and its etched part respectively. EDS data table is shown in table 6.3 which confirms that samples are stoichiometric with an La: Na ratio of 1:1. For further confirmation, the end member of the LNMO series namely LNMO9 is also subjected to EDS analysis. The EDS spectrum of Si/CrAu-LNMO9 is shown is figure 6.6 and the EDS data table is

tabulated and shown in figure 6.4. It can be seen that most of La sites are occupied by Na ions thus maintaining stoichiometry in films.

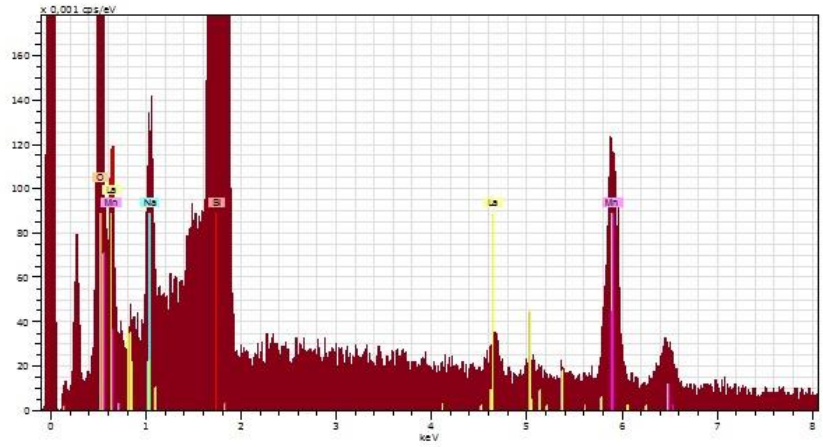

Figure 6.6: EDS spectrum of (a) Si/ Cr Au-LNMO9

Element	Atom C (wt.%)	Error
O 8 K-series	28.64	2.5
Na 11 K-series	1.36	0.1
Si 14 K-series	66.76	3.0
Mn 25 K-series	3.06	0.2
La 57 L-series	0.17	0.1
	100%	

Table 6.4: EDS data of Si/Cr Au-LNMO9

6.3.4. Atomic Force Microscopy

Topographic images of thin films of the series $La_{1-x}Na_xMnO_3$ with x= 0.5, 0.6, 0.7, 0.8 and 0.9 (LNMO) deposited on Si/CrAu substrate using Atomic Force Microscopy (AFM) are shown in

figure 6.7(a) to (d). Topographic images are indicative of a granular structure and are complimentary to that observed in SEM. Figure 6.8 is a three dimensional AFM image of SiCrAu-LNMO9 which gives a more precise view of film growth regions as cone shaped structures on Si substrates.

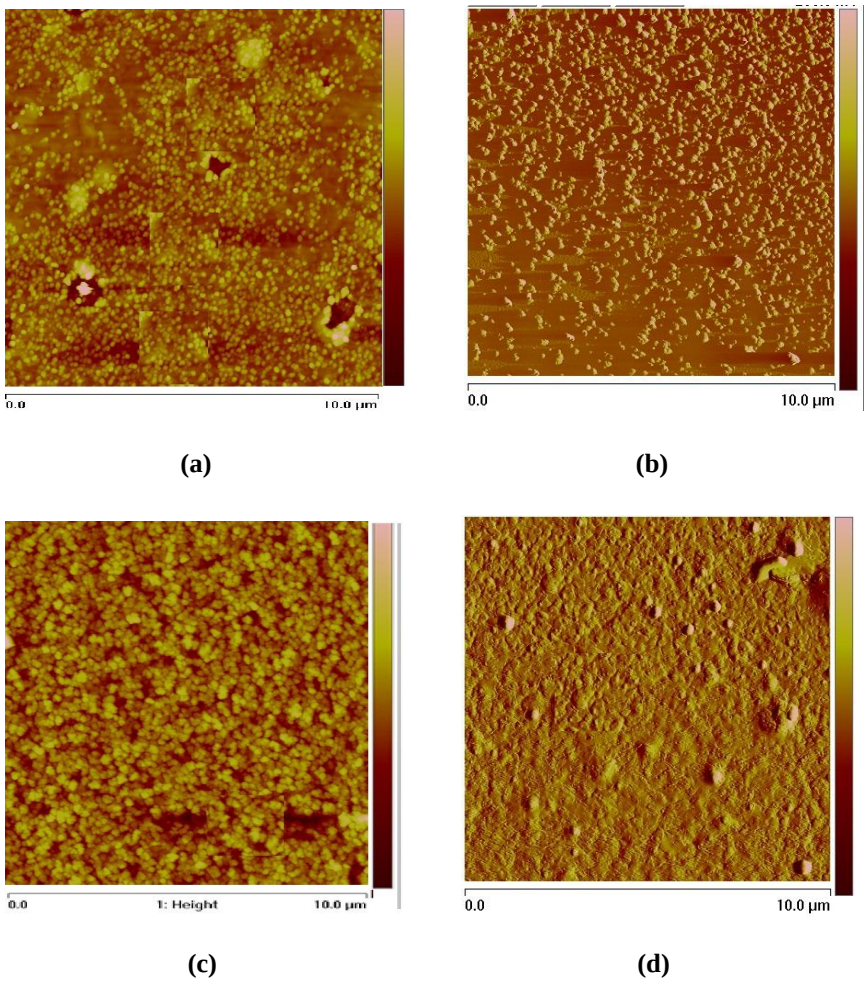

Figure 6.7: AFM of thin films on Si/Cr Au substrate (a) LNMO5 (b) LNMO6 (c) LNMO7 (d) LNMO8

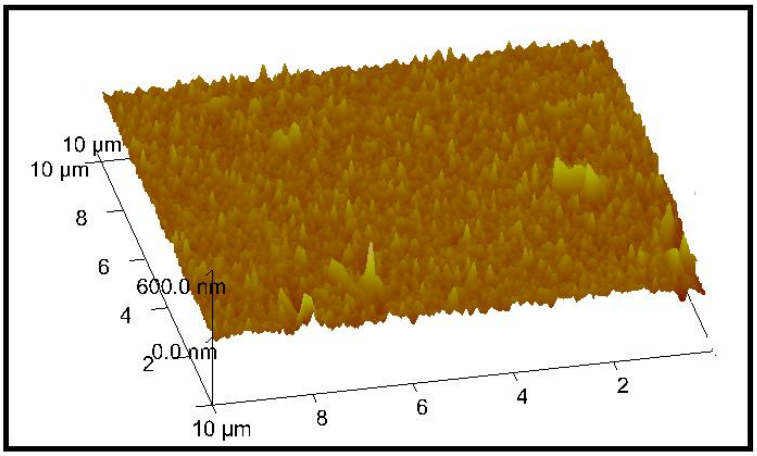

Figure 6.8: AFM of thin films on Si/Cr Au substrate

6.3.5. Vibrating Sample Magnetometer for magnetic characterization

Room temperature magnetic measurements carried out on thin film samples of LNMO series were performed and it indicated that all samples exhibit ferromagnetic ordering as shown in figure 6.8.This is analogous to the ferromagnetic ordering observed at 300 K for bulk samples of LNMO. Magnetization is expressed in terms of µemu/cm^2 after subtracting the diamagnetic contribution of silicon and a highest saturation magnetization of around 22 µemu/cm^2 is observed for SiLNMO5 sample. Saturation magnetization (M_S) is found to be decreasing with increase in Na concentration with nominal coercivity and the minimum M_S has been observed in LNMO9 thin film. Decrease of M_S with increase in Na concentration has been observed earlier for bulk samples also. It is also to be noted even though magnitude of M_S has decreased from that observed in bulk counterparts, magnetization followed the same trend as that of bulk targets and augers well for device

fabrication and promising. There is no special significance of measuring the magnetization in films of different thickness deposited on common substrates like silicon since the magnetization of LNMO films is expressed in terms of area units, μemu/cm^2 rather than μemu/cm^3. Thus magnetic measurements on one set of samples with thickness of 300 nm only are considered here.

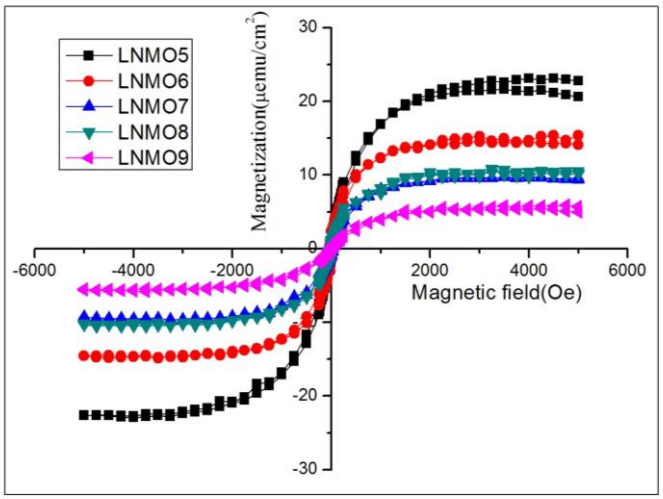

Figure 6.9: Ferromagnetic behaviour in SiLNMO thin films

6.4. Estimation of Magnetic Entropy Change

Magnetic entropy change is an essential criterion in deciding the magnetocaloric or magnetic refrigeration potential of a material. Magnetic entropy change in manganites can be evaluated from the magnetic isotherms [10, 11]. For this, magnetic isotherms in the temperature range of 200 K to 400 K were utilized. The procedure for estimation of entropy change is already discussed in the previous chapters (chapters 2 and 4). The entropy change is evaluated from the area

difference between the isotherms and expressed in terms of $J.Kg^{-1}K^{-1}$. Magnetic entropy change (ΔS_M) for all the samples in the series LNMO5 to LNMO9 is estimated. Evaluation of magnetic entropy change in thin films is a tedious task since the substrate contribution cannot be ignored. In the present case, approximate entropy values are estimated on the assumption that silicon substrates are diamagnetic and thus variation of magnetic parameters with external magnetic fields and temperature are negligible. Figures 6.10, 6.11, 6.12 and 6.13 show the variation of estimated magnetic entropy change in LNMO6 to LNMO9 thin films of thickness 300 nm deposited on Si substrate.

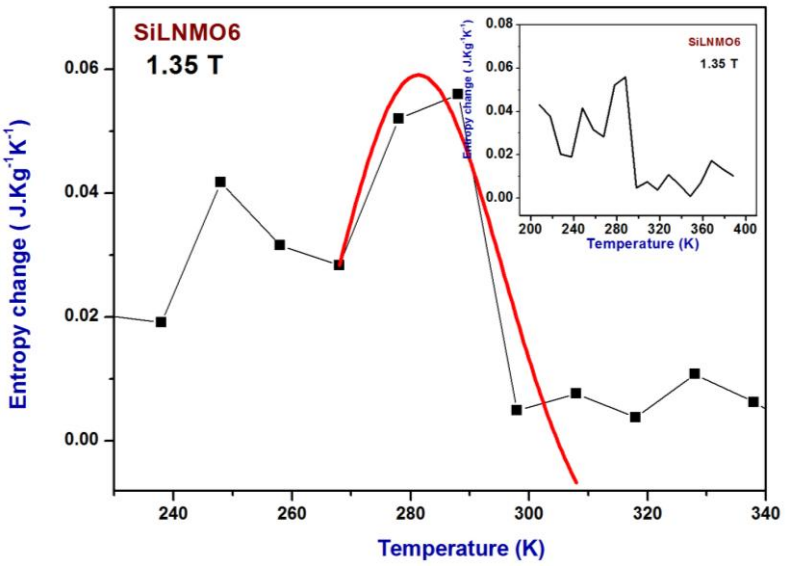

Figure 6.10: Magnetic entropy change in SiLNMO6 film

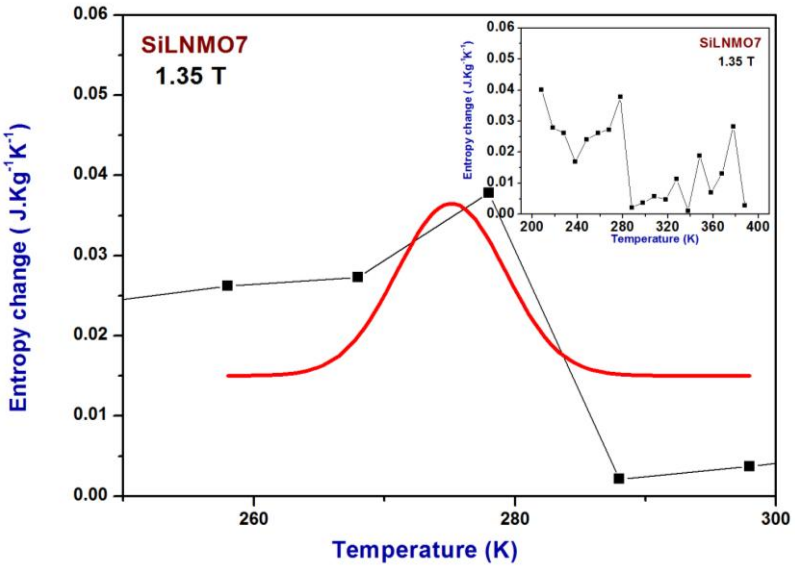

Figure 6.11: Magnetic entropy change in SiLNMO7 film

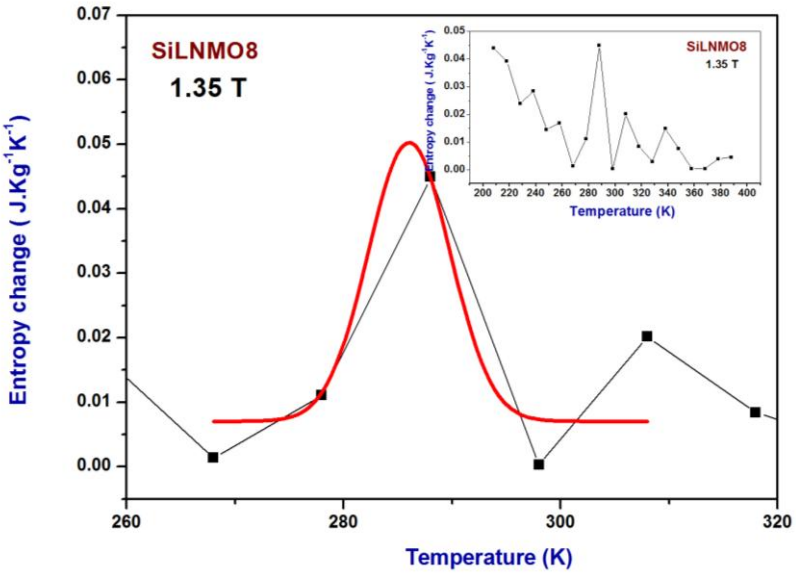

Figure 6.12: Magnetic entropy change in SiLNMO8 film

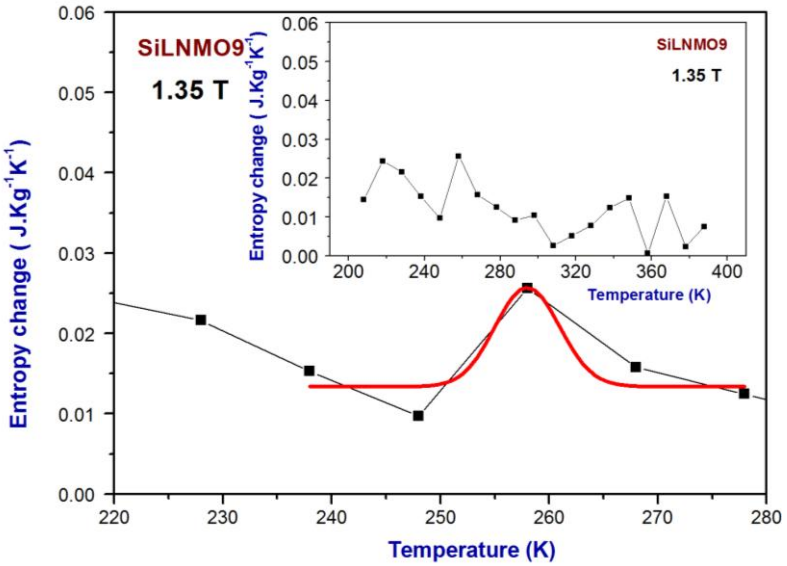

Figure 6.13: Magnetic entropy change in SiLNMO9 film

Magnetic entropy change does not follow a regular pattern with temperature with a peak at around 300 K, i.e, near room temperature. The inset figures (Figures 6.10, 6.11, 6.12 and 6.13) show the estimated magnetic entropy change for LNMO6 to LNMO9 thin film samples. Variation of magnetic entropy near room temperature region in all the films is subjected to a lognormal fitting as indicated in figures 6.10, 6.11, 6.12 and 6.13. The reasons for this anomaly observed in magnetic entropy values could be because of the errors arising out of 1) subtracting the diamagnetic contribution of Si substrate 2) approximation in the integration results during the area calculation between isotherms 3) lower magnetization in thin films 4) approximation in density values for the conversion of magnetization to emu/g units.

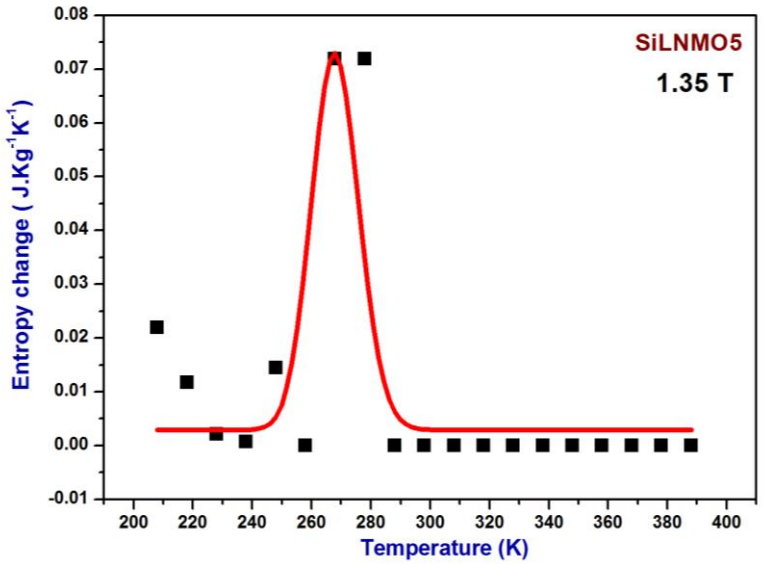

Figure 6.14: Magnetic entropy change in Si-LNMO5 film

In the case of LNMO5 film, magnetic entropy change observed with a thickness of 300nm shows a systematic variation with maximum values in the range 260 K -280 K as shown in figure 6.14. The lognormal fit to the estimated magnetic entropy values shows clearly that the maximum entropy change is within the temperature range of 250 K to 290 K. Thus LNMO5 films exhibit magnetic entropy change of around 0.07 $J.Kg^{-1}K^{-1}$ near room temperature. These observations thus point to the possibility of developing an MCE material from 50 percent sodium substitution for La sites in lanthanum manganites since entropy change is appreciable in their bulk and thin films. For thin films there exists future possibility for determining entropy change by proper choice of substrates,

subtraction of substrate contribution and by tuning the thickness of the films.

6.5. Estimation of Relative Cooling Power (RCP)

Relative Cooling Power (RCP) of a magnetic refrigerant material denotes the cooling efficiency. Larger the RCP value, higher the efficiency of the material for magnetocaloric applications. RCP can be evaluated using the following relation [12, 13]:

$$RCP = \Delta S_M(T,H)\delta_{FWHM} \tag{6.1}$$

where ΔS_M indicates the maximum magnetic entropy change and δ_{FWHM} is the full width at half maximum of magnetic entropy curve. RCP denotes the amount of heat transfer between cold and hot regions of a magnetic refrigerant during a thermodynamic cycle. From figure 6.14, δ_{FWHM} can be determined and it is found to be 18.64 K. Maximum entropy change, ΔS_M at 1.35 T is 0.07 $J.Kg^{-1}K^{-1}$. For bulk samples of $La_{0.67}Sr_{0.33}MnO_3$, an RCP value of 42 $J.Kg^{-1}$ and for $La_{0.8}0Ca_{0.20}MnO_3$, an RCP of 72 $J.Kg^{-1}$ has been reported earlier. RCP value of 1.3 JKg^{-1} is substantial and appreciable for thin film samples [13-15].

Conclusion

Thin films of sodium substituted lanthanum manganite samples were deposited on silicon substrates using PLD. Structural and morphological characterizations using SEM and AFM confirmed granular structure. Compositional analysis using EDS proved that stoichiometry of La, Na and Mn ions are maintained in thin films akin to bulk

compositions. Magnetic measurements proved that all samples exhibit ferromagnetic ordering near room temperature as in the case of bulk samples. It is also observed that saturation magnetization decreased with increase in Na concentration with maximum magnetization of 22 μemu/cm^2 observed for the thin film of LNMO5 on Si substrate. Magnetic isotherms in the temperature range of 200 K to 400 K were utilized for determining magnetic entropy change. Variation of magnetic entropy change for LNMO6 to LNMO9 samples does not follow a regular pattern. On the other hand, a systematic variation is observed for maximum entropy change in LNMO5 thin films. Maximum magnetic entropy change of 0.07 $J.Kg^{-1}K^{-1}$ is observed for LNMO5 sample and entropy change is substantial within the temperature range of 250 K to 290 K. Relative cooling power of the LNMO5 film is also evaluated and it is found to be 1.3 J/Kg. Thus it has been demonstrated that thin film forms of LNMO samples can be deposited on Si substrates without sacrificing stoichiometry. Though the relative cooling power is much less to that of bulk samples, the results are promising and warrants further investigations.

References

[1] A-M Haghiri-Gosnet and J-P Renard, J. Phys. D: ApplPhys. ,**36,** R127 (2003).

[2] W Prellier, Ph Lecoeur and B Mercey, *J*. Phys.: Condens. Matter ,**13,** R915 (2001).

[3] I.W. Boyd, W. Zhang, Appl.Surf. Sci., 127–129, 410–417 (1998).

[4] C. Aruta, M. Angeloni, G. Balestrino, N. G. Boggio, P. G. Medaglia, A. Tebano, B. Davidson, M. Baldini, D. Di Castro, P. Postorino, P. Dore, A. Sidorenko, G. Allodi, and R. De Renz, J. Appl. Phys., **100**, 023910 (2006).

[5] M. Navasery, S.A. Halim, N.Soltani, G.Bahmanrokh, A.Dehzangi, M.Erfani H, A.Kamalianfar, S.K.Chen and K.Y.Pan, Int. J. Electrochem. Sci., **8,** 467 – 476 (2013).

[6]] Dubourdieu C, Audier M, Se´nateur JP, Pierre J. , J. Appl. Phys., 86, 6945 (1999).

[7] T. Nurgaliev, U. Topal , B. Blagoev, E. Mateev, J. Supercond. Nov. Magn. , **25**, 2495–2498 (2012).

[8] Barry Carter, M. Grant Norton, Ceramic Materials: Science and Engineering, Springer, New York (2007).

[9] Milton Ohring, Materials Science of Thin Films, 2nd edn., Academic press, Santiago, USA (2002).

[10] L. M. Wang, Jian-Hong Lai, and Jyh-Iuan Wu, Y.-K. Kuo, C. L. Chang, **102**, 023915 (2007).

[11] A. H. Morrish, The Physical Principles of Magnetism, Wiley, New

York, Chap. 3 (1965).

[12] V. Franco, J. S. Blazquez, B. Ingale, and A. Conde, Annu. Rev. Mater. Res. **42**, 305–342 (2012).

[13] A. Rostamnejadi , M. Venkatesan , P. Kameli , H. Salamati , J. M. D. Coey , J. Magn. Magn. Mater, **323**, 2214–2218 (2011).

[14] Zhiming Wang , Gang Ni, Yulu Che, J. Supercond. Nov. Magn.,**25**, 533–539 (2012).

[15] Z.B. Guo, Y.W. Du, J.S. Zhu, H. Huang, W.P. Ding, D. Feng, Phys. Rev. Lett. **78**, 1 (1997).

CHAPTER 7

Demonstration of a Field Effect Device based on Ferroelectric- Ferromagnetic Heterostructures and Studies on the Influence of Strain on Magnetization

Manganites are perceived as tunable magnetic materials which could serve as excellent candidates for magnetoelectric applications. This chapter deals with the fabrication of a magnetoelectric composite using thin film deposition of sodium substituted lanthanum manganites on a ferroelectric substrate. A material which functions as a ferroelectric as well as a piezoelectric is selected for this purpose. The demonstration of a field effect device based on a heterostructure of a ferroelectric-ferromagnetic combination is attempted here. The magnetic hysteresis loop and the ferroelectric hysteresis loop parameters are also evaluated. Further, the influence of manganite film thickness on the magnetic properties will be investigated by coating films of different thickness on different substrates.

Chapter 7

7.1. Introduction

A magnetoelectric (ME) response is a substantial change in electric polarization with the application of a magnetic field and vice versa [1-3]. The literature is replete with reports on bulk composites comprising of ferromagnetic and ferroelectric components namely CFO/BFO (cobalt ferrite/barium titanate), NZFO/PZT (Nickel Zinc Ferrite/Lead Zirconate [3-6]. However, the ME coupling coefficient in these materials with ferrites as the ferromagnetic phase is not appreciable as ferrites are either conducting or semiconducting and cause leakage current by deteriorating the insulating nature of ferroelectrics. Thus higher dispersion of ferrites in ferroelectric matrix with large final sintering temperatures is undesirable [5]. Also an effective synthesis procedure for developing ME composites using ferrites is novel and have not been achieved yet. Later, Magnetic alloy based composites with Terfenol D and metglas were tested and appreciable ME coupling could be achieved. For a laminate structure of metgalss ribbon and PZT fiber actuator layer, an ME response of 10V cm^{-1} Oe at low frequency and under small magnetic fields has been observed. Polymer based composites and rare earth oxide based composites were also developed but the coupling was found to be lower [7-11].

Among rare earth based oxides, manganites are perceived as potential multifunctional materials since they possess tunable structural, electrical and magnetic properties. They exhibit colossal magnetoresistance, Jahn Teller distortion, charge ordering and metal-insulator transition with a close entanglement between lattice, charge and spin degrees of freedom. Manganites are generally called half metallics as

the lattice offers less resistance to one type of spin and for the other spin, it behaves as an insulator. Spintronics, magnetoelectrics and multiferroics currently utilize the charge as well as spin degrees of freedom of electrons and working towards achieving a strong coupling between these different orders. Manganites with perovskite structure could serve as efficient candidates in these fields since they are excellent electron correlated systems [12].

Doped manganites with high magnetization with tunable magnetic properties are excellent substitutes for ferrites in developing ferrolelectric- ferromagnetic (FE-FM) heterostructures. Correlation of the electrical, structural and magnetic properties renders uniqueness to these materials and paves way for developing multifunctional materials. One such effort is the field effect device with manganites serving as the ferromagnetic part [3,13-19]. Doped lanthanum manganites with varied sodium substitutions were found to be possessing ferromagnetic ordering in bulk and thin films near room temperature. This has been the motivation for the development of a field effect device (FED) using these thin film manganites. Choice of substrate in developing FED is crucial. A substrate which offers dual functionality of serving as a deposition medium and a ferroelectric is ideal for an FED device. Considering all these factors, an ideal substrate of PMN PT is chosen and an FED device using FE-. FM heterostructure is demonstrated in this chapter. Dependence of magnetization of thin films on substrate / strain and the concept of strain dependent magnetism is also presented in this chapter.

7.2. Experimental

Bulk samples of sodium substituted lanthanum manganites which were found to be ferromagnetic were used as targets for thin film deposition. Pellets of the bulk samples of radius 10mm were made and these were used as the targets for PLD. Perovskite type (1-x)$Pb(Mg_{1/3}Nb_{2/3})O_3$-$xPbTiO_3$ (PMN-PT) is chosen as the ferroelectric component in the heterostructure. PMN-PT serves as a piezoelectric substrate which is also relaxor ferroelectric having a high dielectric constant. PLD is chosen for depositing LNMO on PMN PT samples since it has been demonstrated earlier that such films retain their stoichiometry of the bulk (Ref: chapter 6). The detailed description of thin film deposition parameters is described in chapter 6. No individual compositional analysis is performed for thin film deposited on PMN PT as deposition was carried out in situ along with Si substrates. The compositional analysis of films deposited on Si substrates is already presented in chapter 6 and it is assumed that films deposited on PMN PT also retain their parental characterization. Thin films with 50 and 70 percent of Na substitution are chosen for the present study as these compositions are found to be structurally pure and possess high magnetization values. These samples are coded as PMNPT-LNMO5 and PMNPT-LNMO7. A schematic of a field effect device based on ferroelectric and ferromagnetic material is shown in figure 7.1.

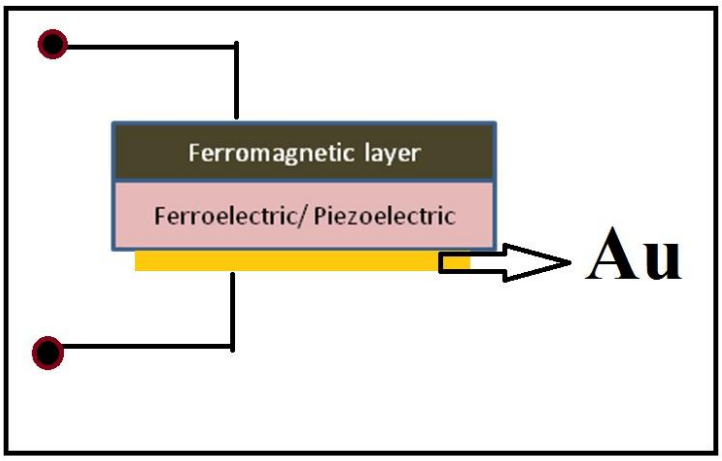

Figure 7.1: A schematic diagram of field effect device

7.3. Structural Characterization

7.3.1. X-Ray Diffraction

X-Ray diffraction pattern of a representative thin film sample of the series, LNMO5 film (2θ range of 20 to 40) with thickness of 300nm deposited on PMN PT substrate is shown in figure 7.2. The characteristic peak corresponding to the plane (110) can be observed at around 32^0[20,21]. However, peaks corresponding to other planes could not be observed. A GXRD could have come handy but could not be carried out for want of time.

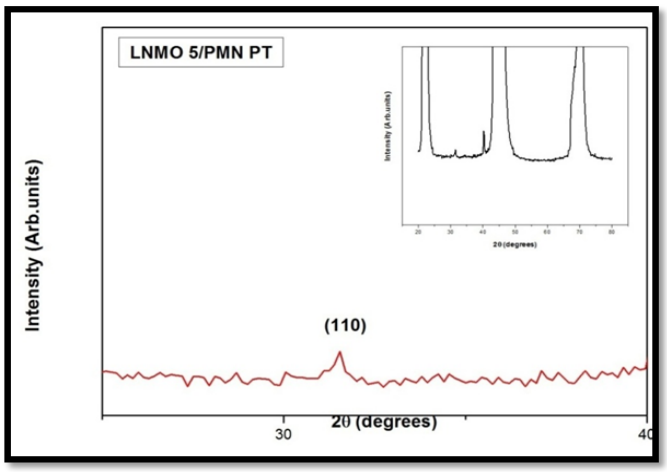

Figure 7.2: XRD pattern of LNMO5 film deposited on PMN PT substrate

7.3.2. Scanning Electron Microscopy

In order to determine the surface morphology of the deposited films, SEM images of LNMO films were recorded and analyzed. SEM images of LNMO5 and LNMO7 films deposited on PMN PT substrate are shown in figures 7.3 and 7.4. It is found that in LNMO5 films, the grains are spherical in nature while for LNMO7, the particles are prismatic. The transformation from spherical to prismatic nature could be because of lattice distortion arising out of increased Na concentration. The effect of substrate also could not be ruled out since no such property was seen in thin films deposited on Si substrate.

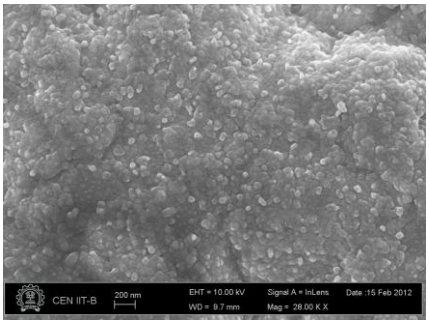

Figure 7.3: SEM image of PMNPT-LNMO5

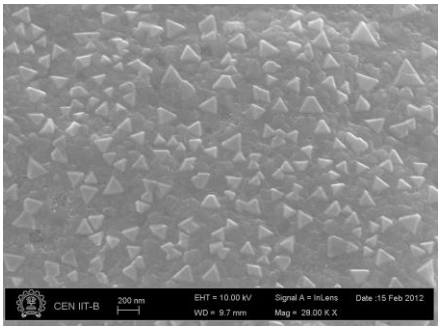

Figure 7.4: SEM image of PMNPT- LNMO7

An AFM image of the PMN PT-LNMO5 is also recorded and is shown in figure 7.5. It can be observed that the AFM image displays a complex structure which can be due to the piezoelectric property of the substrate.

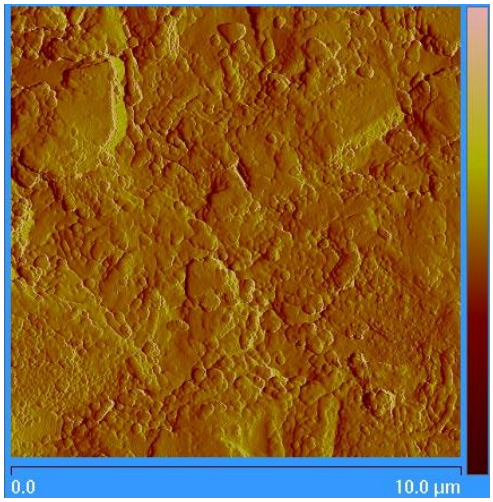

Figure 7.5: AFM image of LNMO5 film deposited on PMN PT substrate

7.3.3. Vibrating Sample Magnetometer for magnetic characterization

Room temperature VSM measurements were carried out in bulk as well as in thin films on Si substrates and it was observed that M_S decreases with increase in Na concentration. The hysteresis loop of all thin films of LNMO series deposited in PMN PT substrate for a thickness of 100nm is shown in figure 7.6. It is observed that LNMO5 exhibits higher magnetization and thereon there is no substantial variation in magnetization. This further justifies our selection of two samples, namely LNMO5 and an intermediate member of the series, LNMO7. Magnetic measurements on PMN PT- LNMO5 and PMN PT- LNMO7 for two different thicknesses of 300 nm and 100 nm are shown in figure 7.7 and 7.8 respectively. For PMN PT-LNMO5, M_S is 167 μ emu/cm^2 for 100 nm film and 31 μ emu/cm^2 for 300 nm thick film while for PMN PT-LNMO7, the values are 28 μ emu/cm^2 and 10 μ emu/cm^2 for 100 nm and 300 nm films respectively.

On the other hand, thin films of LNMO5 and LNMO7 deposited on Si substrates do not show any such thickness dependent magnetization. Thickness dependent magnetization observed in the case of films deposited on PMN PT substrate is quite interesting and needs to be probed from a fundamental perspective. It is known that lattice strain of the substrate can alter properties like structural, electrical and magnetic. It has been observed in the case of STO like substrates that a lattice mismatch can induce a lattice strain on the deposited film [13, 22]. It may be noted here that PMN PT substrate is piezoelectric and iso structural with LNMO5 and LNMO7. Such substrates elongate the lattice parameters which increase the distance between Mn ions leading to a

decreased magnetization in films with respect to bulk materials. The effect of strain is uniform in the case of thinner samples (~ 100nm) while inhomogeneity occurs in the case of thicker samples. This has been suggested as the reason for the decrease in magnetization as film thickness increases [13].

Very recently researchers reported their findings on the theoretical estimation of strain induced magnetism in single layer molybdenum disulphide (MoS_2) system and graphene [13]. They predicted through calculations that strain and vacancies induce enhanced magnetization close to 2μB per vacancy defect. However, it is purely theoretical. A quick scan of literature also tells that another group (Chopdekar et al.)[14] examined strain induced domain structure of $LaSrMnO_3$ thin films grown on BTO substrates. It was found that magnetization can be oriented b 45^0 or 90^0 by the orientation of ferroelectric phase with temperature. There are reports on SrRuO3 films deposited on PMN PT substrates where the reversible biaxial strain from substrate was utilized to probe the response of magnetization to strain [23].

Even though influence of substrate strain in the magnetic properties of LNMO could be observed and is a prominent result for the strain mediated magnetic response, it remains largely speculative and needs further evidence. At present, it can be inferred that the substrate plays a crucial role in deciding the properties (especially magnetic properties) of manganite thin films. Theory of strain dependent magnetization phenomena is still in its infancy and conformational evidences are to be sought for establishing the causes of this phenomenon.

Spectroscopic tools could be employed to evaluate the bond angle and bond length of Mn-O-Mn to verify enhanced magnetization

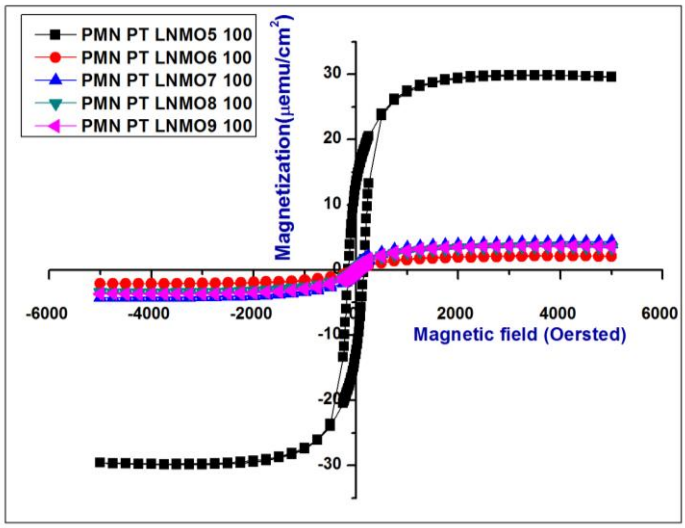

Figure 7.6: Room temperature magnetic hysteresis loop of LNMO films deposited on PMN PT substrate

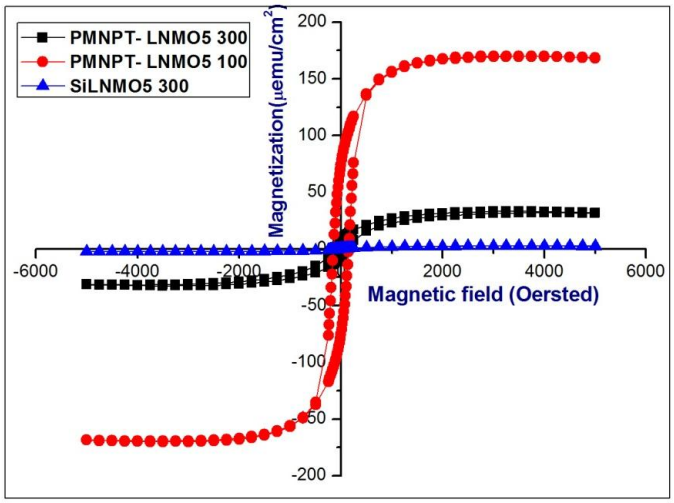

Figure 7.7: Room temperature magnetic hysteresis loop of LNMO5 film deposited on PMN PT and Si substrate

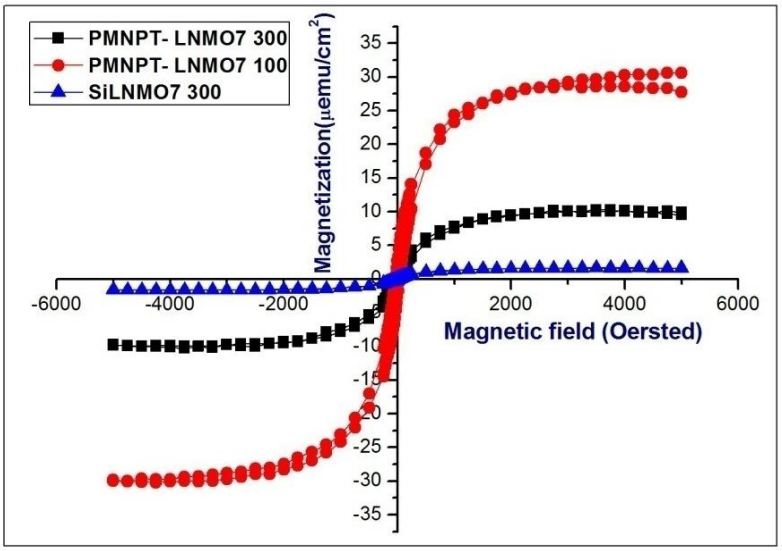

Figure 7.8: Room temperature magnetic hysteresis loop of LNMO7 film deposited on PMN PT and Si substrate

7.3.4. Ferroelectric Loop Tracer Measurements

Strain effects in PMN PT and the films deposited on them need some additional confirmation. It is known that PMN PT substrates are nearly cubic and exhibit inverse piezoelectric effect. To understand the influence of electric field on the substrate, ferroelectric hysteresis loops are plotted with electrical polarization, P vs Electric field, E and are shown in figures 7.9(a) to (d). It is observed that in comparison to bare PMN PT substrate, PMN PT-LNMO shows an increase in coercive field (E_C). In the case of PMN PT-LNMO5, E_C is 100.1kV/cm while PMN PT has 78.7 kV/cm and that for PMN PT-LNMO7 it is 89.6 kV/cm. Such an increase in E_C has been observed for other electric field ranges such as

20kV, 30kV and 40kV. Detailed variation of E_C and remanence (P_R) is tabulated in table 7.2(a) and (b). Coercive field change for LNMO5 is larger than that observed for LNMO7 for all the field ranges. But in LNMO7, the remanence is larger than LNMO5.

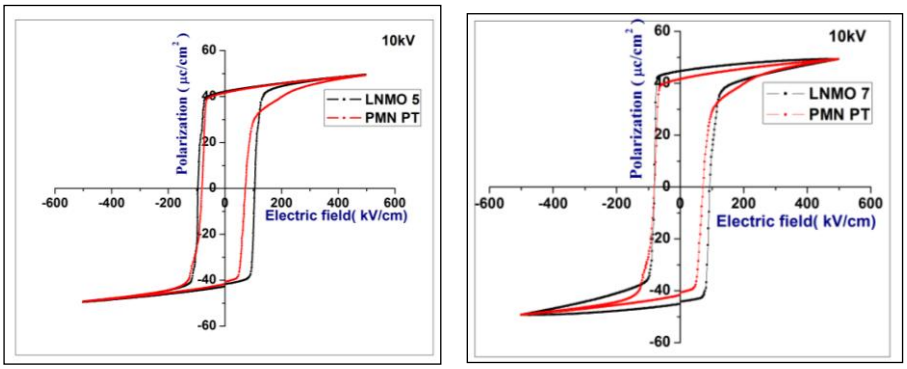

(a)

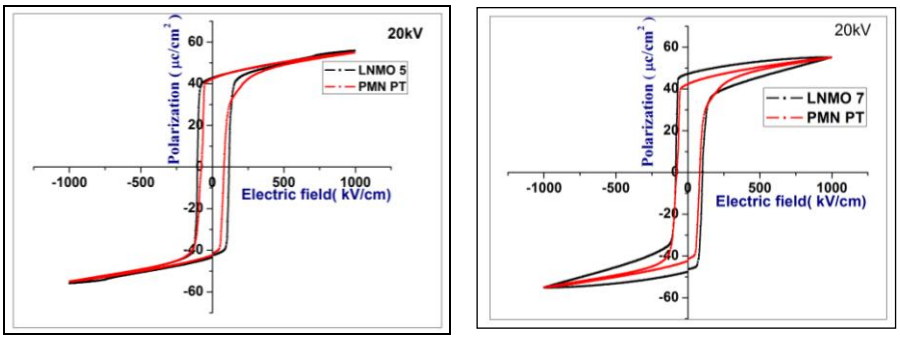

(b)

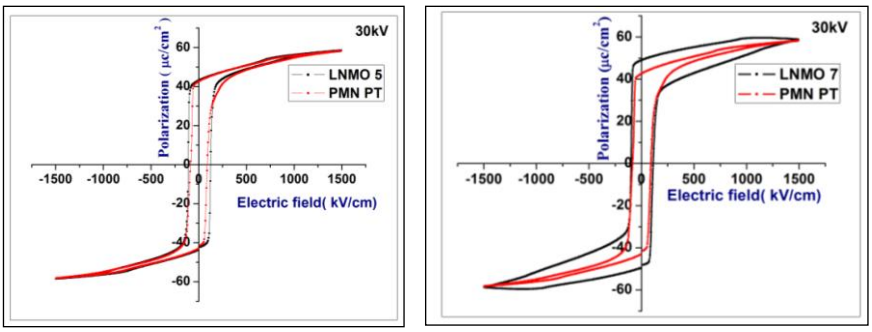

(c)

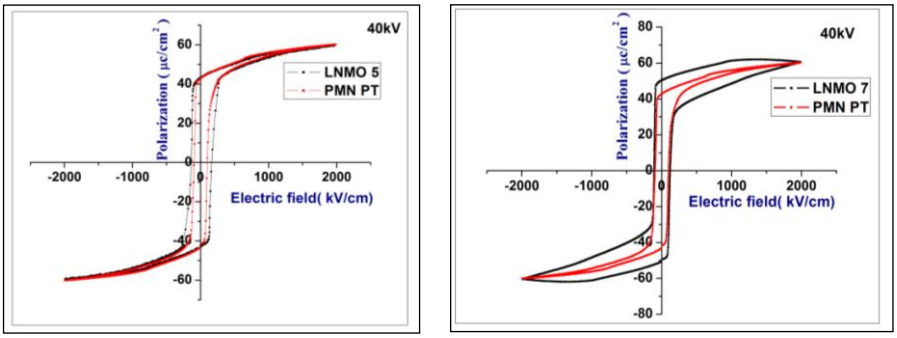

(d)

Figure 7.9(a) to (d): Ferroelectric loop tracer measurements on PMN PT – LNMO5 and PMN PT- LNMO7 films (100nm) for electric field ranges 10kV, 20kV, 30kV and 40kV.

SAMPLE CODE	10 kV			20kV		
	Ec	Pr	Ps	Ec	Pr	Ps
PMN PT	78.7	41.6	48.1	80.5	42.2	54.5
PMN PT-LNMO5	100.1	42.17	49.2	110.6	42.7	55.1
PMN PT-LNMO7	89.6	44.6	49.2	92.6	47.1	55.1

(a)

SAMPLE CODE	30kV			40kV		
	Ec	Pr	Ps	Ec	Pr	Ps
PMN PT	85.4	42.5	57.6	98.3	42.2	59.6
PMN PT-LNMO5	118	43.1	57.9	145.9	43.1	59.7
PMN PT-LNMO7	103.8	48.9	59.1	114.3	50.2	61.3

(b)

Table 7.2(a) and (b): Table showing parameters from ferroelectric hysteresis measurements

There has been reports that strain from the substrate influence the coercive field and remanence of thin films. An increase in coercive field signifies higher epitaxial strain influence which has been observed for thicker BFO thin films in the structure Au/BFO/LSMO/STO. Also in the same structure, an increase of remanence with increase in BFO film thickness has been attributed to strain relaxation. Such an explanation holds for the change in ferroelectric parameters with respect to thickness of films [16]. In the present case, thickness of films is constant and the variation parameter is the concentration of Na in films.

In our case, it is also to be noted that ferroelectric hysteresis loop of bare LNMO bulk materials showed a circular loop typical of a resistive material as in figure 2. Thin films on Si substrate when subjected to P-E loop studies suffered a dielectric breakdown. Thus it could be established that the change in E_C and P_R are substrate effects and the applied electric field influences strain of the substrate which results in the change in E_C and P_R parameters similar to BFO thin films. It has been proved from magnetic measurements conducted in bulk and thin

films that Na concentration significantly influences the saturation magnetization of LNMO structures. Accordingly, LNMO5 was found to be more magnetic than LNMO7. Thus a possible explanation could be that for LNMO7 the strain is in a relaxed state compared to LNMO5 causing an enhancement of remanence compared to LNMO5. A larger strain influence is felt in LNMO5 films which has led to an increase in coercive field E_C in addition to decrease in P_R in agreement with earlier results. This shows the response of PMN PT- LNMO, a ferroelectric-ferromagetic structure with respect to electric field. The magnetic ordering also influences the strain mechanism giving an insight and scope for the dependence of strain, electrical and magnetic ordering. Thus PMN PT-LNMO system can be viewed as a field effect device and can pave way for further studies on thickness dependence on ferroelectric and ferromagnetic parameters possible leading to a multifunctional magnetoelectric material.

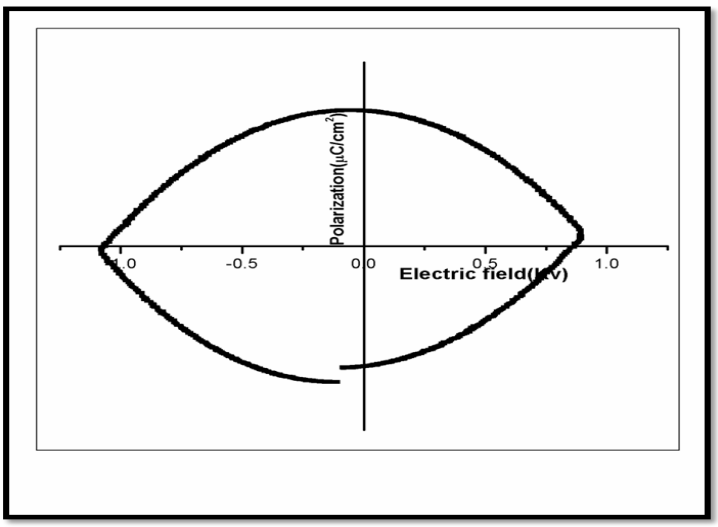

Figure 7.10: Ferroelectric loop tracer measurements on LNMO5 bulk material

Chapter 7

Conclusion

Sodium substituted lanthanum manganite (LNMO) films were deposited on ferroelectric PMN PT substrates with the aim of developing a ferroelectric – ferromagnetic composite. Sodium substitutions of 50 and 70 percent for lanthanum sites were carried out in lanthanum manganites and the thin films were deposited by PLD on normal Si and Ferroelectric PMN PT substrate. Thin films on PMN PT substrate showed higher magnetization for thinner films of 100nm than 300nm films which indicated that substrate strain of PMN PT changes the Mn -O-Mn bond length and bond angles of LNMO responsible for magnetism in manganites and the strain effects are higher for thinner films. Ferroelectric loop tracer measurements carried out in LNMO5 and LNMO7 films showed that there is a considerable change in E_C and P_R of PMN PT substrate on thin film deposition. Such a variation of the ferromagnetic and ferroelectric loop parameters signifies the importance of PMN PT – LNMO composites for magnetoelectric and field effect device applications at room temperature.

References

[1] Daniel Khomskii , Physics ,**2**, 20 (2009).

[2] N.A. Hill, J. Phys. Chem. B, **104**, 6694 (2000).

[3] Jing Ma , Jiamian Hu , Zheng Li , and Ce-Wen Nan Adv. Mater., **20**, 1–26 (2011).

[4] W. Eerenstein, N. D. Mathur & J. F. Scott , Nature, **2** ,442, 17(2006).

[5] Rahul C. Kambale, Dae-Yong Jeong and Jungho Ryu, Adv. Cond.Mat.Phys., **2012,** 824643 (2011).

[6] A. M. J. G. van Run, D. R. Terrell, and J. H. Scholing, J. Mater. Sci. **9**,10, 1710–1714 (1974).

[7] J. Ryu, A. V. Carazo, K. Uchino, and H. E. Kim, J. Electroceram, **7**, 1, 17–24 (2001).

[8] J. Ryu, S. Priya, K. Uchino, D. Viehland, and H. Kim, J. Kor. Ceram. Soc.,, **39**, 813–817, 2002.

[9] G. Srinivasan, C. P. Devreugd, C. S. Flattery, V. M. Laletsin, and N. Paddubnaya, Appl. Phys. Lett., **85**, 13, 2550–2552 (2004).

[10] S. Dong, J.-F. Li, and D. Viehland, Appl. Phys. Lett., **85**, 22, 5305–5306 (2004).

[11] J. Zhai, S. Dong, Z. Xing, J. Li, and D. Viehland, Appl. Phys. Lett., **89**, 8, 083507 (2006).

[12] . B. Salamon and M. Jaime, Rev. Mod. Phys.,**73**, 3 (2001).

[13] Peng Tao, Huaihong Guo, Teng Yang, and Zhidong Zhang, J. Appl. Phys., **115**, 054305 (2014).

[14] R.V. Chopdekar, J. Heidler, C. Piamonteze, Y. Takamura, A. Scholl, S. Rusponi, H. Brune, L.J. Heyderman, and F. Nolting, Eur. Phys. J.

B, **86**, 241 (2013).

[15] Baomin Wang, Lu You, Peng Ren, Xinmao Yin, Yuan Peng, Bin Xia, Lan Wang, Xiaojiang Yu, Sock Mui Poh, Ping Yang, Guoliang Yuan, Lang Chen, Andrivo Rusydi & Junling Wang, Nat. Commu., **4**, 2778 (2013).

[16] Le Wang, Zhen Wang, Kui-juan Jin,a) Jian-qi Li, Huai-xin Yang, Can Wang, Rui-qiang Zhao, Hui-bin Lu, Hai-zhong Guo, and Guo-zhen Yang, Appl. Phys. Lett.,**102**, 242902 (2013).

[17] V. Pen˜a , Z. Sefrioui, D. Arias, C. Leo´n, J. Santamaria, M. Varela, S.J. Pennycook , M. Garcia-Hernandez , J.L. Martinez, J. Phys. Chem. Solids., **67**, 472–475 (2006).

[18] Jizhai Cui, Joshua L. Hockel, Paul K. Nordeen, David M. Pisani, Cheng-yen Liang, Gregory P. Carman, and Christopher S. Lynch, Appl. Phys. Lett., **103**, 232905 (2013).

[19] A-M Haghiri-Gosnet1 and J-P Renard**,** J. Phys. D: Appl. Phys. **36**, R127–R150 (2003).

[20] S.Roy , Y.Q. Guo, S. Venkatesh and N.Ali , J. Phys.: Condens. Matter **13**, 9547(2001)

[21] A. Das, M. Sahana, S.M. Yusuf, L. Madhav Rao, C. Shivakumara, M.S. Hegde, Mater. Res. Bull. **35**, 651–659 (2000).

[22] Yandong Ma, Ying Dai, Meng Guo, Chengwang Niu, Yingtao Zhu, and Baibiao Huang, ACS Nano, **6**, 2,1695–1701 (2012).

[23] A. Herklotz, M. Kataja, K. Nenkov, M. D. Biegalski, H.-M. Christen, C. Deneke, L. Schultz, and K. D¨orr, Phys. Rev.B.,**88**, 144412 (2013).

CHAPTER 8

SUMMARY AND CONCLUSION

Man's pursuit for newer materials is unstoppable and it is this attribute that has led to the development of new technologies. Newer materials and novel phenomena enter the arena of research almost daily. If it was ferrites in 1950's, a material which revolutionized the entire magnetics industry, it is the turn of manganites now. These classes of materials are now the cynosure of scientists and engineers. With the discovery of brand new phenomena like GMR, CMR, colossal magnetoelectric coupling, giant MCE and giant thermoelectric power, novel materials also start rising in the horizon of materials science.

Manganites are an important member of the perovskite family and have been in the forefront of research for the last 50 years or so. They represent a class of materials called correlated systems wherein the principle of correlation is extensively utilized to make storage devices, bolometric sensors, magneto-resistance devices and spin valves. Manganites can also serve as multifunctional devices. The fundamental requirement in the material property for meeting multifunctionality is the correlation of electronic spin and charge. From a fundamental perspective, correlated systems are interesting as they have presented many new concepts like ion mediated exchange, spin dependent transport,

charge and orbital ordering, half metallicity and strain dependent magnetization to the theoretical world.

The central theme of this thesis is also on manganites and is with the twin objectives of a material study leading to the demonstration of a device. This is taken up for investigation. Sincere efforts are made to synthesize phase pure compounds. Their structural evaluation, compositional verification and evaluation of ferroelectric and ferromagnetic properties are also taken up. Thus the focus of this investigation is related to the investigation of amagnetoelectric and magnetocaloric application potentials of doped lanthanum manganites with sodium substitution.

Bulk samples of sodium substituted lanthanum manganites with Na substitution ranging from 50 percent to 90 percent were synthesized using a modified citrate gel method and were found to be orthorhombic in structure belonging to a pbnm spacegroup. The variation in lattice parameters and unit cell volume with sodium concentration were also dealt with. Magnetic measurements revealed that magnetization decreased with increase in sodium concentrations. Vacancies in the lattice were found to have a profound influence on the magnetic behaviour of these materials which was evident from temperature dependent magnetization measurements. Magnetization vs temperature of all the compositions were carried out in the high temperature range, above 300 K, and it was found that the T_C for 50 percent Na substituted sample is around 334 K. Effective Bohr magneton from magnetization values were estimated and were correlated with the composition.

XPS measurements were performed on these samples and the characteristic peaks of major elements like Na, Mn, La and O were

identified. Origin of ferromagnetism in these compounds can be attributed to double exchange or super exchange mechanism between Mn^{3+} and Mn^{4+} ions with double exchange phenomenon dominating the super exchange as indicated by the ferromagnetic ordering at room temperature and partly by the vacancy induced magnetic interactions. Competing ferro/ antiferro regions were dependent on the ration of Mn^{3+}/Mn^{4+} ions and the XPS analysis showed that Mn^{3+}/Mn^{4+} ratio decreased with increase in Na concentration. For the end sample of the series LNMO, LNMO9, it was found that Mn^{4+} ratio exceed Mn^{3+} and antiferromagnetism wins over ferromagnetism.

The exact stoichiometry of LNMO samples could not be established beyond doubt even after employing very sophisticated techniques like XPS. The study using XPS has been instrumental in the estimation of Mn^{3+}/Mn^{4+} ratioin the compounds and this to some extent has helped to correlate the observed magnetization with the composition. Magnetization measurements carried out on these samples are indicative of the fact that there exist magnetic inhomogeneity in the system. These magnetic nhomogeneities could be arising particularly from vacancies. Vacancy driven magnetism is quite new with the advent of graphene/ carbon magnetism. More elaborate studies need to be carried out to spell out the nature of magnetism and the concentration of each component in the compound. Even these compositions could well serve as a rich template for such a study. This could be a futuristic study.

A systematic investigation on the electrical conductivity of these compositions with and without the presence of oxygen with in situ facilities for XRD, DTA, TGA, can be carried out. May be the electrical conductivity data can be correlated with the magnetic data. This coud not

be carried out and is left for future studies. From a fundamental point of view, more needs to be understood, especially, on the nature of magnetism and their exact origin in defect rich compounds like sodium substituted lanthanum manganites.

M-H Isotherms of all samples exhibited ferromagnetic characteristic in the observed temperature range. These isotherms were utilized to determine the magnetic entropy change in the samples. It was found that a maximum magnetic entropy change of 1.5 $J.Kg^{-1}K^{-1}$ was observed for 50 % Na sample and ΔS_M decreased with increase in Na substitution. From the M-H isotherm data, Arrott plots were plotted to determine the nature of magnetic transition and established that all samples possessed second order magnetic transition. The T_C (or T_C range) was determined from Arrott plots which indicated that T_C decreased with increase in Na concentration. For LNMO5, a maximum magnetic entropy change (ΔS_M) of 1.5 $J.Kg^{-1}K^{-1}$ was observed at 290 K for a ΔH of 5 T while 0.12 $J.Kg^{-1}K^{-1}$ was observed for 1.35 T at 308 K. Adiabatic temperature change was evaluated from heat capacity (C_P) measurement and ΔS_M values which was found to be increasing with increase in temperature with a maximum of 0.62 K at 280 K. An appreciable value for magnetic entropy change was observed in all the compositions of sodium substituted lanthanum manganites with the highest value for LNMO5.

Evaluation of magnetic entropy change and adiabatic temperature change for all the compositions in the series is quite tedious and labour intensive. A very systematic set of data for a wide range of temperature could be generated for various substitutions of Na. In short, it has been found that the compositions with Na substitution of 50 percent is

the best and it exhibits a fairly large value of 1.5 $J.Kg^{-1}K^{-1}$ entropy change near room temperature. This is promising.

Thin films of these compositions were prepared on silicon substrates. Excellent films with composition matching their targets could be deposited by pulsed laser deposition. Such studies are very rare in literature and this particular investigation has shed valuable insights on the ΔS_M values of the thin film compositions. Though the absolute values of ΔS_M are very much lower than their corresponding bulk, scope exists to deposit films with appropriate magnetization for application purposes. The relative cooling power evaluated for a representative sample was found to be around 1.3 $J.Kg^{-1}$.

Magnetoelectrics and multiferroics has become synonymous nowadays and efforts are afoot to fabricate field effect devices. A simple field effect device was demonstrated with PMN PT substrtae serving as the ferroelectric component and LNMO5/LNMO7 playing the role of a ferromagnetic component. The field effect device demonstration was carried out with the help of P-E and M-H hysteresis loop tracings. The shift in P-E loop with respect to pristine PMN PT is an indirect evidence to prove that there exist coupling between magnetic and electric behaviour. However, ME coupling experiments need to be carried out to evaluate the coupling coefficients and resonance frequency etc. Such experiments only could shed light on the effectiveness of the device. This needs to be conduted and a proposition postponed for the future.

Strain induced magnetism is a new phenomena predicted on MoS2 like system. We were able to demonstrate enhanced magnetization in the case of less thick samples of LNMO5/LNMO7 on PMN PT substrates. This has been explained by invoking the change

induced in the Mn-O-Mn bond angle and bond length. This mechanism is very much tentative and inconclusive and more experiments need to be carried out by using advanced spectroscopic techniques. Like Raman spectroscopy in combination with Infrared spectroscopy. This is earmarked for a future date.

Sodium substituted mangnaites could exhibit interesting dielectric phenomenon since these compounds are rich in oxygen vacancies. The evaluation of dielectric permittivity at various frequencies is yet another unfinished study. Such a study involving Cole-Cole plot, dielectric spectroscopy could be valuable and can even be correlated with electrical conductivity studies.

Knowledge, research and innovation are deeply intertwined. When researchers carry out investigations, they contribute to the knowledge base by adding new theories and lending new insights on the existing phenomena. This knowledge is for dissemination and this is nothing but teaching. The other link in this chain is innovation and this is the fructification of research. Innovation occurs only if research is put to use for the benefit of humanity to create wealth and for making life more humane. This could be in the form of improved processes, new devices or brand new applications. All investigations leading to Ph.D. degrees must result in atleast 'incremental science'. This investigation may also be viewed in this context. The generated knowledge is just like a drop in the vast ocean of knowledge. However, this 'Δ' is obviously a worthwhile contribution. Generally, Ph.D.s are considered as an exercise in generating the required human resources for dissemination of knowledge and also for sustaining the knowledge - research – innovation chain.

Any research if it does not touch the lives of human beings is meaningless. For this, the 'lab' to 'field' distance must be reduced. This requires the service of entrepreneurs. In short, it is not worthless to be a researcher. Today's researcher is tomorrow's knowledge disseminator, innovator or an entrepreneur or all the three put together.